STUDIES ON HYDROCARBON TRANSFORMATIONS OVER ZEOLITES

A THESIS

SUBMITTED TO THE

UNIVERSITY OF POONA

FOR THE DEGREE OF

DOCTOR OF PHILOSOPHY

(IN CHEMISTRY)

TH-1057

BY

DEBASIS BHATTACHARYA

CATALYSIS DIVISION

NATIONAL CHEMICAL LABORATORY

PUNE - 411 008, INDIA.

(SEPTEMBER 1996)

Dedicated

To

My Parents

TH-1057

CERTIFICATE

Certified that the work incorporated in the thesis entitled "**Studies on Hydrocarbon Transformations over Zeolites**" submitted by **Mr. Debasis Bhattacharya**, for the degree of Doctor of Philosophy, was carried out by the candidate under my supervision in the Catalysis Division, National Chemical Laboratory, Pune, India. Materials obtained from other sources have been duly acknowledged in the thesis.

[Dr. S. SIVASANKER]

(Research Guide)

ACKNOWLEDGEMENTS

I wish to express my sincere gratitude to Dr. S. Sivasanker, Deputy Director, National Chemical Laboratory, Pune, for his valuable guidance and encouragement throughout the course of this investigation without which I would not have completed this thesis successfully.

I am deeply indebted to Dr. A.V. Ramaswamy, Head, Catalysis Division, for providing me all facilities to conduct research and for his stimulating discussions during the course of my research work.

I am grateful to Drs. B.S. Rao, R. Vetrivel, A.P. Singh and S.S. Tambe for their helpful suggestions during the present study.

I am thankful to Drs. A. Chatterjee, M. Chatterjee, S. Kannan and Eric. Edward Lowenthal for their encouragement and moral support during this study.

I would be failing in my duty if I donot thank my friends, Ram, Manna, Binod, Nikhil, Sujit, Asit, Rina, Rita, Sharmistha, Rajib, Bhola, Debasis, Biswajit, Anil, Tapan, Tapas, Asim, Sahida, Ashok, Krishanu, Dr. Raju, Bokade, Priyabrata and Suvendu.

I would like to thank Mr. Ramakrishnan and all the members of Catalysis Division for their cooperation during my study.

I am thankful to Dr. P. Ratnasamy, Director, NCL, Pune, for permitting me to submit this work in the form of a thesis, and University Grants Commission, New Delhi, India, for providing me a research fellowship.

Debasis Bhattacharya

[DEBASIS BHATTACHARYA]

CONTENTS

I. INTRODUCTION

II. EXPERIMENTAL DETAILS

Chapter I

Introduction

1.0. GENERAL INTRODUCTION

Catalysts can be broadly classified into two categories, namely homogeneous catalysts and heterogeneous catalysts. Homogeneous catalysts possess advantages such as milder reaction conditions, better mixing between the reactant and the catalyst and the presence of well-defined active sites. But they also possess disadvantages such as difficulty in separation from the reactants and products, regeneration and stability problems. As a result, heterogeneous catalysts have been found to be preferable in many industrial processes. The world market for heterogeneous catalysts has already exceeded 4 billion dollars per year *[1]*. Zeolites constitute a major portion of the heterogeneous catalysts used in the industry. Systematic studies of the synthesis of zeolites were first carried out by Barrer in 1948 *[2]*. As of today, more than 150 synthetic zeolites and 37 natural zeolites are known with different structures.

1.1. ZEOLITES

Zeolites *[2,3]* are crystalline microporous silico-aluminates made up of a three-dimensional network of $[SiO_4]$ and $[AlO_4]$ tetrahedra linked by corner sharing of oxygen ions. The number of alumina tetrahedra present in the structure determines the framework charge, which is balanced by either H^+ and / or metal cations. If H^+ ions are the charge balancing species, Brönsted acid sites are generated. The Al^{3+} ion itself has a tendency to acquire a pair of electrons to fill its vacant p orbitals resulting in the formation of a Lewis acid site. A representative empirical formula for a zeolite can be written as:

$M_{2/n}O.Al_2O_3.xSiO_2.yH_2O$

where "M" represents the exchangeable cations and "n" represents the valency of the cation M, which is generally from the elements of group I and II, although other metal, non-metal

and organic cations may also balance the framework charge. The value of "x" is always equal to or greater than 2 since two Al^{3+} cannot occupy adjacent tetrahedral sites *[4]*.

1.1.1. STRUCTURAL OVERVIEW

The primary building unit of a zeolite framework is the individual tetrahedral TO_4 unit, where T is either Si or Al. Loewenstein has formulated that whenever two tetrahedra are linked by an oxygen bridge, the center of only one of them can be occupied by aluminium; the other center must be occupied by silicon or by another small ion of electrovalence 4 or more (such as phosphorous) *[4]*.

A secondary building unit (SBU) consists of a selected geometric grouping of the primary tetrahedra. There are nine such building units which can be used to describe all of the known zeolite structures. These SBUs consist of 4, 6 and 8 membered rings, 4-4, 6-6 and 8-8 membered double rings and 4-1, 5-1 and 4-4-1 branched rings *[3]*. The structures of these units are shown in Fig.1.1.

However, in many instances, it is necessary to take into account the arrangements of these secondary building units in space to describe structural similarities among the zeolites of the same group. For example, when we look at the tetrahedra that comprise the 4-membered ring SBU, we find that there is more than one way of joining the tetrahedra together to form the 4-ring SBSs. There are several possible orientations for the tetrahedra in the 4-rings. Therefore, the linking of these 4-rings to form the chain building units results in four completely different sequences of the tetrahedra. The chain building units stack further to form the final lattice. The use of chains composed of the SBUs simplifies visualization of the structural aspects of zeolites.

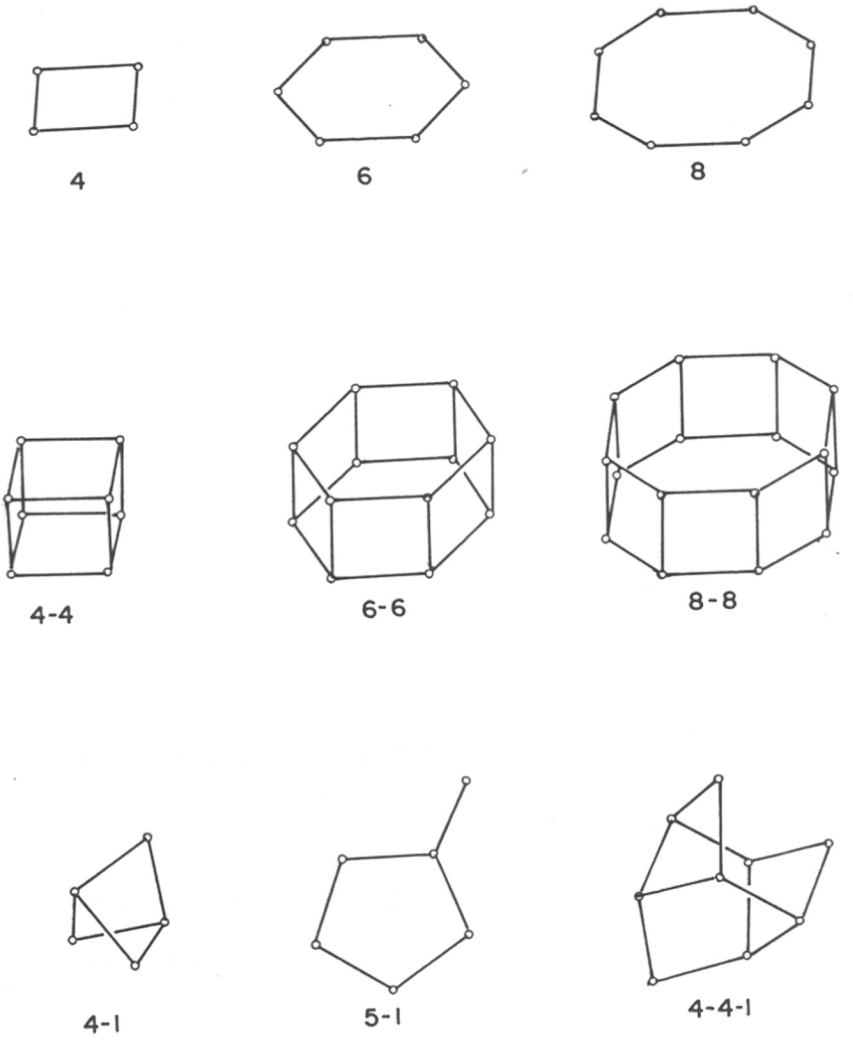

Fig. 1.1. Secondary building units (SBUs) found in zeolite structures *[3]*.

1.1.2. SYNTHESIS OF ZEOLITES

Zeolites are formed by the crystallization of ingredients composed of alumina, silica, alkali-salts, water and organic templates under hydrothermal conditions. The nature of the zeolite thus obtained is influenced by the composition of the precursors and synthesis conditions such as temperature, pH of the reactant mixture and the duration of crystallization *[3,5]*.

1.1.3. CLASSIFICATION OF ZEOLITES

Zeolites are classified according to their chemical composition *[6]* and effective pore diameters *[2,7]*. Classification of zeolites according to their chemical composition has been made on the basis of their silica to alumina ratio (SAR). These are grouped as (a) low silica (SAR = 1-1.5) (b) medium silica (SAR = 1.5-5) (c) high silica (SAR = 5-several thousands) and (d) Al-free, pure materials, "Silicalites". Zeolites can also be classified based on their pore opening, made up of either 8-, 10- or 12- membered rings and referred to as small, medium and large pore zeolites respectively.

1.2. CHARACTERISTIC PROPERTIES OF ZEOLITES

Zeolites are useful as heterogeneous catalysts due to their many characteristic properties *[8]*, namely, ion exchange capacity, high acidity, large adsorption capacity, high thermal stability and resistance to coke deposition. The above properties are described in detail in this section.

1.2.1. ION-EXCHANGE

The ion exchange capacity of a zeolite is determined by the amount of aluminium present in the framework positions. Each $[AlO_4]$ tetrahedron in the zeolite framework is

associated with a net (unit) negative charge. The charge is usually compensated by cations of alkali or alkaline earth metals present in the synthesis formulation. These cations, present in their hydrated form are loosely attached to the framework and have a high degree of mobility. These ions can be partially or completely replaced by other univalent, divalent or multivalent ions by ion-exchange, hydrothermal fusion or vapor-phase treatments *[9]*. Barrer *[10,11]*, Rees *[12]* and Sherry *[13,14]* have studied the ion-exchange equilibria in X and Y zeolites in detail. A comprehensive review on the ion-exchange phenomenon is also available in the literature *[15]*. The effective pore size of the zeolites can be modified in a controlled way by changing the nature of the exchangeable cations which are located near the pore openings. For example in the case of zeolite A, ion-exchange with the divalent ion Ca^{2+} opens the pore aperture to 5.6 Å, whereas larger univalent ions (Na^{+}) diminish the pore aperture to 4.7 Å *[16]*. Similar effects have also been observed in other zeolites like mordenite, chabazite, zeolite X and offretite *[17,18]*.

Due to their interesting ion-exchange properties, zeolites are also used as detergent builders replacing the traditionally used phosphates. Zeolite A is generally used to replace the Ca^{2+} and Mg^{2+} ions present in the hard water by ion-exchanging with the Na^{+} ions, present in the zeolite *[19]*. The present worldwide production of NaA zeolite for detergent applications exceeds 500,000 metric-ton per year *[19]*.

1.2.2. ACIDITY

The introduction of Faujasites (X and Y zeolites) as industrial catalysts for fluid catalytic cracking (FCC) which is an acid catalyzed reaction is a landmark in zeolite catalysis *[20-22]*. The creation and the nature of the two types of acidic sites (Brönsted and Lewis) has already been explained in section 1.1. It has been established that the total number and strength of the acid sites can be varied, respectively, by changing the aluminium content and

by isomorphous substitution of Al by Ga and Fe. Acidity of zeolite HY also increases on exchanging with rare-earth cations (RE). The enhanced acidity of RE-Y has been attributed to the formation of new Brönsted acid sites with stronger acid strengths compared to HY *[23]*. In addition, different zeolite structures possessing the same Al content possess different acidities. This difference in acid strength based on zeolite morphology may be attributed to the differences in the Si-O-Al bond angles. The change in acid strength on isomorphous substitution of Al by Ga and Fe and the effect of the Si-O-Al bond angle on the Brönsted acidity has been explained theoretically by the molecular orbital (MO) theory *[24]*. The presence of both types of acidities plays an important role in catalyzing reactions such as cracking, alkylation, isomerization and aromatization.

1.2.3. ADSORPTION

Zeolites attract and hold organic molecules strongly and this property is now being exploited in zeolite-based adsorption systems. The size of the pores in each zeolite structure determines the size of the molecule that can be adsorbed. Thus the diameter of the organic molecule of interest determines the type of zeolite to be used. The polarity of the organic molecules also influences the adsorption properties of the zeolites. The separation of close boiling species, for which distillation is impractical, can now be done by adsorptive processes. For example, adsorptive separation processes are already used for the separation of xylene isomers *[19]* and n-paraffins from kerosene *[25]*. Silicalite-1 (Al free form of ZSM-5) has been found to be a good adsorbent for the separation of cyclohexane from naphtha due to channel diameter being close to the critical diameter of cyclohexane *[26]*. Tantet *et al. [27]* have correlated the adsorption properties of zeolites to their silica to alumina ratio. They showed that the rate of SO_2 adsorption (ml/min.g) increases with increasing silica to alumina ratio of H-ZSM-5. Recently, Richter *et al. [28]* have reported that SAPO-17, with its small

pore opening (3.6 x 5.1 Å), is able to discriminate between the stereoisomeric cis and trans-butenes. Due to their interesting adsorption properties, zeolites can also be used in the removal of pollutants such as n-alcohols from water by selective adsorption *[29]*. A silica analog of NCL-1 has been reported to be useful in the removal of bulkier water pollutants like dimethyl phenols *[30]*.

1.2.4. DIFFUSION

The theory and the role of diffusion in heterogeneous catalysis were developed first by Thiele *et al.[31]* and later on by Wheeler *[32]*. Classically, diffusion in porous materials consist of two main parts: "bulk diffusion" from the gas phase to the external surface of the catalysts and "Knudsen diffusion" inside the pores, whose dimensions are smaller than the mean free path of the gas. In bulk diffusion, molecular translational velocity is proportional to the square root of the temperature and inversely proportional to the square root of the molecular weight of the diffusing molecule. In Knudsen diffusion, a molecule within the pore, on an average, will strike the pore wall more often than it strikes a second molecule. Hence, the Knudsen diffusion coefficient (D_k) $\propto \sqrt{}$ (T/M).r, where M = mol. wt of the diffusing species and r is the radius of the pore. It has been found that a slight difference in configurational structure between cis and trans-butenes causes their diffusion coefficients to differ by more than two orders of magnitude during the diffusion of these two isomers in Ca-A zeolite *[33]*. To explain the diffusional behavior of the two butene isomers, Weisz *et al. [34]* have proposed a new class of diffusion called "configurational diffusion" in zeolites. Here, the diffusion process is affected by the configuration of the molecule as it penetrates the void space of the zeolites. Apparent and intrinsic rate constants of catalytic reactions can be correlated with an effectiveness parameter "η" by using the relation:

$$\eta = \frac{k^{app}}{k^{intr}}$$

where k^{app} and k^{intr} are the apparent and intrinsic 1st order rate constants. The effectiveness parameter, η, can be related to diffusivity (D_{eff}) through the equation *[35]*.

$\eta = (\tanh \varphi) / \varphi$,

The Thiele modulus, φ, is defined as $\varphi = R (k^{intr}/D)^{1/2}$; R is the particle radius.

Diffusion plays an important role in molecular shape selective catalysis and the diffusion process can have a profound effect upon the activity and selectivity of zeolite catalysts.

1.2.5. THERMAL STABILITY

Zeolites, in general, possess high thermal stability compared to other conventional heterogeneous catalysts. Barrer *[2]* has summarized the thermal properties of various zeolites and reported that the thermal stability of the zeolite structure increases with increasing Si /Al atomic ratio *[36]*. Zeolites such as ZSM-5, mordenite and USHY possess high thermal (upto 1283K) and hydrothermal stabilities compared to other catalytically important zeolites *[37,38]*. These properties permit reactions to be carried out in the presence of water vapour and regeneration of the deactivated catalysts at relatively high temperatures.

1.2.6. COKE FORMATION

Catalysts generally deactivate during organic transformation due to the formation of heavy olefinic secondary products (coke) which either strongly adsorb on the active sites or irreversibly block the pores. It has been demonstrated that coking is a shape selective process, the rate of coking and the molecular structure of the coke depending on the composition and the pore structure of the zeolite *[39,40]*. The rate of coking also depends on

the reaction temperature, the nature of the reactant, the reaction pressure and the nature of the added gases (H_2 or N_2) *[41]*. Guisnet *et al. [42]* have studied the nature and the location of the coke in zeolites possessing different channel structures, namely, mordenite, Y and H-ZSM-5. Bulow *et al. [43]* have studied coke deposition on H-ZSM-5 samples of polycrystalline, spherical and polyhedral morphology during n-hexane and mesitylene cracking and have distinguished between intracrystalline and surface coke. They have also demonstrated the influence of intracrystalline and surface coke on the diffusional behavior of guest molecules in the zeolite pore system. It was observed that a partially deactivated surface of ZSM-5 showed a reduction in the pore apertures and channel dimensions, favouring p-xylene formation. This phenomenon is known as coke-induced shape selectivity *[44]*.

Dimon *et al.[45]* have studied the kinetics of coking at various temperatures and at different partial pressures of propene (between 0.33 KPa and 13 KPa) over USHY and H-ZSM-5. They showed that irrespective of the nature of the zeolite, with increasing temperature and the partial pressure of propene, the amount of coke deposited (wt.%) on the catalyst increases rapidly with time and reaches a constant steady state value.

1.3. ISOMORPHOUS SUBSTITUTION

The modification of the zeolite framework by isomorphous substitution produces a new class of zeolites, often possessing catalytic properties different from the parent structural isomorph. The first isomorphous substitution (in the lattice) was reported by Goldsmith *[46]*, who replaced Si by Ge. The isomorphous substitution of ions into the zeolite framework has been reviewed in many articles *[2,47-49]*. The framework T-atoms can be substituted by

other tri, tetra and penta-valent metal ions. To date, many ions, of the metals such as Be, Ga, Fe, B, Cr, Ti, Zr, Sn, Ge, V and P have been introduced into the lattice of different zeolites.

Pauling *[50]* had predicted theoretically the stability of a metal ion in a tetrahedral oxygen surrounding. According to Pauling *[50]*, a metal ion is stable in the framework when ρ (pauling criterion) is in the range $0.414 > \rho > 0.225$, where ρ is defined as $\rho = r_c / r_0$, and r_c is the cationic radius and r_0 is the radius of oxygen. When ρ is out of this range, the substitution is either impossible or it can take place only on a limited scale. However, some metal ions like Fe^{3+}, Ti^{4+}, Ga^{3+} and V^{4+}, for which ρ is out of the criterian range, have been successfully substituted into the zeolite tetrahedral framework *[3,51-53]*.

1.4. ACTIVE SITES

Both Brönsted and Lewis acid sites act as active sites in zeolite catalysis *[54-56]*. Besides, strong electric fields in the small volume within the zeolite channels, arising from the various charged species are believed to create large energy gradients within the pores, affecting the activity and selectivity of the zeolites in many reactions *[57]*.

1.5. CATALYSIS BY ZEOLITES

The use of zeolites as catalysts in industrial processes began in the early 1960s. Since then they have been used in many reactions such as isomerization of xylenes, cracking and hydrocracking of heavy oils, the dewaxing of petroleum oils, methanol to gasoline conversion, olefin oligomerization, isomerization of n-paraffins and alkylation of benzene. Zeolites possess the following properties which often distinguish them from other heterogeneous catalysts *[58]*:

- well defined crystal structure,
- high internal surface area,

- uniform pores of one or more discrete sizes,
- good thermal stability,
- ability to sorb and concentrate reactant molecules,
- shape-selective properties,
- tailoring of acidity of the zeolites through various methods such as changing Si/Al ratio, ion-exchange with rare-earth ions, changing calcination conditions and isomorphous substitution,
- zeolites can also be converted into solid bases through ion-exchange with alkali metal cations such as Cs^+ and Rb^+ *[59]* and by impregnating with sodium azide *[60]* or with cesium acetate *[61]*,
- zeolites can be used as selective oxidation catalysts by substituting early transition metal ions such as V or Ti into their framework *[62]*.

1.5.1. SHAPE SELECTIVITY IN ZEOLITES

The basic concept of shape selectivity has been discussed in detail by many authors *[63-65]*. Recently, Chen *et al. [66]* underlined the impact of shape selective zeolite catalysis in the petroleum and petrochemical industries with a special emphasis on the pentasil family of zeolites. The different types of shape selectivity observed in zeolites are discussed in the following sections.

1.5.1.1. REACTANT SHAPE SELECTIVITY

Reactant shape selectivity occurs when only some of the reactant molecules in the reaction mixture are small enough to diffuse through the zeolite pores and are thus converted to products while the other molecules are excluded. Chen *et al.[67]* have explained reactant shape selectivity on the basis of coulombic interaction between the reactant and the zeolite.

An important application of reactant shape selectivity is in the dewaxing of petroleum oils to lower their "pour point" by selectively cracking the long chain waxy paraffin molecules, while "sieving" out branched molecules which enhance the quality of the lube oils.

1.5.1.2. PRODUCT SHAPE SELECTIVITY

Product shape selectivity occurs when one or more of the products formed within the pores or cavities diffuse out faster than the other products, leaving behind the bulkier molecules which are either converted to less bulky molecules that can diffuse out of the pore network or eventually from coke and deactivate the catalyst *[68]*. Product shape selectivity has been suggested to be responsible for the higher yields of the p-isomer during the isomerization of m-xylene over medium pore zeolites *[69]*.

1.5.1.3. RESTRICTED TRANSITION STATE SHAPE SELECTIVITY

Restricted transition state shape selectivity depends upon the size and shape of the transition state complex formed during catalytic transformations inside the cavities of the zeolite. The products which result from transition states that can be accommodate inside the zeolite pore system are preferentially produced. The resistance of ZSM-5 to deactivation by coke deposition has been attributed to the fact that large "coke molecules" cannot be formed inside the pores due to restricted transition state selectivity. Additionally, the chemical nature of the active sites, the strength of the acid sites and electronic as well as thermodynamic effects have also been found to influence the overall selectivity patterns in certain reactions *[70]*. It has been found that the restricted transition state shape selectivity does not always guide the reaction path in zeolites, but electronic as well as thermodynamic effects predominate over steric effects *[71]*.

1.5.1.4. MOLECULAR TRAFFIC CONTROL

According to this concept, in the case of zeolites with more than one type of intersecting channels, the reactant molecules preferentially enter through one type of channel, while the products diffuse out through the other one, minimizing counter diffusion. Derouane and Gabelica *[72]* explained the concept of molecular traffic control in the conversion of methanol over H-ZSM-5. The smaller reactant molecules (methanol) enter through the sinusoidal circular channels, while the larger product molecules exit from the straight elliptical channel. However, the existence of molecular traffic control is not yet experimentally confirmed.

1.5.1.5. MOLECULAR ORBITAL INDUCED SHAPE SELECTIVITY

Recently, the role of the chemical nature of the reactant in directing selectivity has been interpreted by Corma *et al. [73]* on the basis of Pearson's principle of soft and hard acids and bases (SHAB). The SHAB principle can be extended to show that the energy levels of HOMO and LUMO orbitals play an important role in determining the path of the reaction *[73]*. The principle can also be used to explain the preferential position of attack (ortho, meta, para) of electrophiles on substituted aromatic compounds during electrophilic aromatic substitution and the ortho/para ratios of the products.

1.5.2. COMMERCIAL SHAPE SELECTIVE PROCESSES USING ZEOLITE CATALYSTS

Zeolites are used mainly as cation exchangers (as components in detergents to scavenge Ca^{2+} and/or Mg^{2+} ions), selective adsorbents (in moisture removal from petroleum gases) and as cracking catalysts in the petroleum industry. The combination of acidity, basicity and shape selectivity provides a good opportunity to use these catalysts in many industrial

processes other than in cracking reactions *[66,70,74,75]*. Some major petrochemical processes based on zeolite catalysts are listed in Table 1.1.

1.5.3. ZEOLITES IN THE SYNTHESIS OF FINE CHEMICALS

The pioneering work of Venuto and Landis *[38]* showed that zeolites could be used to synthesize compounds free from undesirable by-products. As the number of zeolite structures have increased and the basic understanding of the acidity and shape selective properties of the zeolites have improved, it has now become possible, by proper tailoring of the acidity and basicity of zeolites, to use them in the synthesis of many fine chemicals. Numerous economically interesting organic reactions, which were hitherto not feasible because of low activity and selectivity of the earlier catalysts, can now be commercially exploited using zeolites. Some of these reactions are discussed in the following sections:

1.5.3.1. CONDENSATION REACTIONS

Condensation reactions are of industrial importance and can be catalyzed by either acids or bases. Accordingly, such reactions represent a suitable area of application for zeolites, since their acidity and basicity can be tailored. For example, β-substituted pyridines can be synthesized by the reaction of acrolein and an alkanal with ammonia over boron containing zeolites *[91]*.

1.5.3.2. ELECTROPHILIC AROMATIC SUBSTITUTION

Zeolite-catalyzed, aromatic alkylation is well established as testified by the numerous patents and papers on the alkylation of aromatic compounds. Industrial examples include the Mobil-Badger process for ethyl-benzene and the ethylation of toluene over a modified H-ZSM-5 catalyst to yield selectively the p-isomer. Zeolite- catalyzed, Friedel-Craft acylation of aromatic compounds like benzene, toluene and naphthalene have been reported over RE-Y

Table 1.1

Commercial process based on zeolites (announced / in operation)

Name of the process	Catalyst used	Purpose	Developed by
Selecto-forming	Erionite	Octane boosting	Mobil *[76]*
M-forming	ZSM-5	-do-	-do- *[77]*
MDDW (Mobil Distillate Dewaxing)	ZSM-5	Distillate dewaxing	-do- *[78]*
MLDW (Mobil Lube oil Dewaxing)	ZSM-5	Lube dewaxing	-do- *[80]*
M2-forming	ZSM-5	Light hydrocarbons to aromatics	-do- *[81]*
Aroforming	Ga-ZSM-5	LPG to aromatics	Salutec (Australia) IFP (France) *[82]*
Cyclar Process	-do-	-do-	BP-UOP *[83]*
MOGD (Mobil Olefins to Gasoline and Diesel)	ZSM-5	Olefins to gasoline and aromatics	Mobil *[83]*
MTG (Methanol to Gasoline)	-do-	Methanol to gasoline	-do- *[84]*
MTO (Methanol to Olefins)	-do-	Methanol to olefins	-do- *[85]*
MVPI (Mobil Vapour Phase Xylene Isomerization)	-do-	Xylene isomerization	-do- *[86]*
MHTI (Mobil High Temperature Xylene Isomerization)	-do-	-do-	-do- *[86]*
MTDP (Mobil Toluene Disproportionation)	-do-	Toluene disproportionation	-do- *[87]*
Albene	-do-	Ethylbenzene synthesis	NCL (India) *[88]*
Cumene Synthesis	Beta	Cumene synthesis	-do- *[89]*
PDEB (Para Diethylbenzene)	Modified ZSM-5	Synthesis of para-diethylbenzene	-do- *[90]*

zeolites. Recent studies have shown that H-beta is also a promising catalyst for the acylation of aromatic hydrocarbons *[92-94]*, it produces selectively β-benzoyl-naphthalene during the benzoylation of naphthalene *[94]*. TS-1 *[95]*, TS-2 *[96]*, VS-1 *[97]*, VS-2 *[98]* and other Ti or vanadium containing zeolites are active in the hydroxylation of toluene, phenol and anisole.

1.5.3.3. RING TRANSFORMATION REACTIONS

Ring transformation reactions are a class of reactions in which the heteroatom in a cyclic carbonyl compound is exchanged by another heteroatom. Such exchange reactions are, in some cases, catalyzed by bases and in others, by acids. For example, tetrahydrofuran reacts with NH_3 on acidic boron zeolites to yield pyrrolidine *[99]*.

1.5.3.4. SYNTHESIS OF PHARMACEUTICAL INTERMEDIATES

Zeolites have been found to be effective in the synthesis of pharmaceutical intermediates. For example, HX and HY zeolites have been used as disproportionation catalysts to convert ortho and/or meta-isobutylbenzenes into p-isobutylbenzene *[100]*. The latter is dehydrogenated in another step to produce p-isobutylstyrene, an intermediate in the manufacture of α-(4-isobutylphenyl) propionic acid (Ibuprufen).

1.6. PENTASIL ZEOLITES

The generic name "Pentasil zeolites" was proposed by Kokotailo and Meier *[101]* to designate the group of structures having 5-1 secondary building units. The secondary building units are linked through edges to form chains and these chains are connected to form sheets which in turn link to form a three dimensional framework. ZSM-5, ZSM-22, ZSM-48 and EU-1 belong to the pentasil family, but due to the differences in their secondary building unit, framework density and different Si-O-Si bond angles, they form different types of structures. A comparison of the four zeolites has been made (see below) on the basis of SBU, framework density, symmetry of point group, unit cell volume and channel characteristics.

TH-1057

RR
66·097·3:661·183·6(043)
BHA

1.6.1. ZSM-5

ZSM-5 is a member of the pentasil family with its SBU made up of eight 5-membered rings (Fig. 1.2a). These SBUs can be linked to form chains as shown in Fig. 1.2b. The combination of these building units results in a framework containing two intersecting channel systems, one sinusoidal and the other one straight. The elliptical, 10-membered ring (MR) apertures are the entrances to straight channels. The nearly circular 10-membered ring apertures are the entrance to the sinusoidal channels. In ZSM-5, the straight channels have a diameter about 5.3 x 5.6 Å and sinusoidal channels about 5.1 x 5.5 Å *[102]*.

Chemical composition	$Na_n[Al_nSi_{96-n}.O_{196}] \sim 16H_2O$
Symmetry	Orthorhombic
Framework density	17.9 T / 1000 $Å^3$
Unit cell constants	a = 20.1 Å
	b = 19.9 Å
	c = 13.4 Å
Unit cell volume	5345.6 $Å^3$
Pore structure	[010] **10** MR; 5.3 x 5.6 Å, [100] 5.1 x 5.5 Å, (two channels are interconnecting and three dimensional).

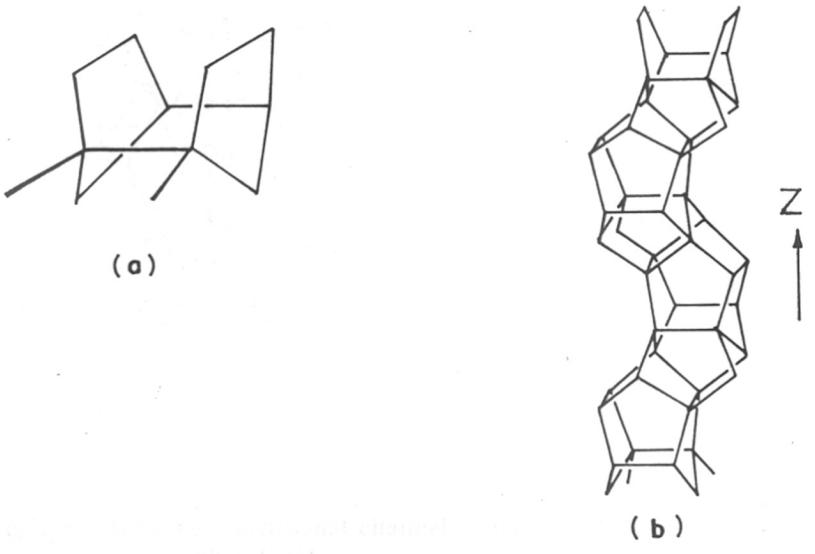

Fig. 1.2. **Building units in ZSM-5: (a) secondary building unit; (b) chain building unit *[102]*.**

1.6.2. ZSM-22

ZSM-22 is a high silica zeolite with orthorhombic symmetry with its SBU made up of repeated connections of a 6-ring. The structure contains ferrierite sheets. The channel system is linear with openings constituted by 10-membered rings which are parallel to the c-axis and has a maximum and a minimum diameter of 5.5 and 4.5 Å (Fig. 1.3a & 1.3b) *[103].*

Chemical composition	$Na_n[Al_nSi_{24-n}O_{48}] \sim 4H_2O$
Symmetry	Orthorhombic
Framework density	19.7 T / 1000 $Å^3$
Unit cell constants	a = 13.86 Å
	b = 17.41 Å
	c = 5.04 Å
Unit cell volume	1220.3 $Å^3$
Pore structure	[001] **10** MR; 4.4 x 5.5 Å, (one dimensional)

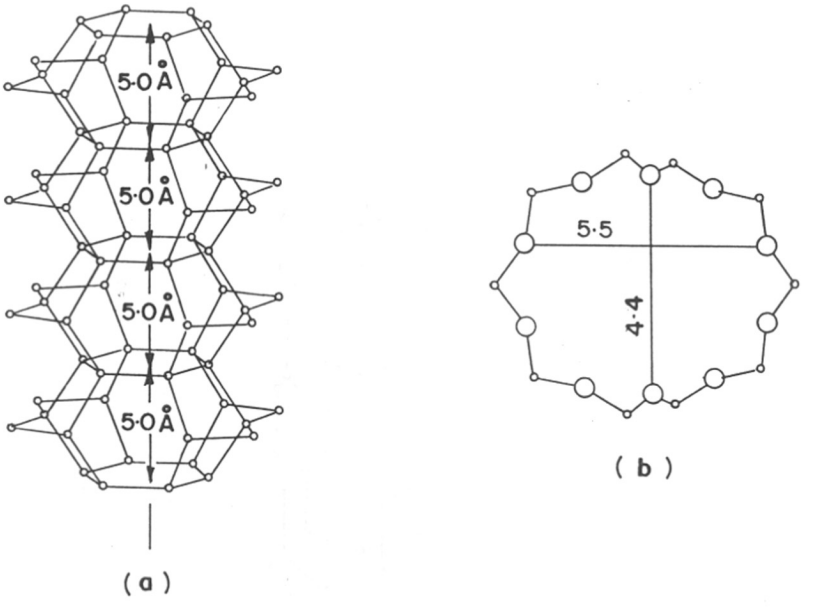

Fig. 1.3. (a) One dimensional channel system in ZSM-22; (b) 10-ring viewed along <001> *[103].*

1.6.3. ZSM-48

ZSM-48 is a high silica zeolite with orthorhombic or pseudo-orthorhombic symmetry. It has a framework structure consisting of ferrierite sheets linked via bridging oxygen located on the mirror plane. ZSM-48 has a 10-ring pore structure with 6-ring windows (Fig. 1.4). The channel dimensions are 5.3 x 5.6 Å *[104].*

Chemical composition	$Na_n[Al_nSi_{48-n}O_{97}] \sim 6H_2O$
Symmetry	Orthorhombic
Framework density	19.7 T / 1000 Å
Unit cell constants	a = 14.24 Å
	b = 20.14 Å
	c = 8.40 Å
Unit cell volume	1703.55 $Å^3$
Pore structure	[001] **10** MR; 5.3 X 5.6 Å, (one dimensional).

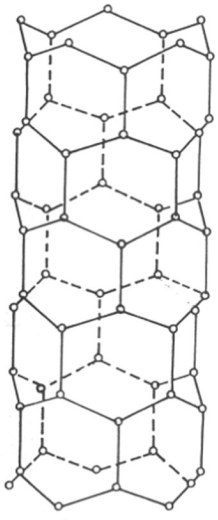

Fig. 1.4. **10-ring channel structure in ZSM-48** ***[104].***

1.6.4. EU-1

EU-1 is a member of the pentasil family with its SBU made up of one 4-membered ring and four 5-1 membered rings. The structure of EU-1 consists of unidimensional channels with 10-T windows having dimensions 5.7 x 4.1 in the [100] plane. However, there are side pockets off these channels of cross section 6.8 x 5.8 Å and 8.1 Å deep (Fig. 1.5a and 1.5b). These side pockets are present in the [001] direction, with respect to the channel direction *[105]*.

Chemical composition	$Na_n[Al_nSi_{112-n}O_{224}] \sim 26H_2O$
Symmetry	Orthorhombic
Framework density	18.2 T / 1000 $Å^3$
Unit cell constants	a = 13.74 Å
	b = 22.33 Å
	c = 20.18 Å
Unit cell volume	6173.5 $Å^3$
Pore structure	[100] **10** MR; 4.1 x 5.7 Å (6.8 x 5.8 Å, pocket 8.1 Å deep; one dimensional).

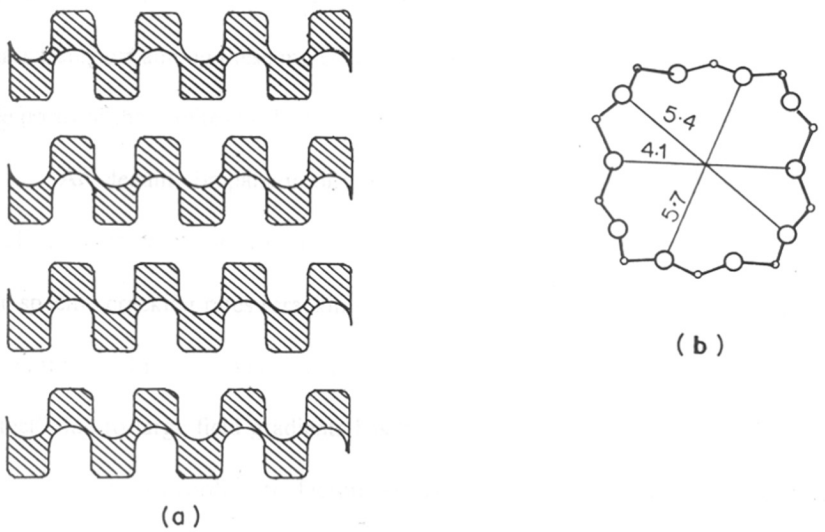

Fig. 1.5. **Schematic of the channel/side pocket network in EU-1: (a) the channels run in the <100> direction and the side pocket in <001> directions off these; (b) 10-ring viewed along <100> *[105]*.**

1.7. CRACKING OF ALKANES

The first major industrial application of zeolites as catalysts was in the catalytic cracking of heavy petroleum oils (FCC). Along with the development of cracking catalysts, fundamental studies on the cracking of various model hydrocarbons over different catalysts have been in progress to understand the mechanism of cracking reactions. A number of reviews on the cracking of model hydrocarbons over zeolites have been published in recent years *[35,106,107]*. Haag *et al. [35]* have showed that in the cracking of linear alkanes, reactivity increases with increasing chain length. The ratio of initial cracking rates of nonane to hexane over Pt-Ca-Y is about 8.5 *[106]* . This ratio is however much less on ZSM-5 (3.2) *[36]*. Based on the studies of the cracking of normal and branched alkanes over ZSM-5 of different crystallite sizes, Haag *et al. [35]* have proposed the formation of transition state complexes during the cracking of paraffin molecules. They have observed that the differences in the initial rate constants in paraffin cracking are not caused by the differences in diffusional mass transport among these molecules but are mainly due to differences in steric inhibition (in the pores of the zeolite) to the formation of the intermolecular transition state complexes.

An elegant comparison of the activities of a number of small, medium and large pore zeolites in the cracking of n-pentane has been made by Derouane *[108]*. He has found that the specific cracking rates (cracking activity per Al^{3+} ion) is highest for the pentasil zeolites. Even the small pore erionite has a larger cracking activity than Y. The operation of a "nest effect" due to large field gradients has been attributed to the greater activity of the medium pore zeolites. According to Derouane *[108]*, the adsorbed molecules, depending on their ability to form a "nest". Adsorption (or activity) will be favoured for the molecules (or intermediates) which can easily adopt this geometry. Besides, the strength of the acid centers

in small and medium pore zeolites with higher silica / alumina ratios is greater than in the other zeolites, leading to larger activities.

Several hypotheses for the initiation step in catalytic cracking of paraffins have been made by several authors *[109-112]*. According to one mechanism, carbonium ions are formed by the abstraction of hydride ions from a saturated hydrocarbon by strong Lewis acid sites (tricordinated Al species) *[113-115]*. On Brönsted sites, a carbonium ion may readily formed from an olefin by the addition of a proton to the double bond or, more rarely, via abstraction of a hydride ion from a paraffin molecule by a strong Brönsted proton. The latter process leads to the formation of hydrogen as an initial product *[116,117]*, though for many years the role of Brönsted acid sites in H-abstraction during paraffin cracking was often neglected. It is now accepted that the initiating step in the cracking of paraffins is the protolysis of a molecule by a strong Brönsted acid on the catalyst surface *[118]*. Paraffin molecules are protonated by the Brönsted acid sites to form a carbonium ion. This carbonium ion then decomposes to form either hydrogen and a paraffin carbenium ion or into a smaller paraffin and a small carbenium ion. Depending on the probability of the various steps, the carbenium ion can desorb as an olefin or participate in bimolecular chain reactions. Corma *et al.[119]* and Wielers *et al.[120]* experimentally verified the possibility of bimolecular processes during n-butane and n-hexane cracking respectively. The chain transfer process involves the rearrangement of an adsorbed carbonium ion through hydride transfer from the feed molecule. By this process, isomeric paraffins are formed. In the chain termination step, carbenium ions desorb from the catalyst surface as olefins after β-scission or remain on the surface to form coke.

1.8. AROMATIZATION PROCESS

The transformation of lower hydrocarbons (C_2-C_6) into aromatics is an industrially important process. ZSM-5 is known to be an excellent catalyst for the aromatization of lower hydrocarbons *[80-82, 121,122]*. Many commercial processes such as Cyclar *[82]*, M-2-forming *[80]*, Aroforming *[81]* are based on ZSM-5. Aromatics selectivity of ZSM-5 can further be improved by introducing promoters such as Ga, Zn and Pt *[121-124,]*. However, the mechanism of the activation of lower alkanes and the role of the metal cations in the aromatization have not been well established. Mole *et al. [122]* have studied the conversion of propane over H-ZSM-5 and concluded that propane activation occurs through the abstraction of a hydride ion. However, Shibata *et al.[125]* and Ono *et al. [121]* have reported that the initial step in the activation of propane by H-ZSM-5 involves the formation of penta cordenated carbonium ions by reaction with Brönsted acid sites. The formation of carbonium ions during lower hydrocarbon transformation has also been suggested by Haag and Dessau *[126]*. It is now accepted that the initial step during the aromatization of lower hydrocarbons is the protonation of hydrocarbon molecules by strong Brönsted acid sites on the catalyst surface *[126]*. Meriaudeau *et al. [127]* have proposed the following sequence of steps in the aromatization of propane over H-ZSM-5:

- Protonation of propane produces a carbonium ion of the formula $C_3H_9^+$, which after cracking and dehydrogenation produces ethane, methane and propene respectively.
- Formation of higher alkenes by oligomerization.
- Cyclization through internal alkylation of the mono-olefins to form alkyl-cyclohexanes or diolefins, produced from hydride transfer reactions to form alkyl-cyclohexenes.
- Aromatization by hydride transfer between cyclic hydrocarbons and olefins.

- Additional cracking of the oligomers occurs during the process of aromatization.

Over Ga or Zn promoted H-ZSM-5, alkanes undergo direct abstraction of a hydrogen atom (or ion) to form olefinic species, which oligomerize over acidic sites to form olefin oligomers. These olefin oligomers further dehydrogenate over metallic (oxidic) sites to form allylic species such as dienes and trienes *[127]*. At high temperatures, trienes are rapidly cyclized into cyclohexadienes. Alternatively, the protonation of the dienes results in the formation of olefinic carbonium ions which undergo intramolecular double bond alkylation subsequently forming 5 and 6-ring cycloalkenes *[127]*. The dehydrogenation of the olefinic oligomers into dienes during aromatization over Ga and Zn promoted H-ZSM-5, has also suggested by Ono *et al. [128]* and Kanai *[129]*. Finally, over Ga/H-ZSM-5 (Zn/H-ZSM-5), aromatics are formed by dehydrogenation of cyclohexenes and cyclohexadienes over the metal oxide component *[127]*.

Meriaudeau *et al. [127]* have studied the aromatization of n-hexane over H-ZSM-5 and Ga/H-ZSM-5 at low pressures and at low contact times to observe the primary kinetic products. At these reaction conditions H-ZSM-5 produced almost exclusively cracked products, whereas over Ga/H-ZSM-5 the main products were propene and benzene. Rapid dehydrogenation of n-hexane over Ga/H-ZSM-5 into hexadiene and hexatriene which could easily form cyclohydrocarbons by intramolecular alkylation catalyzed by H^+ has been suggested to explain the differences between H-ZSM-5 and Ga/H-ZSM-5 *[127]*.

A knowledge of the interplay between the acidic and dehydrogenating catalytic functions is thus of key importance in understanding the behavior of aromatization catalysts. Such information is vital for the design of catalysts with optimal activity, selectivity and long life.

1.9. SCOPE OF THE THESIS

In the preceding sections, the properties of zeolites with special reference to their shape selectivity, acidity, framework structure and their application in industrial catalytic processes were reviewed. It was noted that ZSM-5 has many advantages over others in hydrocarbon transformation reactions due to its high acidity and optimal pore geometry. In fact, many novel petrochemical processes based on ZSM-5 have become possible due to the above mentioned properties.

It has been found that the addition of a small amount of ZSM-5 to cracking catalysts increases the octane rating of FCC gasoline, through selective cracking of the low octane n-paraffin components *[130]*. Chester *et al. [131]* have reported that besides ZSM-5, other zeolites such as ZSM-11, ZSM-12, ZSM-23, ZSM-35 and ZSM-38 also possess octane boosting capability. *It should, therefore, be interesting to study the cracking activity of another medium pore zeolite ZSM-48.* Recently, kinetic and mechanistic studies of the cracking of C_6-paraffins carried out on H-Y and other large-pore zeolites have indicated that the cracking of these molecules follow both protolytic and chain reaction modes *[132-135]*. So far, most of the kinetic studies on the cracking of paraffins available in the literature have been carried out over large pore zeolites and detailed kinetic studies of paraffin cracking over medium pore zeolites are scarce. *It is therefore be useful to examine in detail the mechanism of n-hexane cracking over H-ZSM-48.*

In early works, Csicsery *[136-139]* has described the dehydrocyclodimerization of lower hydrocarbons over bifunctional catalysts such as Pt on alumina or Cr_2O_3 on alumina. It was established that dehydrocyclodimerization reactions proceed through the formation of olefins in the intermediate step. Csicsery *[138]* showed that more C_5-C_8 olefins and

naphthenes and less bi and poly-cyclic aromatics are formed over alumina and silica-alumina than over catalysts containing a dehydrogenation component. As the amount of bi and poly-cyclic aromatics and naphthenes increased, the coke content of the catalysts also increased. So frequent regenerations were required, thereby reducing the initial activities of these catalysts. Recent studies have revealed that zeolites also possess very good aromatization activity. Among the zeolites studied so far, ZSM-5 has been found to be an excellent catalyst for the aromatization of lower hydrocarbons. The excellent aromatization activity of ZSM-5 may be due to its optimum pore structure and high acidity. In this context it is interesting to compare the performance of other medium pore high-silica zeolites with different pore structures and acidities. The aromatization activity of ZSM-5 can be further increased by introducing promoters such as Ga, Zn and Pt *[121-124]*. Metal oxides such as, Ga_2O_3 and ZnO improve the aromatization activity, but these catalysts deactivated rapidly for various reasons. *It is therefore interesting to study in detail the againg characteristics of these catalysts, especially at different process conditions.* Such data are not available in the literature. *Again, as most early studies have been carried out over model hydrocarbons, it is again interesting to study the aromatization of a typical commercial feedstock containing mixtures of different hydrocarbons.*

The main objective of this thesis is to study the cracking and aromatization of lower hydrocarbons (C_4 - C_6) over different medium pore high-silica zeolites.

Synthesis and characterization of the catalysts used in this study are reported in Chapter II. The different experimental techniques adopted for the reactions are also presented in Chapter II.

The influence of different process parameters, SiO_2/Al_2O_3 molar ratio, size of the hydrocarbons and isomorphous substitution of Al by Ga and Fe have been investigated for the cracking of n-hexane over ZSM-48. The kinetic reaction modelling of n-hexane cracking has also been studied over ZSM-48. All these results are reported in Chapter III.

In Chapter IV, a comparative study of the aromatization of C_4 and C_6 hydrocarbons carried out over three medium pore zeolites, ZSM-5, ZSM-22 and EU-1 is presented. The deactivation characteristics of the three zeolites in the presence of added gas such as H_2 and N_2 have been compared. Both the product yield and the deactivation characteristics of Ga, Zn, Cr and Fe promoted H-ZSM-5 catalysts have been studied during n-hexane aromatization. The influence of different process parameters on the aromatization of n-hexane has been investigated. Aromatization of a commercial light raffinate feed has also been studied over H-ZSM-5 based catalysts.

A summary of the present investigation and the conclusions made have been presented in Chapter V.

References

1. Wilkinson, S., and Hunter, D., *Chem. Week*, 24 (1989).
2. Barrer, R. M., "Hydrothermal Chemistry of Zeolites", Academic Press., New York (1982).
3. Szostak, R., in "Molecular Sieves, Principles of Synthesis and Identification", Van Nostrand Reinhold Catalysis Series, New York (1989).
4. Loewenstein, W., *Am. Minerals*, **39,** 92 (1954).
5. Meier, W. M., in "Molecular Sieves", Society of Chem. Industry, London (1968).
6. Sand, L. B., *Econm. Geol.*, (1967) 191.
7. Flanigen, E. M., *Pure and Applied Chemistry,* **52,** (8) 2191 (1980).
8. Dewkenewieg, R. P., *J. Material Edn.*, 9(5), 518 (1989).
9. Barrer, R. M., and Hinds, L., *J. Chem. Soc. Chem. Commun.*, 1879 (1953).
10. Barrer, R. M., Davis, J. A., and Rees, L. V. C., *J. Inorg. Nucl. Chem.*, **31,** 2599. (1969).
11. Barrer, R. M., Bartholamew, R. F., and Rees, L. V. C., *J. Phys. Chem.*, **24,** 309 (1963).
12. Rees, L. V. C., and Rao, A., *J. Chem. Soc. Faraday. Trans.*, **62,** 2103 (1970).
13. Sherry, H. S., *J. Phys. Chem.*, **72,** 4068 (1968).
14. Sherry, H. S., *J. Collid. Interface. Sci.*, **28,** 218 (1968).
15. Sherry, H. S., in "Molecular Sieve Zeolites - 1", Adv. Chem. Ser., **101,** 350 (1971).
16. Vansant, E. F., *Stud. Surf. Sci. Catal.*, **37,** 143 (1988).
17. Rees, L. V. C., *Stud. Surf. Sci. Catal.*, **46,** 661 (1989).
18. Breck, D. W., Eversole, W. G., Milton, R. M., Reed, T. B., and Thomas, T. L., *J. Am. Chem. Soc.*, **78,** 5963 (1956).
19. Johnson, J. A., and Oroskar, P. B., *Stud. Surf. Sci. Catal.*, **46,** 451 (1989).
20. Magee, J. S., and Blazek, J. J., in "Zeolite Chemistry and Catalysis", (J. A. Rabo, Eds.), p. 625, ACS, Washington, DC (1976).
21. Vaughan, D. E. W., in "Properties and Applications of Zeolites" (R. P. Townsend), p. 294, The Chemical Society, London (1980).
22. Weitkamp, J., *Chemic-Technik*, **11,** 707 (1982).
23. Herreros, B., Man, P. P., Manoli, J. M., *J. Chem. Soc. Chem. Commun.*, 464 (1992).
24. Barthomeuf, D., *Stud. Surf. Sci. Catal.*, **37,** 365 (1987).

25. Meyers, R. A., "Hand book of Petroleum Refining Process", p. 236, McGrew Hill, New York, NY, 1986.
26. Cavalcante, C. L., and Ruthven, D. M., *Stud. Surf. Sci. Catal.*, **84,** 1209 (1994).
27. Tantet, J. E. M., and Desai, R., *Stud. Surf. Sci. Catal.*, **84,** 1269 (1994).
28. Richter, M., Roost, U., and Lohse, U., *J. Chem. Soc. Chem. Commun.*, 1616 (1993).
29. Milestone, N. B, and Bibby, D. M., *J. Chem. Tech. Biotech.*, **31,** 732 (1981).
30. Reddy, K. R., *J. Chem. Soc. Chem. Commun.*, 559 (1993).
31. Thiele, E. W., *Ind. Eng. Chem.*, **31,** 916 (1939).
32. Wheeler, A., "Advance in Catalysis and Related Material", **3,** 249 (1951).
33. Chen, N. Y., and Weisz, P. B., *Chem. Eng. Progr. Symp. Ser.*, **63,** 86 (1967).
34. Weisz, P. B., *Chemtech*, **6,** 498 (1973).
35. Haag, W. O., Lago, R. M., and Weisz, P. B., *Faraday Discussion.*, **72,** 317 (1982).
36. Kuhl, G. H., *J. Catal.*, **29,** 270 (1973).
37. Nayak, V. S., and Choudary, V. R., *Appl. Catal.*, **10,** 137 (1984).
38. Venuto, P. B., and Landis, P. S., *Adv. Catal.*, **18,** 269 (1968).
39. Rollmann, L. D., and Walsh, D. E., *Adv. Catal.*, **56,** 139 (1979).
40. Derouane, E. G., Lonelik, B., Naccache, C., Coudurier, G., Ben Taarit, Y., and Vedrine, J. C., *Stud. Surf. Sci. Catal.*, **20,** 221 (1985).
41. Bhattacharya, D., and Sivasanker, S., *Appl. Catal.*, **141,** 105 (1996).
42. Guisnet, M., and Magnoux, P., *Appl. Catal.*, **54,** 1 (1989).
43. Bulow, M., Caro, J and Volter, J., *Stud. Surf. Sci. Catal.*, **34,** 434 (1983).
44. Kaeding, W. W., and Young, L. B., U.S. Pat., 4,034,053 (1977).
45. Dimon, B., Cartraud, P., Magnoux, P., and Guisnet, M., *Appl. Catal.*, **101,** 351 (1993).
46. Goldsmith, J. R., *Min. Mag.*, **29,** 952 (1952).
47. Ione, K. G., and Vostrikova, L. A., *Russ. Chem. Rev.*, **56,** 231 (1987).
48. Ione, K. G., Vostrikova, L. A., and Mastikhin, V. M., *J. Mol. Catal.*, **31,** 355 (1985).
49. Taramasso, G., Perego, G., and Notari, B., in "Proc. 5th Int. Zeolite. Conf.", Napoli, (L. V. C. Rees, Eds.), p. 40, Heyden, London, 1980.
50. Pauling, L., in "The nature of the Chemical Bond", Goskhimizdat, Moscow, 1947.
51. Taramasso, M., Perego, G., and Notari, B., US. Pat., 4410501 (1983).
52. Naccache, C., and Ben. Tarrit, Y., in "Zeolite Science and Technology", (F R.

Ribeiro, A. E. Rodrigues, L. D. Rollmann, and C. Naccache, Eds.), p. 373, Martinus, Nijhoff (1984).

53. Kornatowski, J., Sychev, M., Goncharuk, V., and Baur, W. H., *Stud. Surf. Sci. Catal.*, **65** (1991) 581.

54. Vedrine, J. C., Auroux, A., Coudurier, G., "Catalytic Materials: Relationship between Structure and Reactivity", American Chemical Society, p. 253, Washington, DC (1984).

55. Barthomeuf, D., "Molecular Sieves-II", American Chemical Society, p. 453, Washington, D.C. (1977).

56. Kramer, G. M., McVicker, G. B., and Ziemiak, J. J., *J. Catal.*, **92,** 355 (1985).

57. Mirodatos, C., and Barthomeuf, D., *J. Catal.*, **93,** 246 (1985).

58. Jacobs, P. A., and Von Ballmoos, R., *J. Phys. Chem.*, **86,** 3050 (1982).

59. Chen, N. Y., and Degnan, J. F., *Chem. Eng. Progr.*, **84,** 32 (1988).

60. Yashima, T., Sato, K., Hayasaka, T., and Hara, N., *J. Catal.*, **26,** 303 (1972).

61. Marleus, L. R. M., Grobet, P. J., and Jacobs, P. A., *Nature*, **315,** 568 (1985).

62. Hathaway, P. E., and Davis, M. E., *J. Catal.*, **116,** 263 (1989).

63. Chen, N.Y., and Weisz, P. B., *Chem. Eng. Progr. Symp. Ser.*, **63,** 86 (1967).

64. Csicsery. S. M., *ACS. Monograph*, **171,** 680 (1976).

65. Derouane, E. G., "Interrelation Chemistry" (M.S. Whittingham and A. J. Jacobson, Eds.), p. 101, Academic press, New York,1982.

66. Chen, N. Y., in "Shape Selective Catalysts in Industrial Applications", Marcel Dekker, Inc., New York, 1989.

67. Chen, N. Y., and Garwood. W. E., *Catal. Rev. Sci. Eng.*, **28,** 1 (1986).

68. Weisz, P. B., *Stud. Surf. Sci. Catal.*, **7A,** 3 (1981).

69. Dewing, J., *J. Mol. Catal.*, **27**, 25 (1984).

70. Lerchert, L., *React. Kinet. Catal. Lett.*, **46**, 153 (1992).

71. Weisz, P. B., Frilette, V. J., Matman, R. W., and Momer, E. B., *J. Catal.*, **1,** 307 (1962).

72. Derouane, E. G., and Gabelica, Z., *J. Catal.*, **65,** 486 (1980).

73. Corma, A., "Guidlines of Mastering the Properties of Molecular Sieves" NATO series. p 221.

74. Heineman, H., *Catal. Rev. Sci. Eng.*, **23,** 315 (1981).

75. Wu, E. L., Landolt, G. R., and Chester, A. W., *Stud. Surf. Sci. Catal.*, **28,** 547 (1986).

76. Chen, N. Y., Maziuk, J., Schwartz, A.. B., and Weisz, P. B., *Oil and Gas J.*, **66** (47), 154 (1968).

77. Heineman, H., *Catal. Rev. Sci. Eng.*, **15,** 53 (1977).

78. Chen, N. Y., Gorring, R. l., Irelard, H. R., and Stein, T. R., *Oil and Gas J.*, **75** (23), 165 (1977).

79. Smith, K. W., Starr, W. C., and Chen, N. Y., *Oil and Gas J.*, **78** (21), 75 (1980).

80. Chen, N. Y., and Yan, T. Y., *Ind. Eng. Chem. Process. Des. Dev.*, **25,** 151 (1986).

81. Guisnet, M., and Gnep, N. S., *Appl. Catal.*, A: General, **89,** 1 (1992).

82. Johnson, J. A., Weiszmann, J. A., Hilder, G. K., and Hall, A. H. P., paper presented at the 1984 NPRA Annual Meeting, March 25-27, 1984, San Antonio, TX.

83. Tabak, S. A., Krambeck, F. J., and Garwood, W. E., "Conversion of Propylene and Butylene over ZSM-5 Catalyst" paper presented at the AlChE meeting, San Francisco, Nov., 25-30, 1984 ; AlChE. J., 32 (1986) 1526.

84. Kam, A. Y., Schreiner, C and Yurchak, S., "Handbook of Synfuels Technology" (R.A. Meyers, Eds.), p. 2, Mcgrew Hill., New York, (1984).

85. Gould, R. M, Avidam, A. A, Sato, J. L., Chang, C. D., and Socha, C. J., paper presented at the AlChE. Nat. meeting. New Orleam, Apr., 6-10, 1986.

86. Haag, W. O., and Olson, D. H., U.S. Pat. 3856871, Dec. 24, 1974.

87. Olson, D. H., and Haag, W. O., *Am. Chem. Soc. Symp. Ser.*, **248,** 275 (1984).

88. Saikh, R. A., Rao, B. S., Balkrishnan, I., and Ratnasamy, P., Indian Patent., application, 56/DEL/1992.

89. Pradhan, A. R., Rao, B. S., and Ratnasamy, P., Indian Patent., application, 1169/DEL/1988.

90. Rao, B. S., Saikh, R. A., Balkrishnan, I., and Ratnasamy, P., Indian Patent., application, 119/DEL/1994.

91. Hoelderich, W. F., in Proc. Int. Symp on Catalysts, "Sorbent and Detergent Builders", Wurzburg, FRG, 1988, p. 193, Elsevier, Amsterdam (1989).

92. Singh, A. P., and Bhattacharya, D., *Catal. Lett.*, **32,** 327 (1995).

93. Singh, A. P., Bhattacharya, D., and Sharma, S., *J. Mol. Catal.*, **102,** 139 (1995).

94. Bhattacharya, D., Sharma, S., and Singh, A. P., *Appl. Catal.*, (in press).

95. Perego, G., Bellussi, G., Corno, L., Taramasso, M., Buonomo, F., and Esposito, A., *Stud. Surf. Sci. Catal.*, **28,** 129 (1986).

96. Thangaraj, A., Kumar, R., and Ratnasamy, P., *Appl. Catal.*, **58,** L1(1990).

97. Rigutto, M. S., and Bekkum, H. van., *Appl. Catal.*, **68,** L1 (1991).

98. Rao, P. R. H. P., Ramaswamy, A. V., and Ratnasamy, P., *J. Catal.*, **137,** 225 (1992).

99. Ono, Y., Hatada, K., Fujita, K., Halgeri. A., and Keii, T., *J. Catal.*, **41,** 322 (1976).

100. Shiznizu, I., Matsumura, Y., Tokumoto, Y., Uchida, K., Eur. Patent., 0373,362 (1990).

101. Kokotailo, G. T., and Meier, W. M., in "The Properties and Applications of Zeolites", (R.P. Townsend, Eds.), p. 133, The Chemical Soc. London, (1979).

102. Olson, D. H., Kokotailo, G. T., Lawton, S. L., and Meier, W. M., *J. Phys. Chem.*, **85,** 2238 (1981).

103. Kokotailo, G. T., Schlenker, J. L., Dwyer, F. G., and Valyocsik, E. W., *Zeolites*, **5,** 349 (1985).

104. Schlenker, J. L., Rohrbaugh, W. J., Chu, P., Valyocsik, E. W., and Kokotailo, G. T., *Zeolites*, **5,** 355 (1985).

105. Briscoe, N. A., Johnson, D. W., Shannon, M. D., Kokotailo, G. T., and McCusker, L. B., *Zeolites*, **8,** 75 (1988).

106. Hedden, K., and Weitkamp, J., *Chemie-ing-Techn.*, **47,** 505 (1975).

107. Weitkamp, J., *ACS Symp. Ser.*, **20,** 1 (1975).

108. Derouane, E. G., *J. Catal.*, **100,** 541 (1986).

109. Bandeira, J., and Ben, Taarit, Y., *Appl. Catal.*, **62,** 309 (1990) 309.

110. Abbot, J., *J. Catal.*, **123,** 383 (1990).

111. Planelles, J., Sanchez-Marin, T., Thomas, F., and Corma, A., *J. Chem. Soc. Perkin Trans.*, **2,** 333 (1985).

112. Abbot, J., *Appl. Catal.*, **57,** 105 (1990).

113. Tung, S. E., and McIninch, *J. Catal.*, **10,** 166 (1968).

114. Nace, D. M., *Ind. Eng. Prod. Res. Dev.*, **8,** 31 (1969).

115. Borodzinski, A, Corma, A., and Wojciechowski, B. W., *Can. J. Chem. Eng.*, **58,** 219 (1980).

116. Janardhan, P. B., and Rajeswari, R., *Ind. Eng. Prod. Res. Dev.*, **16,** 52 (1977).

117. Gates, B. C., Katzer, J. R., and Schuit, G. C. A., "Chemistry and Catalytic

118. Abbot, J., and Wojciechowsk, B. W., *Can. J. Chem. Eng.*, **66,** 825 (1988).
119. Corma, A., Miguel, J., and Orchilles, A. V., *J. Catal.*, **145,** 171 (1994).
120. Wielers, A. F. H., Var Kamp, M., and Post, M. F. M., *J. Catal.*, **127,** 51 (1991).
121. Ono, Y., *Catal. Rev.-Sci.Eng.*, **34,** 179 (1992).
122. Mole, T., Anderson, J. R., and Creer, G., *Appl. Catal.* **17,** 141 (1985).
123. Kanai, J., and Kawata, N., *Appl. Catal.*, **55,** 115 (1989).
124. Kanai, J., and Kawata, N., *J. Catal.*, **144,** 284 (1988).
125. Shibata, M., Kitagawa, H., Sendoda, Y., and Ono, Y., "New Development in Zeolite Science and Technology", (Y. Murakami, A. Iijima, J.W. Ward Eds.), p. 717, Kodansa, Elsevier, Tokyo, Amsterdam, 1986.
126. Haag, W. O., and Dessau, R. M., in Proc. of 8th Int. Congr. Catal., Berlin, Dechema, Frankfurt, 1984, vol 2, p 305.
127. Meriaudeau, P., Sapaly, G., and Naccache, C., *Stud. Surf. Sci. Catal.*, **60,** 267 (1990).
128. Ono, Y., Nakatami, Y., Kitagawa, H., Suzuki, E., *Stud. Surf. Sci. Catal.*, **44,** 279 (1989).
129. Kanai, J., *Stud. Surf. Sci. Catal.*, **44,** 211 (1989).
130. Plank, C. J., and Rossinski, E. J., and Given, E. N., US. Pat., 4,141,859 (1979).
131. Chester, A. W., Cormier, W. E., and Stoner, W. A., US. Pat., 4368 (1983) 114.
132. Abbot, J., and Wojciechowski, B. W., *J. Catal.*, **113,** 353 (1988).
133. Abbot, J., *J. Catal.*, **126,** 628 (1990).
134. Wielers, A. F. H., Var Kamp, M., and Post, M. F. M., *J. Catal.*, **127,** 51 (1991).
135. Zhao, Y., Bamwenda, G. R., and Wojciechowski, B. W., *J. Catal.*, **142,** 465 (1993).
136. Csicsery, S. M., *J. Catal.*, **17,** 207 (1970).
137. Csicsery, S. M., *J. Catal.*, **17,** 216 (1970).
138. Csicsery, S. M., *J. Catal.*, **17,** 315 (1970).
139. Csicsery, S. M., *J. Catal.*, **17,** 323 (1970).

CHAPTER II

EXPERIMENTAL DETAILS

2.0. INTRODUCTION

In this chapter, the preparation and the different techniques used in the characterization of the zeolites used in this study, namely, ZSM-48, ZSM-22 and EU-1, and metal promoted ZSM-5 catalysts are described. A detailed description of the experimental set up and the procedure adopted for the reactions of the different hydrocarbons (C_4-C_6) are also presented. The materials used in the synthesis of the different zeolites and in the different reactions are summarized in Table 2.1. The purity of these materials used is also presented in the same Table.

2.1. SYNTHESIS

The synthesis of the zeolites was carried out in stainless steel autoclaves under hydrothermal conditions. The autoclaves were cleaned with aqueous hydrofluoric acid (40%, wt.) and polished with a carbon brush prior to use. The typical synthesis procedures for the catalysts used in this study are presented below.

2.1.1. ZSM-5

The sample of ZSM-5 used in this study was obtained as the Na-form from United Catalysts India, Ltd. (India). The H-form of the sample was prepared by three exchanges of the Na-form with an aqueous ammonium acetate solution (5N; solid/solution (g/g) = 1:10; 6h at 353K) and by calcination of the NH_4^+- form at 813K for 16h in the presence of air.

2.1.2. ZSM-22

ZSM-22 was synthesized according to the procedure reported in the literature *[1]*. In a typical synthesis, 2.18 g of potassium hydroxide in 25 g of doubly distilled water was added slowly under stirring to 20.76 g of silica sol and stirred for 45 min. The resulting mixture was then added slowly to a solution of 4.8 g of aluminium sulfate in 15 g of doubly distilled water

under vigorous stirring. The resulting gel was stirred for 1 hr and then a solution of 3.76 g of 1-ethyl pyridinium bromide in 18 g water was added to the above gel and stirred for 15 min before transferring it to the autoclave. The resulting gel was heated in a stirred condition (60 rpm) at 433K for 4days under autogeneous pressure.

2.1.3. ZSM-48

A typical synthesis of ZSM-48 *[2]* consisted of adding 21.22 g tetra-ethyl orthosilicate to a solution of 0.12 g aluminium sulfate in 30 g distilled water while stirring. The mixture was stirred for 45 min before adding it to a solution of 1.6 g hexamethonium bromide in 20 g distilled water. Finally, a solution of 0.42 g sodium hydroxide in 20 g distilled water was added to the above mixture under vigorous stirring. The resulting white gel was further stirred for 1 h and crystallized at 433K under tumbling (60 rpm) for 7 days. A similar procedure was adopted for the synthesis of the isomorphs, Ga-ZSM-48 and Fe-ZSM-48, using 0.16 g of gallium nitrate and 0.25 g of ferric nitrate, respectively, which were added to the to the synthesis gel in lieu of the aluminium sulfate.

2.1.4. EU-1

EU-1 was synthesized according to the procedure described by Casci *et al. [3].* A typical synthesis of EU-1 consisted of adding 12.3 g sodium silicate in 49 g distilled water to a solution containing 0.95 g aluminium sulfate, 0.40 g sodium hydroxide and 20 g distilled water. The resulting mixture was stirred for 1h. Hexamethonium bromide monohydrate (0.95 g) was added to the above mixture followed by distilled water (10 g). The resulting gel was transferred into a stainless steel autoclave, capped tightly and rotated at 60 rpm in an oven at 433K for 8 days.

Table 2.1

Specifications of the materials used in the study

Reagent and Source	Chemical Formula or Composition	Purity(%)
Tetra ethyl ortho silicate (Aldrich, USA)	$Si(OC_2H_5)_4$	98
Sodium silicate (Loba chemicals, India)	(SiO_2 = 28.5%, Na_2O = 49%, H_2O = 22.5%)	
Silica sol (Loba chemicals, India)	(SiO_2 = 28.9%, Al_2O_3 = 0.05%, Na_2O = 0.5%, and H_2O = 70.55%	
Hexamethonium bromide [Hexmethylene bis [trimethyl ammonium dibromide], diquat-6 (Aldrich, USA)	$[Br(CH_3)_3N\text{-}(CH_2)_3]_2.H_2O$	99
1-ethyl pyridinium bromide (Aldrich, USA)	$[C_2H_5\text{-}C_5H_5N]^+\text{-}Br^-$	99
Ferric nitrate (BDH, India)	$Fe(NO_3)_3.9H_2O$	98
Aluminium sulfate (Merck, India)	$Al_2(SO_4)_3.16H_2O$	98
Aluminium nitrate (Merck, India)	$Al(NO_3)_3.9H_2O$	98
Zinc nitrate (Loba chemicals, India)	$Zn(NO_3)_3$	97
Gallium nitrate (Aldrich, India)	$Ga(NO_3)_3$	99
Chromium nitrate (BDH, India)	$Cr(NO_3)_3\ 9H_2O$	98
Chloroplatinic acid (Aldrich, USA)	H_2PtCl_6	99
Perrhenic acid (Aldrich, USA)	$HReO_4$	99
n-hexane (Merck, India)	C_6H_{14}	98
n-butane (Matheson, USA)	C_4H_{10}	99
Butene-1 (Matheson, USA)	C_4H_8	99
(C_5-C_7, raffinate, obtained from a refinery, India)	C_5-C_7 hydrocarbon mixture	
Na-ZSM-5 (United Catalysts India Limited, India)	Na-ZSM-5	

All the zeolites were separated from the mother liquior, washed, dried (383K; 12h) and calcined at 783K for 8h to burn away the template. The calcined samples (alkaline forms) were converted into the H-form as described in the case of H-ZSM-5.

2.1.5. Preparation of extrudates

Catalyst extrudates were prepared using alumina as a binder (zeolite : binder (wt/wt) = 70:30). The required amount of a commercial alumina mono hydrate (catapol B) and the H-form of the zeolite were blended thoroughly and then kneaded by adding a solution of acetic acid (4 wt%) such that the total amount of acid in the mixture was around 2 wt%. Extra water (deionised) was added, if necessary, to give the consistency of a very stiff dough. This resulting material was extruded using a hand extruder. The extrudates were dried initially at 423K for 2h and then calcined at 723K for 6 h. The diameter of the extrudates was 1.5 mm, which were broken into 4-6 mm pieces and stored. Metals were loaded on the extrudates by impregnation. Table 2.1 and Table 2.6 list the metal salts used and the amount of metal impregnated.

2.1.6. Preparation of M_xO_y/H-ZSM-5 catalysts (M = Ga, Zn, Cr, Fe)

Samples of H-ZSM-5 were loaded with different metal oxides by an impregnation technique using respective metal nitrate salts. In a typical preparation, 5 g of H-ZSM-5 was added to 0.34 g zinc-nitrate in 12.6 g water. The water slurry was kept over a water bath and stirred gently to evaporate it nearly to dryness. A small amount (3g) of water was added to the extrudates and redried with stirring. The procedure was repeated twice. The oxides of other metals, namely, Ga, Cr and Fe were also impregnated following the same procedure employing 0.50 g gallium(III)-nitrate, 0.39g, chromium(III)-nitrate and 0.37g ferric(III)-nitrate, respectively. All the metal impregnated H-ZSM-5 samples were calcined slowly by

stepwise heating (100 degree steps) starting from room temperature to 773K at a fixed rate of heating (1°/min). At each step the catalyst was kept for 1 h and finally at 773K for 6 h.

2.2. CHARACTERIZATION

2.2.1. Chemical analysis

A known weight of the sample was placed in a platinum crucible, covered with a lid and heated for 2h over a Mekker burner. The crucible was kept in a dessicator and cooled. The anhydrous weight of the sample was noted and this procedure continued until a constant weight of the anhydrous sample was obtained. This residue was then dissolved in 10 ml of aqueous hydrofluoric acid (40% wt.) and evaporated. The procedure was repeated to ensure that all the SiO_2 was evaporated as H_2SiF_6. The remaining part of the sample was heated again and the weight of the sample was noted after cooling it in a dessicator. The difference between the weight of the residue and the original weight (weight after initial heating) yielded the weight of SiO_2 in the sample. The residue was then dissolved in 1:1 HCl till a clear liquid was formed and this solution was diluted to a known volume by adding doubly distilled water. Chemical analysis of this solution was then performed by atomic absorption spectroscopy Hitachi; model Z-8000) to estimate the other components.

2.2.2. Powder X-ray diffraction (XRD)

The samples were analyzed by XRD for phase identification. The XRD patterns of the samples were recorded using a computer automated diffractometer (Model D-MAX III VC, Rigaku, Japan) using Ni-filtered CuKα radiation (λ = 1.5404 Å). The samples were equilibrated over a saturated $CaCl_2$ solution at room temperature for 6h prior to the measurement. The samples were then packed on glass sample holders. Data were collected in the 2θ range of 4-50° with a step size of 0.02° and a step time of 10s with continuous

rotation of the samples during the scan. Silicon was used as an internal standard to calibrate X-ray line positions.

2.2.3. Scanning electron microscopy

The morphology of the samples was studied using a scanning electron microscope (JEOL; Stereoscan 440). The samples were slurried with ethanol and deposited as a thin film over a brass sample holder. All the samples were sputtered with Au before conducting the SEM analysis to avoid surface charging of the sample in the electron beam.

2.2.4. Infrared Spectroscopy

Samples (~ 1mg) were mixed with KBr (100 mg) and pressed into pellets which were used for recording the IR spectra. IR spectra were scanned in the range 400-1300 cm^{-1} using a Perkin-Elmer (Model 1620) spectrometer.

2.2.5. Magnetic susceptibility measurements

Magnetic susceptibility of the Fe-ZSM-48 sample was found out at room temperature using a Faraday balance (Cahn-Ventron, Ceritos, CA, USA). The magnetic moment of the sample was calculated using standard procedures. The general formula for the calculation of the magnetic moment of the ferrisilicate is given below. Zeolites have a complex cage structure for which the molecular weight is not a well defined parameter. In ferrisilicate molecular sieves, since only the iron acts as a magnetic center and contributes to the magnetic susceptibility of the material, the molar susceptibility can be defined with respect to the number of moles of iron present in the material. Therefore, the molar susceptibility was calculated as follows:

$$\chi_M = \frac{\text{gram magnetic susceptibility } (\chi_g)}{\text{moles of iron in the sample } (M_{Fe})}$$

$$\text{where, } \chi_g = \frac{\text{magnetic susceptibility}}{\text{sample weight (g)}}$$

$$M_{Fe} = \frac{Z}{100 \times 55.8}$$

where, Z is the amount of iron (wt%) present in the ferrisilicate sample.

$$\chi_M = \frac{\chi_g \times 55.8 \times 100}{Z}$$

The magnetic moment μ can then be derived as

$\mu = 2.83\ (\chi_M xT)$ BM, where T is the temperature in Kelvin.

2.2.6. Temperature programmed desorption (TPD) of ammonia

Acidity measurement of the samples were carried out by temperature programmed desorption of ammonia. The sample 20-30 mesh (~ 1g) was placed in a silica tube (1.5cm i.d. x 30cm long) and activated in a flow of dry N_2 at 773K for 6h. The sample was then cooled in flowing N_2 (flow rate : 100 ml/min) to room temperature. NH_3 gas (25 ml/min) was introduced into the sample holder and passed continuously for a period of 30 min. N_2 (25 ml/hr) was passed for a period of 15 h at 300K to desorb the physically adsorbed NH_3 . The sample was then heated step wise at the rate of 10°/min in N_2 flow (25 ml/min) and held for 1/2 h at each step. The amount of NH_3 desorbed at each step was absorbed in 1N HCl and estimated titrimetrically.

2.2.7. Surface area measurement

A commercial adsorption apparatus (Omnisorb 100 CX; Coulter Corporation, USA) was used for measuring the BET surface area of the samples. The sample was usually

evacuated at 673K for 2h under high vacuum (10^{-6} mm). The anhydrous weight of the sample was measured. The sample was then cooled to 94K using liquid nitrogen and then allowed to adsorb nitrogen gas. Surface area of the sample was calculated by the BET method. The general form of the BET equation can be written as follows:

$$1 / V_{ads} (p_o - p) = 1 / V_m C + [C-1/ V_m C] p/p_o \quad [1]$$

where,

V_{ads} = volume of the gas adsorbed at pressure p,

p_o = saturated vapour pressure,

V_m = volume of the gas adsorbed for monolayer coverage,

C = BET constant

By plotting left side of the Eq. [1] against p/p_o , a straight line is obtained with a slope of $(C-1)/V_m.C$ and an intercept $1/V_m.C$. The BET surface area is calculated by using the formula

$$S_{BET} = X_M.N.A_m.10^{-20}$$

where N is the Avogardo's number, A_m is the cross-sectional area of the adsorbate molecule (N_2 , 16.2 $Å^2$) and X_M is the moles of N_2 adsorbed.

2.2.8. Adsorption measurements

n-hexane adsorption for all the samples were carried out using a vacuum electromicrobalance (Cahn-2000 G, USA). The sample (~60mg) was pressed into a pellet and weighed in a aluminium bucket attached to the balance. The sample was outgased at 675K for 12 h at 10^{-5} torr prior to the sorption measurement. The temperature was then lowered to the required value. The sorbate vapour was admitted into the sample at a constant pressure and temperature (p/po = 0.5 and 298K) and the weight gain was recorded as a function of time.

2.2.9. ESR Spectroscopy

ESR spectra of Fe-ZSM-48 and Cr-ZSM-5 were recorded in a Bruker ER 200D spectrometer at room temperature. A standard sample (weak pitch, varian, g = 2.0029) was used for calibration purposes.

2.2.10. Temperature programmed reduction (TPR) studies

Temperature programmed reduction (TPR) spectra for metal modified H-ZSM-5 samples were recorded using an automated instrument (Sorbstar, Model 200) with a thermal conductivity detector. Catalyst (~ 1 g; 10-20 mesh size) was taken in a sample holder, and heated from room temperature to 1073K slowly at a fixed rate of heating (15°C/min). Reduction of the sample was carried out by passing a reducing gas mixture of Ar and H_2 (10% by volume of H_2), which was passed first through the reference compartment of thermal conductivity cell and then through the sample holder and finally through a cold trap to the other compartment, of the TCD cell. In this way, a profile of hydrogen consumed was obtained as a function of temperature. Specific species being reduced showed up as peaks in the profile. All the samples were dried at 673K in argon prior to the TPR measurements.

2.2.11. Coke measurement

The coke content of the used catalysts were estimated by careful burning of the carbonaceous material with air at 773K. Air (25ml/hr) was passed through the catalyst first and then over a bed of Pt (0.3%)-Al_2O_3 at 773K to convert CO to CO_2. The outlet gas was then passed slowly (25ml/min) through two bubblers, each containing 75ml of 0.5N NaOH. The amount of coke was determined titrimetrically on the basis of the amount of CO_2 absorbed in the NaOH solution.

2.3. CATALYTIC STUDIES

2.3.1. Apparatus

2.3.1.1. Atmospheric pressure reactor

A microreactor was used to carryout the reactions at atmospheric pressure. The reactor consisted of a fused silica tube, 1.5 cm i.d. and 30 cm long, with a B-14 ground silica socket and a side limb (5 cm long) with a stop cock attached to it at the top. Schematic drawing of the reactor set up is shown in Fig 2.1. The temperature of the catalyst bed was controlled using an analog temperature controller (Aplab, India) and a digital indicator. An infusion pump (Sage Instruments, Model 352, USA) was used to deliver the feed to the catalyst bed. Added gas flow (H_2 or N_2) was controlled by a mass flow controller (Matheson, USA). After the reaction, the product gas mixture was passed through a cold water condenser to condense the liquid fraction (C_5^+) . Liquid products were collected periodically and weighed. Both the liquid and gaseous products were analyzed by gas chromatography.

2.3.1.2. High-pressure reactor

High pressure catalytic studies were carried out in a commercial high-pressure reactor supplied by Autoclave Engineers (Erie, PA, USA) and Metrimpex (Model: 087014, Hungary); the latter was used during aromatization of the commercial raffinate feed using large amounts (20-30g) of the extruded catalysts. A simplified diagram of the high pressure reactor is shown in Fig 2.2. Added gas (N_2 /H_2) was introduced via a mass flow controller, and the desired reaction pressure was maintained by a back pressure regulator (BPR). Outlet gas flow was measured by a wet gas flow meter. Reactions at high pressure, without any added gases, was carried out by pressurising the system with N_2, the required reaction pressure being

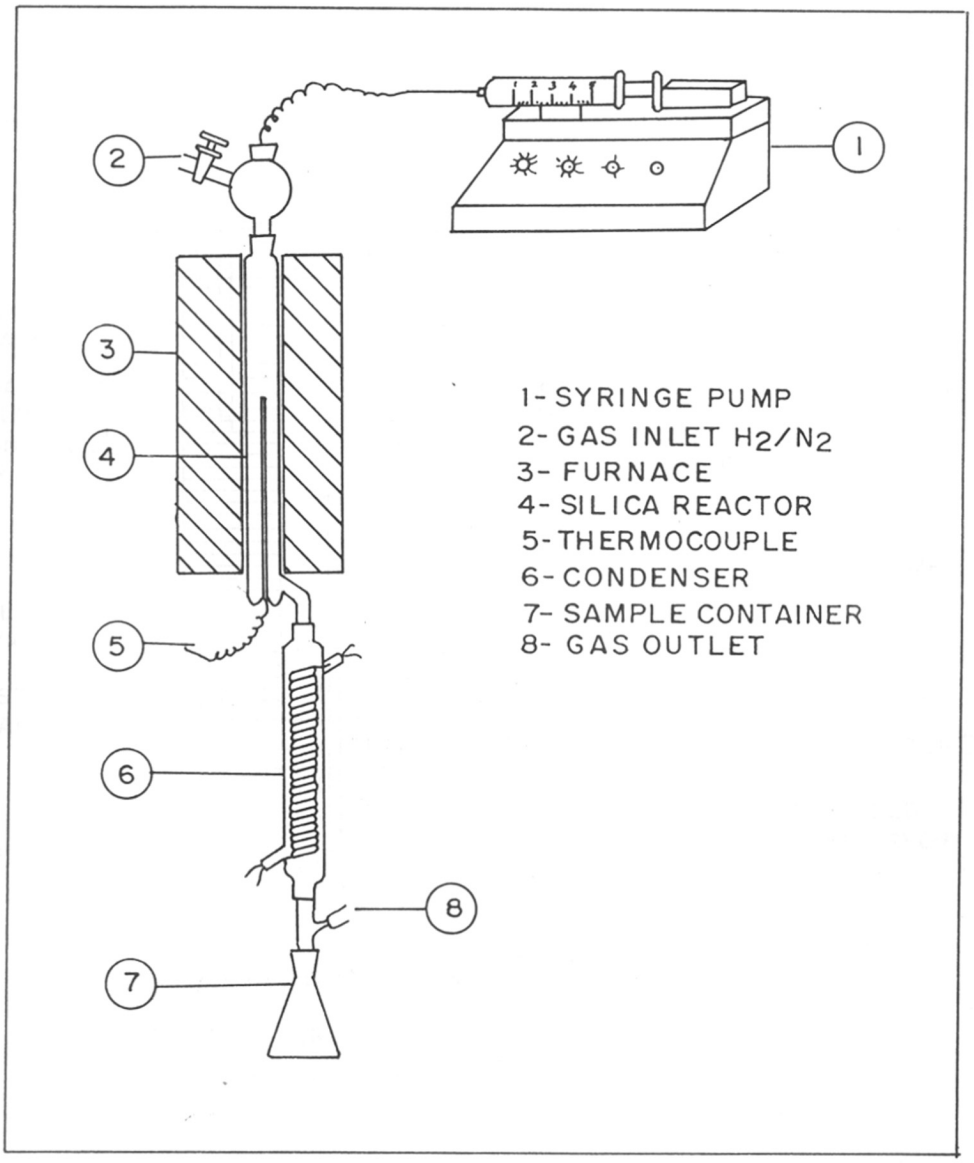

Fig. 2.1. Fixed bed, down flow atmospheric pressure reactor used in this study.

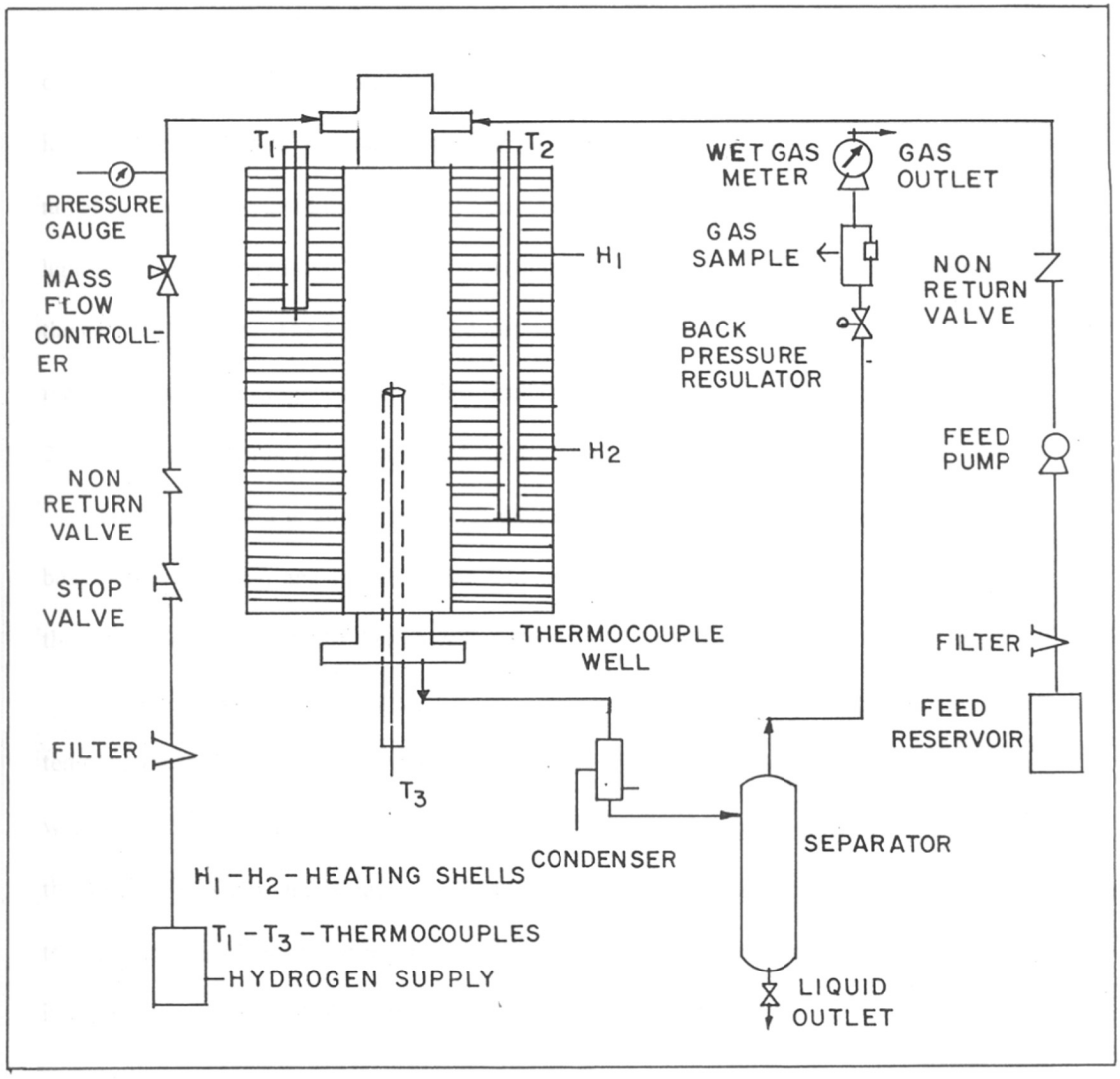

Fig. 2.2. High pressure reactor used in this study.

maintained by the product gases during the reaction. The procedure for product collection and analysis was the same as mentioned for low-pressure reaction studies.

2.3.2. Methodology for catalytic reactions

20-30 g (1.5 mm dia; 3-4 mm length) of the catalyst extrudates and 2-3 g (20-30 mesh) of the compacted powder samples (binder free) were used in the catalytic studies. Pure n-hexane (Merck, India), n-butane, 1-butene (Matheson gas products, USA), hydrogen, and nitrogen (Indian Oxygen Limited, India) were used without further purification. A commercial light hydrocarbon mixture (C_5-C_7 - raffinate), obtained from a refinery (India), was also used in the catalytic studies. The general procedures adopted for both atmospheric and high pressure reactions and for the regeneration of the coked catalysts are described below.

2.3.2.1. Aromatization of n-hexane at both atmospheric and higher pressures

The catalyst (2-3 g; 20-30 mesh) was diluted with the same volume of crushed porcelain beads of similar size and loaded in the mid-section of the reactor so that the tip of the thermocouple kept inside the thermowell was at the middle of the catalyst bed.

The temperature of the catalyst was increased slowly and stepwise starting from room temperature to 773K and kept for 6h for complete activation. A flow of dry air (50 ml/min) was maintained during activation of the catalyst. After completing the catalyst pretreatment, the air flow was changed to nitrogen (25ml/min), to flush the reactor for 1hr. The reactor temperature was then cooled down to the reaction temperature and added gas (H_2/N_2) was introduced at the required flow rate.

For high pressure reactions, the reactor pressure was raised slowly (after activation at 773K at 6h at atmospheric pressure) by controlling the BPR and the final/desired pressure was allowed to equilibriate for 1h. After equilibriation of both the temperature and pressure, n-hexane was introduced at the required flow rate from the top of the reactor. Liquid products were collected periodically, and mass balances were obtained by analysis of both the liquid and gaseous fractions in a gas chromatograph.

2.3.2.2. Regeneration of the catalyst

After completing the catalytic runs, the catalyst bed was flushed with nitrogen (50 ml/min) at 723 K for 2 h to remove the organic materials from the catalyst surface.

The reactor was cooled to 423 K and air was introduced at the rate of 25-50 ml/min for the pelleted samples and at 100ml/min for the extrudate samples.

The reactor temperature was raised slowly to 773 K. During regeneration of the coked catalysts, the catalyst bed temperature was maintained very carefully. The reactor temperature did not exceeded 813K during regeneration of the coked catalysts.

2.3.3. Analysis and Calculations

2.3.3.1. Gas chromatographic analysis

Both the liquid and gaseous products were analyzed. The gases (C_1-C_5) were analyzed using a gas chromatographic refinery gas analyzer (RGA, Model: 5880A, HP, USA) with multiple columns and fitted with a thermal conductivity detector. Additionally, the gas was also analyzed using a capillary column (crosslinked methyl silicone gum, used in PONA analysis, 50m x 0.2 mm, 0.5 μm film thickness; flame ionization detector; HP 5890 gas chromatograph) to estimate the C_5^+ components present in the gas fraction. The same capillary column was used for the analysis of the liquid products also.

2.3.3.2. Mass balance calculations

Both gaseous and liquid products were obtained during the reaction in most of the microreactor experiments. The gaseous and liquid products were analyzed separately to obtain correct conversion and product yields. For mass balance calculations, the liquid product was collected for a given period of time and weighed. Knowing the weight of the feed injected during that time interval, the weight of the gaseous fraction (weight of feed input - weight of liquid product) was calculated and from the analysis of the gaseous and liquid products, the conversion and product break up were calculated. Independently, the gaseous weight was also calculated based on the volume of gas generated and its composition. The weight of the gas obtained by the two methods agreed well within experimental error. For all the reactions, mass balance calculations have been done without considering the amount of H_2 and coke deposited on the catalyst surface. The overall error in the mass balances was always < 5 wt.%.

2.4. RESULTS AND DISCUSSION

The synthesis of ZSM-22, EU-1, and ZSM-48 (Al-, Ga-, Fe-) were carried out in a basic medium under hydrothermal conditions. The sequence of addition of the reactants do not affect the incorporation of Al^{3+} and Ga^{3+} in the framework of zeolites due to the solubility of their oxides in the highly alkaline medium. However, in the case of the ferrisilicate molecular sieves, the formation of insoluble and stable Fe_2O_3 retards the incorporation of Fe^{3+} into the framework of the molecular sieves *[4]*. In order to avoid the precipitation of Fe^{3+} as hydroxide, the basic sodium silicate was added slowly to the acidic ferric salt solution to get a white/yellow ferrisilicate gel *[5]*. Once the ferrisilicate gel was formed, the desired template

was added followed by the addition of the alkali. The molar gel composition and other gel parameters for the different samples used in this study are given in Table 2.2.

X-ray powder diffraction patterns (Fig 2.3 & 2.4) of all the samples are similar to those reported in the literature *[6,7,8,9]*. The XRD patterns of these molecular sieves did not show the presence of any other crystalline impurity phases. The XRD pattern of the samples before and after calcination were similar with a slight change in pattern only for the MFI samples as expected from a symmetry change from orthorhombic to monoclinic. XRD patterns did not suggest any damage to the zeolite structure due to metal loading. Also, no change in the XRD patterns was observed after the reaction indicating the absence of any structural damage during reaction/regeneration.

ZSM-48 was obtained as bundles of needle-shaped crystals with the individual needles being 1μm long and 0.05 μm diameter (Fig. 2.5). The crystals of ZSM-22 were more elongated in one direction (2.5-3.0μm), where as the crystals of EU-1 were nearly cuboid (0.5-1μm). The ZSM-5 crystals were ball-shaped with diameters in the range 2-3 μm (Fig. 2.5)

The framework infrared spectra of the samples were characteristic of each of the zeolites *[6]*. The prominent bands attributed to the different internal tetrahedral and external linkage vibrations are summarized in Table 2.3. The IR data of all the samples are similar to those reported in the literature *[6,7,8,9]*. Table 2.3 also compares the IR spectra of Al-, Ga-, and Fe-ZSM-48. In Fe-ZSM-48, most of the lattice vibration bands are shifted towards the lower wave numbers (in comparison with the Al analog), as has been reported in the case of the other ferrisilicate systems *[10,11,12]*.

Table 2.2

Molar gel composition and synthesis parameters of different metallosilicate molecular sieves

Zeolites	Si/M	Si/ Na or K	Si/R[1]	OH/Si	H_2O/Si	Gel pH	Yield (%)
Al-ZSM-48	153	10	24.2	4.1	38.1	12.1	92
Ga-ZSM-48	154	10	24.2	4.1	38.1	12.0	90
Fe-ZSM-48	158	10	24.2	4.1	38.1	11.8	83
Al-EU-1	21	2.0	12.3	0.3	21.4	11.7	75
Al-ZSM-22	22	8.8	18.4	2.6	11.8	12.2	80

[1]R = organic template used for the synthesis.

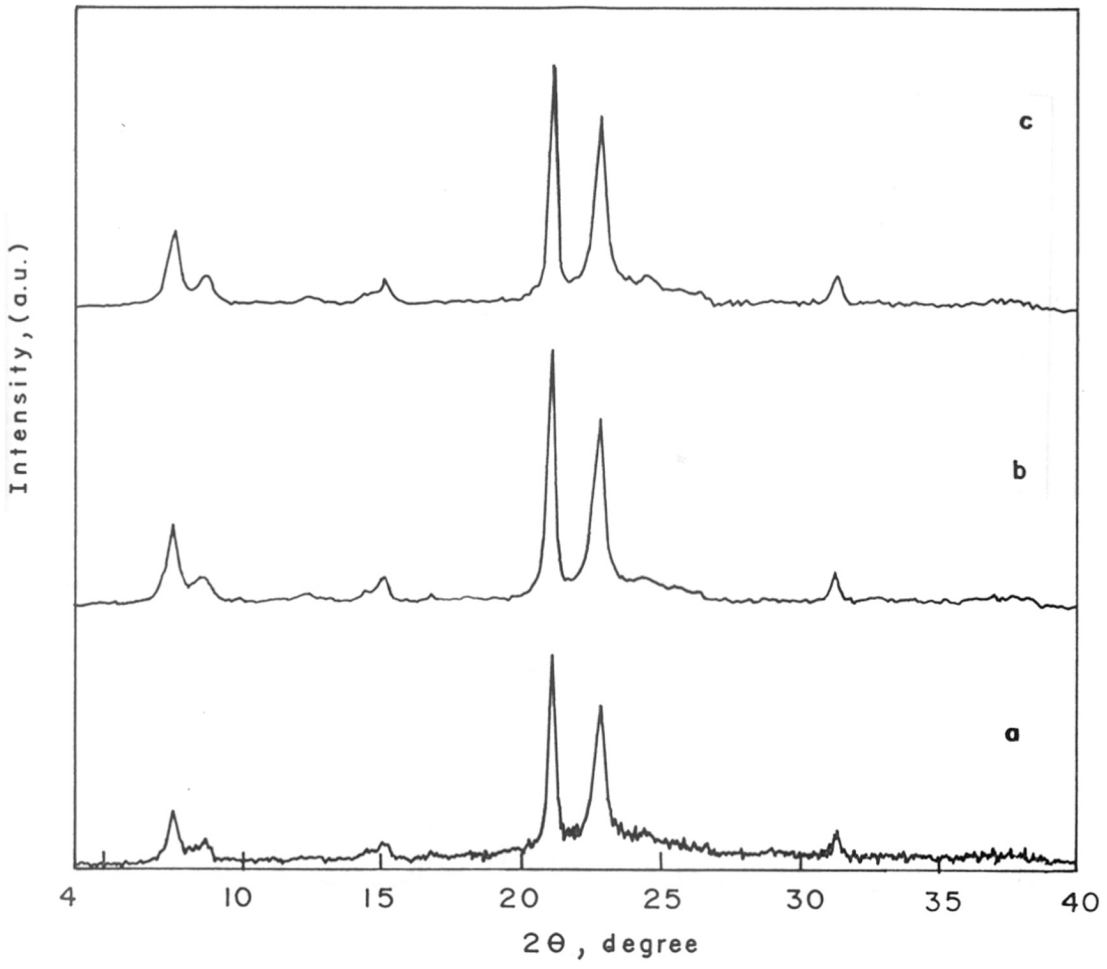

Fig. 2.3. Powder X-ray diffraction patterns of metallosilicates of ZSM-48: (a) H-Al-ZSM-48; (b) H-Ga-ZSM-48; (c) H- Fe-ZSM-48.

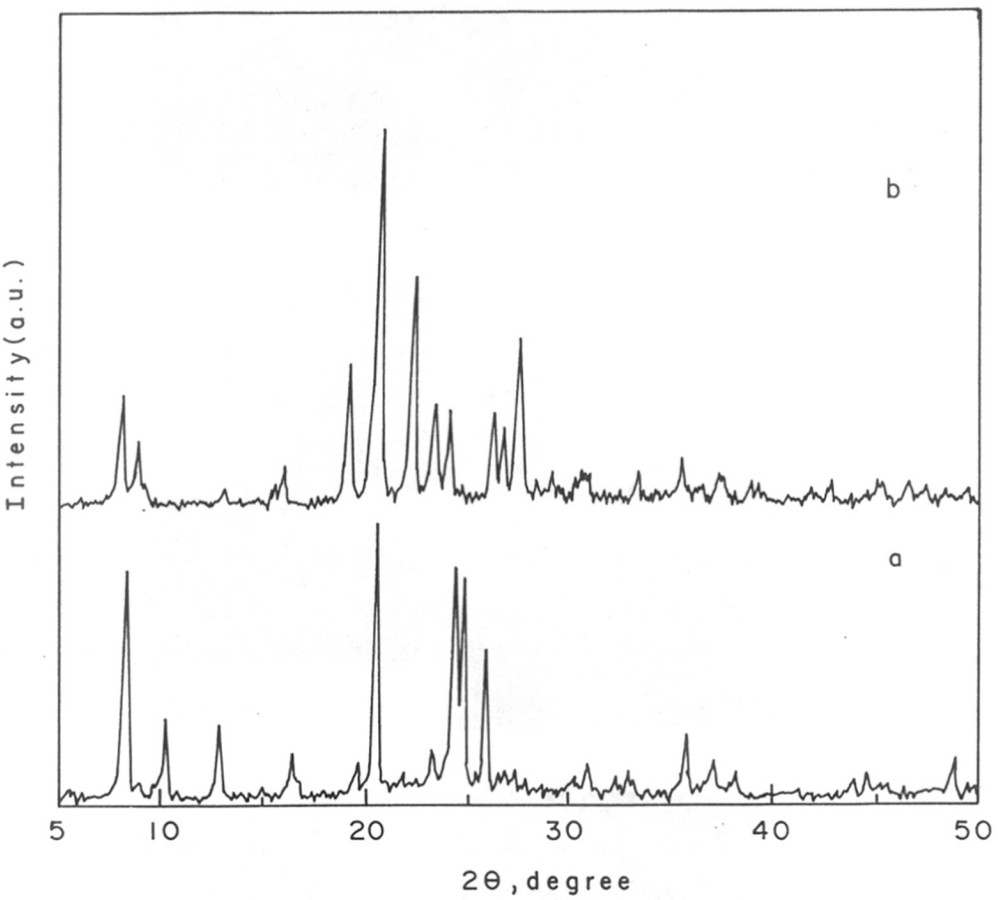

Fig. 2.4. Powder X-ray diffraction patterns of (a) H-ZSM-22; (b) H-EU-1.

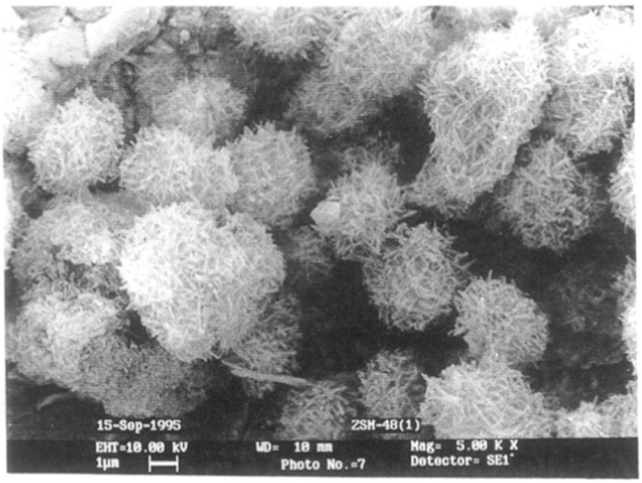
15-Sep-1995
ZSM-48(1)
EHT=10.00 kV
WD= 10 mm
Mag= 5.00 K X
1µm
Photo No.=7
Detector= SE1

a

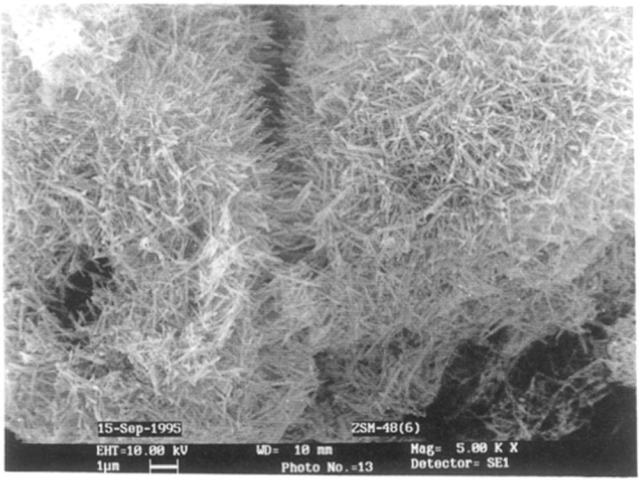
15-Sep-1995
ZSM-48(6)
EHT=10.00 kV
WD= 10 mm
Mag= 5.00 K X
1µm
Photo No.=13
Detector= SE1

b

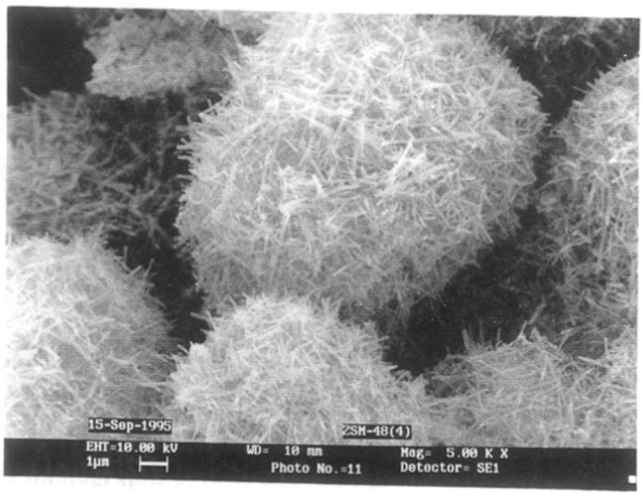
15-Sep-1995
ZSM-48(4)
EHT=10.00 kV
WD= 10 mm
Mag= 5.00 K X
1µm
Photo No.=11
Detector= SE1

c

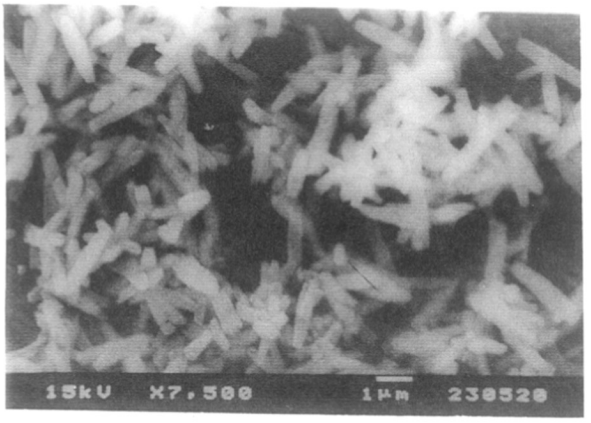

d

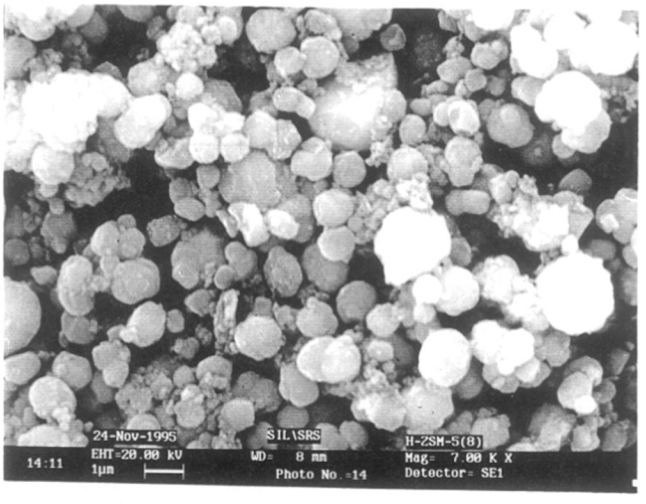

e

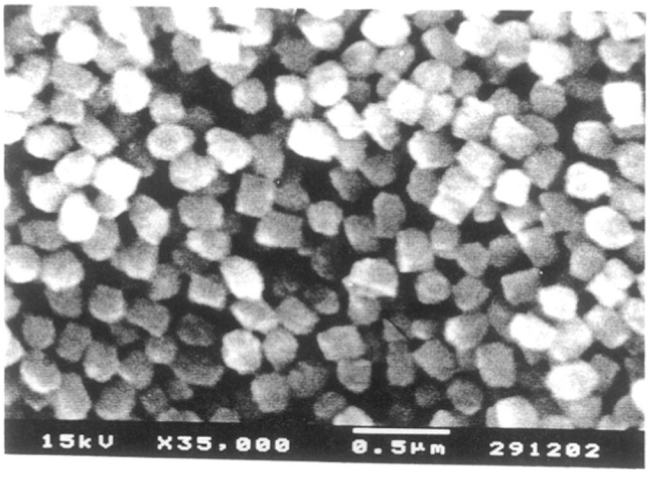

f

Fig. 2.5. SEM photographs of (a-c) ZSM-48; (d) ZSM-22; (e) ZSM-5; (f) EU-1. (a) SiO_2 / Al_2O_3 = 228; (b) SiO_2 / Ga_2O_3 = 309; (c) SiO_2 / Fe_2O_3 = 314; (d) SiO_2 / Al_2O_3 = 44; (e) SiO_2 / Al_2O_3 = 40; (f) SiO_2 / Al_2O_3 = 42.

Table 2.3

IR data for ZSM-5, ZSM-22, EU-1, Al-, Ga- and Fe-ZSM-48

Mode of vibration	Al-ZSM-5	Al-ZSM-22	Al-EU-1	Al-ZSM-48	Ga-ZSM-48	Fe-ZSM-48
Asym. Stretching						
External	1225	1220	1370	1376	1376	1376
Internal	1095	1084	1085	1103	1103	1097
Sym. Stretching						
External	793	808	795	807	801	784
Internal	630	641	620	621	621	620
Double ring	545	549	572	552	550	546
T-O	448	462	470	458	458	457

Magnetic susceptibility measurements can be used to access whether the iron is present in a magnetically dilute environment (with Si-O-Fe-O-Si bonds) or as a condensed oxide phase (with Fe-O-Fe bonds). In the case of high-silica, ferrisilicate zeolites, the framework Fe^{3+} ions are normally present in a magnetically dilute environment and have non-interacting Fe^{3+} ions in a diamagnetic matrix and are expected to possess a magnetic moment less than 6 BM *[12]*. The magnetic moment values of the as synthesized and protonic form of Fe-ZSM-48 sample at 297K were found to be 5.4 and 5.5 BM respectively. Iron oxides such as Fe_2O_3 and Fe_3O_4 if present, are expected to exhibit much higher values of magnetic moment as well as a marked dependence on temperature, depending upon the extent of agglomeration *[12]*. There was no change in the magnetic moment value at 94K. Thus, magnetic susceptibility data confirm that Fe/ZSM-48 does not contain a detectable amount of bulk iron oxide phase like Fe_2O_3 or Fe_3O_4.

The results of the NH_3-TPD experiments carried out over ZSM-48 samples in the temperature range 413-773K are presented in Table 2.4. The NH_3 desorbing over the entire temperature range (413K to 773K) is due to acid sites of differing strengths, from weak to strong. For convenience, these sites have been lumped into two categories, namely, the weak and strong acid sites, corresponding to the desorption of NH_3 in the temperature ranges of 413-523K and 523-773K, respectively. The total amount of NH_3 desorbed from ZSM-48 ($SiO_2/Al_2O_3 = 228$) in the temperature range 413-773K is similar to that reported by Suzuki *et al.[13]*. The concentration of strong acid sites decreases with increasing SiO_2/Al_2O_3 ratios and on isomorphous substitution of Al by Ga or Fe, whereas the quantity of weak acid sites does not change significantly either with changing SiO_2/Al_2O_3 ratios or with isomorphous substitution (see Table 2.4).

The effect of promoters on the acidities of the metal promoted H-ZSM-5 catalysts was also studied (Table 2.5). The data presented in Table 2.5, show that there is no observable change in both weak and strong acid sites after the introduction of Ga and Zn, whereas the number of strong acid sites decreases on introducing Cr and Fe.

n-hexane sorption data for all the ZSM-48 samples are presented in Table 2.4. The data (Table 2.4) demonstrate that neither a variation in the SiO_2/Al_2O_3 ratio, nor isomorphous substitution by Ga and Fe, have any significant influence on the adsorption of n-hexane. A slight decrease in both the surface area (S_{BET}) and the sorption of n-hexane is observed on impregnation of metal oxides over the H-ZSM-5 samples (Table 2.5). The lower n-hexane sorption values for Cr/ZSM-5 and Fe/ZSM-5 suggest that some pore-size modification or pore-mouth blockage has occurred during the loading of these metals. n-Hexane sorption capacities of the ZSM-22 and EU-1 samples were similar to those reported in the literature *[14]*.

The ESR spectrum of Fe-ZSM-48 (Fig. 2.6) exhibits two main signals at g = 4.301 and 2.085 *[8,15]*. The first peak (g = 4.301) has been attributed to Fe^{3+}, in distorted tetrahedral positions, probably in the framework. There is no change in the ESR spectrum of Fe-ZSM-48 before or after calcination, suggesting that framework Fe^{3+} ions are not affected by calcination. Fig. 2.7a and 2.7b show the ESR spectra of the calcined and reduced samples of Cr/H-ZSM-5. The calcined sample shows two signals at g = 2.123 and at g = 1.945, (Fig. 2.7a) whereas after reduction, a broad signal (g = 2.208) is observed (Fig. 2.7b). The ESR spectrum of the calcined Cr/H-ZSM-5 sample (Fig. 2.7a) shows a narrow line superimposed over a broad intense line. The sharp narrow line (Fig. 2.7a) indicates the presence of Cr^{5+} in the sample *[16]*. The broad line is probably due to the large anti ferromagnetic crystals of α-Cr_2O_3

Table 2.4

Catalysts used in n-hexane cracking

Sample	Unit cell composition[a]	SiO_2/M_2O_3[b] (molar ratio)	Adsorption of n-hexane (molecules/ unit cell)[c]	No. of M atoms /unit cell	Acidity[d] (mmol/g)	
					Weak	Strong
1.	$H_{.41}Na_{.01}(SiO_2)_{47.58}(AlO_2)_{.42}$	228	1.8	0.4	0.09	0.04
2.	$H_{.30}Na_{.02}(SiO_2)_{47.66}(AlO_2)_{.32}$	307	1.6	0.3	0.08	0.03
3.	$H_{.20}Na_{.03}(SiO_2)_{47.75}(AlO_2)_{.23}$	394	1.7	0.2	0.07	0.02
4.	$H_{.14}Na_{.02}(SiO_2)_{47.84}(AlO_2)_{.16}$	605	1.7	0.1	0.03	0.01
5.	$H_{.28}Na_{.03}(SiO_2)_{47.69}(GaO_2)_{.42}$	309	1.6	0.3	0.07	0.03
6.	$H_{.30}Na_{.01}(SiO_2)_{47.69}(FeO_2)_{.31}$	314	1.6	0.3	0.06	0.02

[a]Unit cell composition calculated on anhydrous basis; [b]M = Al, Ga and Fe; [c]at $p/p_0 = 0.5$ and 298K; [d]weak and strong acid sites are defined as the NH_3 desorbed in the temperature ranges (413-523K), (523-773K) respectively.

Table 2.5

Catalysts used in n-hexane aromatization

Catalysts	SiO_2/ Al_2O_3 (molar ratio)	Metal loading[a] (wt.%)	BET surface area (m^2/g)	Adsorption of n-hexane (g/100g)[b]	Acidity[c] (mmol/g)	
					Weak	Strong
H-ZSM-5	40	-	423	12.01	0.70	0.47
H-ZSM-22	42	-	275	8.8	0.65	0.17
H-EU-1	38	-	300	10.0	0.72	0.39
Ga/H-ZSM-5	40	3.1	401	11.85	0.81	0.44
Zn/H-ZSM-5	40	3.2	389	11.89	0.51	0.35
Cr/H-ZSM-5	40	2.8	375	9.73	0.65	0.35
Fe/H-ZSM-5	40	3.0	340	9.56	0.61	0.35

[a]Metal loading as oxide basis; [b]at $p/p_o = 0.5$ and 298K; [c]weak and strong acid sites are defined as the NH_3 desorbed in the temperature ranges (413-523K), (523-773K) respectively.

located on the outer surface of the zeolites *[16]*. Hence, it appears that the major portion of chromium is located on the outer surface of the zeolite as Cr^{3+}.

The TPR profiles of Ga/ZSM-5, Zn/ZSM-5, Cr/ZSM-5 and Fe/ZSM-5 are presented in Fig 2.8. The TPR spectrum of Ga/ZSM-5 reveals an unresolved broad peak in the range 773-923K (Fig. 2.8a). Based on TGA and microbalance studies, Price *et al. [17]* have suggested that Ga_2O_3 is reduced to Ga^+, and the different Ga-species formed during reduction are dispersed over the zeolite support. The formation of different Ga-species during reduction and their extent of dispersion within the channels of the zeolite have been confirmed by FTIR *[18]*, STEM *[19]*, and XPS *[20]* studies. H_2 consumption data (Table 2.6) shows that 59% of the Ga_2O_3, were reduced to Ga^+ under our experimental conditions, although this transition (Ga^{3+} to Ga^+) has a negative reduction potential (Table 2.7), suggesting that it is thermodynamically less favourable. The considerable reduction may be due to the intimate mixing between Ga_2O_3 and H-ZSM-5 and the higher acidities of H-ZSM-5 as suggested by Price *et al. [17]*. Other factors such as the amount of Ga_2O_3 loaded and the calcination temperature also influence for the reduction of Ga_2O_3. The TPR spectrum of Zn/ZSM-5 shows two peaks at 723K and at 923K (Fig. 2.8d), similar to the results reported by Zaihui *et al [21]*. The low temperature peak has been associated with the reduction of ZnO, present on the surface of the catalyst, whereas the higher temperature peak corresponds to the reduction of ZnO inside the zeolite pore system *[21]*. H_2 consumption during reduction (Table 2.6) indicate that only 13.5% of Zn^{2+} ions were reduced to the metallic state. Probably, some low valent Zn ions were also formed during reduction along with metallic zinc *[21]*. The TPR profiles and the percentage of reduction of Cr^{3+} and Fe^{3+} in Cr/ZSM-5 and Fe/ZSM-5 reveal that Cr^{3+} and Fe^{3+} species are present in the respective samples and these trivalent species are

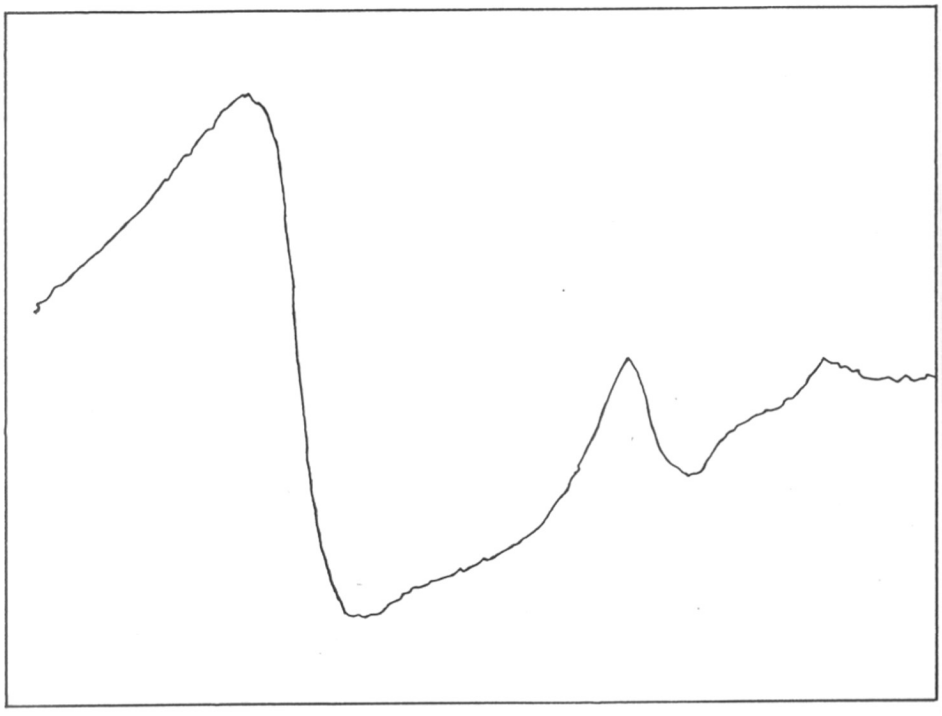

Fig. 2.6. Electron spin resonance spectrum of Fe-ZSM-48 (297K).

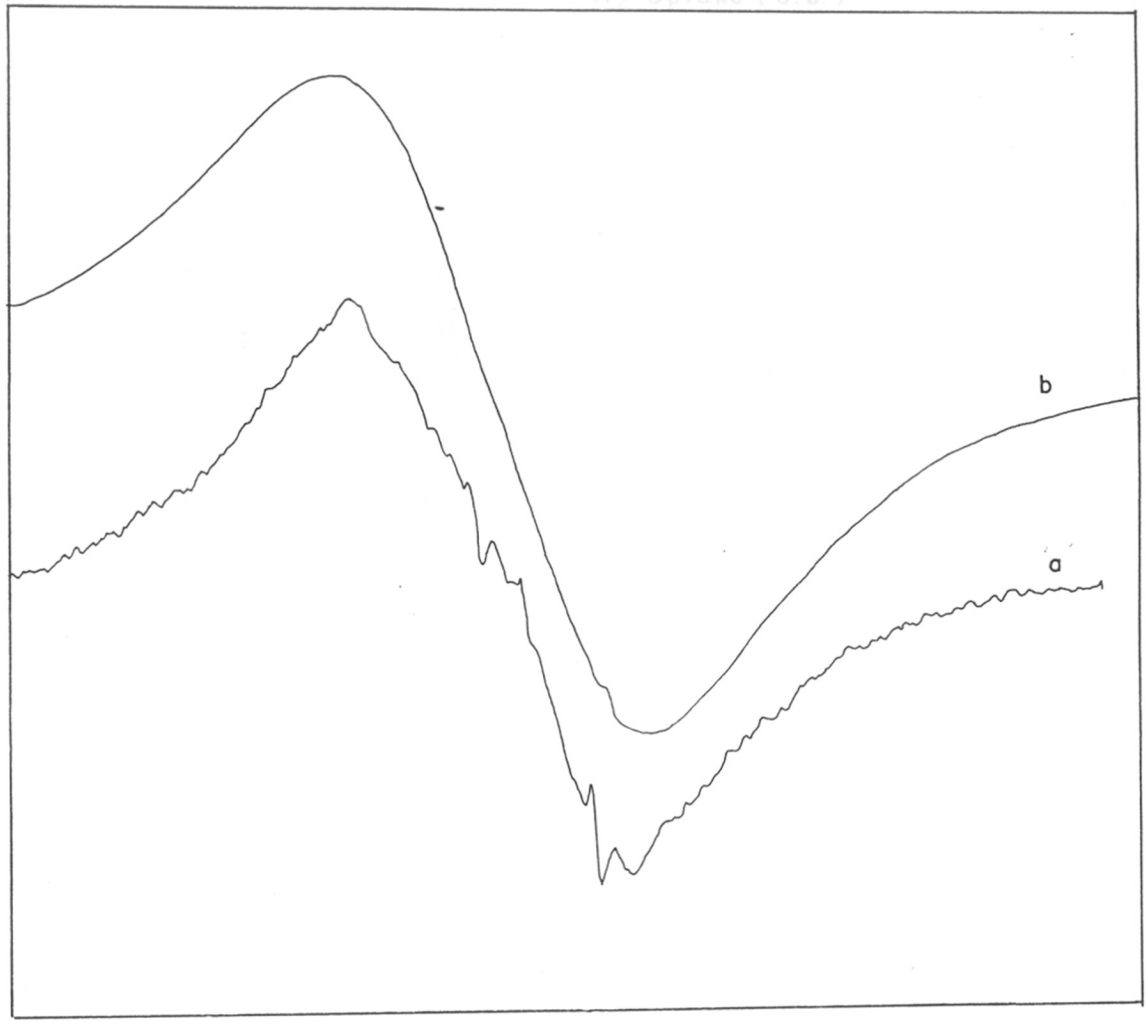

Fig. 2.7. Electron spin resonance spectrum of Cr-ZSM-48: (a) calcined; (b) reduced.

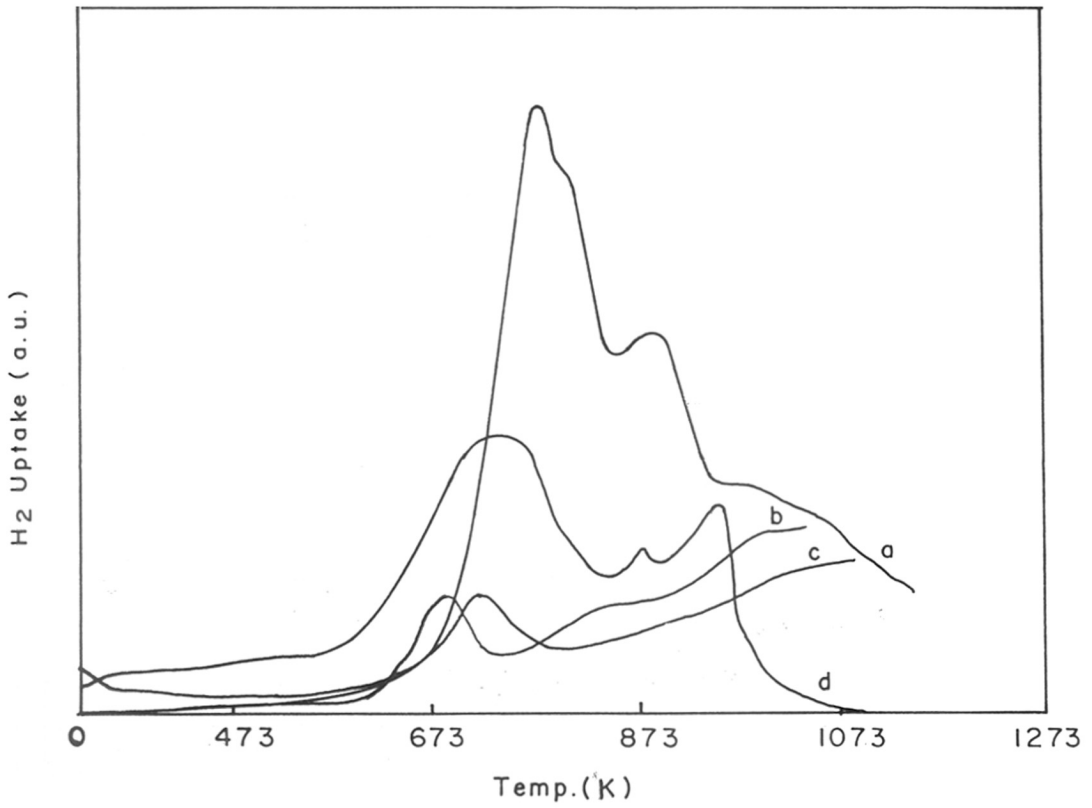

Fig. 2.8. TPR spectra of Ga, Zn, Fe and Cr promoted H-ZSM-5: (a) Ga/H-ZSM-5; (b) Cr/H-ZSM-5; (c) Fe/H-ZSM-5; (d) Zn/H-ZSM-5.

Table 2.6

TPR data for metal promoted H-ZSM-5

Catalyst	Metal loading	Peak Temperature (K)		H_2 uptake (μ mol/g)	% of reduction[a]
		T_{m1}	T_{m2}		
Ga/ZSM-5	2.23	773	-	188.95	59.30
Zn/ZSM-5	2.41	723	923	49.82	13.51
Cr/ZSM-5	2.11	673	-	30.55	7.42
Fe/ZSM-5	2.09	715	-	33.25	7.31

[a] Ga^{3+} to Ga^{+}; Zn^{2+} to Zn^{o}; Cr^{3+} to Cr^{0}; Fe^{3+} to Fe^{0}.

Table 2.7

Standard electrode potential values of Ga, Zn, Cr and Fe ions *[22]*

No.	Reaction	ΔE_0 (kcal /mole)
1.	$Ga^{3+} + e \rightarrow Ga^{2+}$	-0.677
2.	$Ga^{3+} + 2e \rightarrow Ga^{+}$	-0.560
3.	$Zn^{2+} + 2e \rightarrow Zn$	-0.792
4.	$Cr^{3+} + 3e^{-} \rightarrow Cr$	-0.744
5.	$Cr^{3+} + e^{-} \rightarrow Cr^{2+}$	-0.407
6.	$Cr^{5+} + 2e^{-} \rightarrow Cr^{3+}$	1.477
7.	$Fe^{3+} + 3e^{-} \rightarrow Fe$	-0.037
8.	$Fe^{2+} + 2e^{-} \rightarrow Fe$	-0.477
9.	$Fe^{3+} + e^{-} \rightarrow Fe^{2+}$	0.771

difficult to reduce to the metallic or lower oxidation states (Fig. 2.8b & 2.8c; Table 2.6). Reduction potential values show that the reduction of Cr^{5+} to Cr^{3+} is thermodynamically more favourable than the reduction of Cr^{3+} to Cr^{+} or Cr^{3+} to Cr^{2+} (Table 2.7). So the small amount of Cr^{5+} (as shown by ESR) present in the sample is probably reduced to Cr^{3+}. Data in Table 2.7, show that reduction of Fe^{3+} to Fe^{2+} is thermodynamically more favorable than Fe^{3+} to metallic iron. The low level of H_2 consumption during the reduction of Fe_2O_3 in Fe/H-ZSM-5 also suggests that the Fe-oxide species interact strongly with zeolite support and are difficult to reduce.

References

1. Olson, D. H., Calvert, R. B., and Valyocsik, E. W., Eur. Patent, 0102716, (1984).
2. Valyocsik, E. W., Eur. Patent, 0142317 (1984).
3. Casci, J. L., Lowe, B. M., and Whitam, T. M., Eur. Patent, 042226, (1981).
4. Ratnasamy, P., Kumar, R., *Catal. Today.*, **9,** 341 (1991).
5. Szostak, R., Thomas, T. L., *J. Catal.*, **100,** 555 (1984).
6. Jacobs, P. A., and Martens, J. A., *Stud. Surf. Sci. Catal.*, **33,** 26 (1987).
7. Borade, R. B., Adnot, A., and Kaliaguine, S., *Zeolites*, **11,** 710 (1991).
8. Ruifeng, L., Xu, W., and Wang, J., *Zeolites.*, **12,** 716 (1992).
9. Rao, G. N., Joshi, P. N., Shiralkar, V. P., and Kotasthane, A. N., in "Recent Development in Catalysis, Theory and Practice", (B. Viswanathan & C.N. Pillai, Eds.), p. 164, Narosa Publishing House 1990.
10. Kumar, R., Ratnasamy, P., *J. Catal.*, **121,** 89 (1991).
11. Chandwadkar, A .J., Bhat, R. N., and Ratnasamy, P., *Zeolites*, **11,** 42 (1991).
12. Kumar, R., Thangaraj, A., Bhat, R. N., and Ratnasamy, P., *Zeolites*, **11,** 85 (1990).
13. Suzuki, K., Kiyozumi, Y., Shin, S., Fujisawa, K., Watanabe, H., Saito, K., and Noguchi, K., *Zeolites*, **6,** 290 (1986).
14. Szostak, R., "Hand book of Molecular Sieves", Van Nostrand Reinhold, New York (1994)
15. Bellusi, G., Millini, R., Carati, A., Maddinelli, G., and Gervasini, A., *Zeolites*, **10,** 642 (1990).
16. Slinkin, A. A., Kucherov, A. V., Gorjachenko, S. S., Aleshin, E. G., and Slovetskaja, K. I., *Zeolites*, **10,** 111 (1990).
17. Price, G. L., and Kanazirev, V., *J. Catal.*, **126,** 267 (1990).
18. Meriaudeau, P., and Naccache, C., *Appl. Catal.*, **73,** L13 (1991).
19. Joly, J. F., Ajot, H., Merlen, E., Raatz, F., and Alario, F., *Appl. Catal.*, **79,** 249 (1991).
20. Meitzner, G. D., Iglesia, E., Baumgartner, J. E., and Huang, E. S., *J. Catal.*, **140,** 209 (1993).
21. Zaihui, Fu., Dulin, Y., Yang, Y., and Guo, X., *Appl. Catal.*, **124,** 59 (1995).
22. Milazzo, G., and Caroli, S., "Tables of standard electrode potentials" Eds. John. Wiley and Sons., 1978.

CHAPTER III

n-HEXANE CRACKING OVER ZSM-48

3.0. INTRODUCTION

The introduction of zeolite -X as a cracking catalyst by Planck and Rosinski *[1]*, revolutionized the petroleum refining industry. Subsequently, Y, USY and RE-Y have been used in FCC catalyst formulations. The addition of a small amount of ZSM-5 to cracking catalysts has been found to increase *[2]* the octane rating of FCC gasoline through selective cracking of the low octane (n-paraffin) components. Chester *et al. [3]* have reported that besides ZSM-5, other zeolites such as ZSM-11, ZSM-12, ZSM-23, ZSM-35 and ZSM-38 also possess octane boosting capability.

It is now understood that the cracking of hydrocarbons proceeds through the formation of a positively charged organic species (*carbocation).* On Brönsted acid sites a carbenium ion may be readily formed by the protonation of an olefinic intermediate (produced by thermal cracking). The Lewis acid sites, which are strongly deficient in electrons can abstract a hydrogen atom from an alkane molecule in the form a of hydride ion (H^-) with the formation of the complementary carbonium ion. Since the C-H bond is covalent, its ionization energy considerations do not favour the above process and it can only take place on very efficient acidic sites *[4]*. Such a carbocation, once formed on the catalyst surface, may react in various ways. The primary cracking reaction is the heterolytic cleavage of the C-C bond, located in the β position corresponding to the positive charge, with the formation of a paraffin and a new carbonium ion, which continues the chain reaction *[4]*.

The thermodynamic aspects of the cracking reactions can be understood by considering the following cracking reaction.

$$C_{m+n}H_{2(m+n)+2} \rightarrow C_nH_{2n+2} + C_mH_{2m} \qquad [1]$$

The equilibrium constant K_p can be expressed in terms of the partial pressure of the reactants and products as *[5]*:

$$K_P = \frac{P_{CnH2n+2} \cdot P_{CmH2m}}{P_{C(n+m).H2(m+n)+2}}$$

The equilibrium constant can also be correlated to the change in free energy (ΔG_T) by the expression:

$-RT\ln K_p = \Delta G_T$

According to Le Chatelier's principle, cracking will proceed more readily at high temperatures and at low pressures.

This chapter is divided into two parts; in the first, the n-hexane cracking activity of ZSM-48 at different process parameters such as temperature, space velocity and H_2 : n-C_6 molar ratio are described. The effects of isomorphous substitution of the zeolite and the size of the reactant molecule are also reported. The importance of the acid strength in cracking is also examined. In the second part, the n-hexane cracking mechanism over H-ZSM-48 is examined in detail. The conversion of n-hexane (x) is plotted against the contact time (τ) at different reaction times (t) and the conversion vs. contact time plot is optimized in order to estimate the kinetic parameters. By analyzing the experimental data, the probability of the chain mechanism in the cracking network is estimated. The optimum values of the kinetic parameters at different temperatures have been calculated. Also, the average activation energy for the protolytic process and the difference in the enthalpy of adsorption between the reactant and the average product have been computed. Additionally, the reactivities of the C_2-C_4

olefins in the hydrogen transfer step, and the dependence of their yields on the zeolite pore structure, is also reported.

Part 1

3.1. n-HEXANE CRACKING OVER H-ZSM-48

3.2. INTRODUCTION

Apart from ZSM-5, other medium pore zeolites also possess shape selective cracking properties and hence can be used as octane boosting additives. In this context, it is interesting to study the cracking activity of the medium pore zeolite ZSM-48. ZSM-48 is a high silica medium pore zeolite with a disordered structure consisting of ferrierite sheets linked via bridging oxygen located on the mirror planes, and characterized by ten ring, non interpenetrating linear channels with ideal dimensions of 5.3 × 5.6 Å (see Chapter 1)

3.3. EXPERIMENTAL

ZSM-48 with different SiO_2/Al_2O_3 ratios and its Ga and Fe-analogs used in these studies were synthesized as per published procedure *[6]*. The synthesis and physicochemical characterization of the catalysts used in these studies has been reported in chapter 2. The experimental procedures adopted for the catalytic studies and product and coke analysis have also been described in Chapter 2.

3.4. RESULTS AND DISCUSSION

3.4.1. Effect of SiO_2/Al_2O_3 molar ratio

Conversion of n-hexane decreases on increasing the SiO_2/Al_2O_3 ratio of the samples (Table 3.1). The SCA (specific catalytic activity; no. of n-hexane molecules converted / Al^{3+}.sec) increases with increasing number of strong acid sites (mmol/g) (Fig. 3.1). The yields of C_2-C_4 olefins in the product increase with increasing SiO_2/Al_2O_3 ratio. A higher yield of olefins in the product is related to a lower hydrogen transfer ability *[7]*, which depends on the density of the Brönsted acid sites. Corma *et al. [8]* have shown that paraffin to olefin

Table 3.1

Influence of SiO_2/Al_2O_3 molar ratio on n-hexane cracking over H-ZSM-48

	SiO_2/Al_2O_3 molar ratio			
	228	307	394	605
Conversion (wt%)	62.8	47.8	32.6	19.4
Product distribution (wt%)				
C_1	3.2	2.7	2.0	2.7
$C_2^= + C_2$	17.7	17.2	13.5	15.1
$C_3^= + C_3$	49.5	50.2	55.1	46.0
$C_4 + C_4^=$	20.8	20.0	17.0	18.8
C_5	1.2	0.9	0.7	0.9
C_6 isomers	4.8	7.4	9.2	13.6
others	2.8	1.6	2.6	2.9
$C_2^=/C_2$	1.0	0.7	0.7	0.7
$C_3^=/C_3$	0.5	0.4	0.4	0.4
$C_4^=/C_4$	1.3	2.3	2.3	4.5
SCA[a] (10^{-3})	1.4	1.2	1.0	0.6
n[b](10^{-1})	2.0	1.7	1.0	0.9

Reaction conditions: Temperature (K) = 773; pressure =1 atm; H_2 : nC_6 (mole) = 1.5; TOS = 20min; WHSV (h^{-1}) = 1.5: [a]SCA = No. of n-hexane molecules converted/Al^{3+}.sec; [b]Deactivation coefficient (for conversion of n-hexane) determined (0 to 3 h) by fitting into Voorhies' equation ($C = a.t^{-n}$, where C = conversion, t = time on stream, n = deactivation coefficient and a = constant) *[9]*.

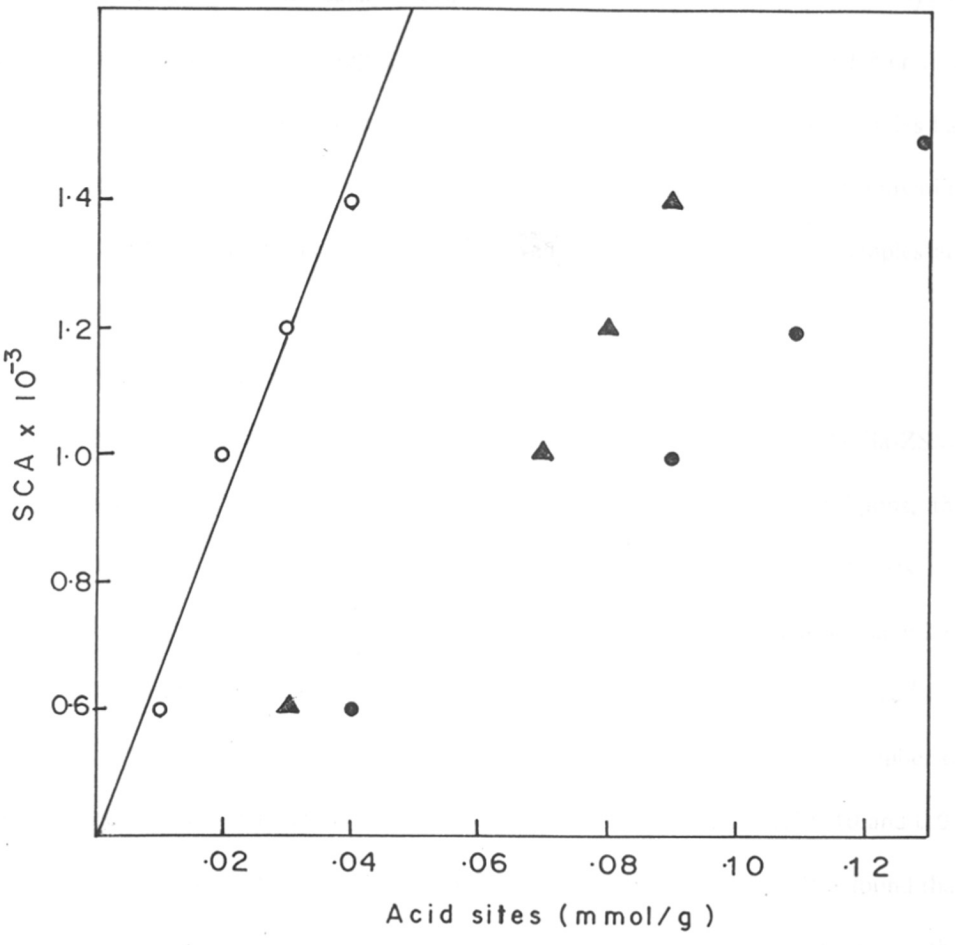

Fig. 3.1. Variation of SCA with different acid sites (mmol/g) for n-hexane cracking over H-ZSM-48: (o) strong acid sites; (▲) weak acid sites; (●) total acid sites.

ratio decreases with decreasing density of the Brönsted acid sites in HY and H-Beta zeolites during n-heptane cracking. All the catalysts deactivate rapidly in the beginning (within 1h) and then the deactivation becomes less rapid, catalysts with higher Al^{3+} deactivating faster than those with lower Al^{3+} content (Fig. 3.2). The rate of deactivation of the different samples has been quantified using the Voorhies' equation *[9]*, $C = a.t^{-n}$, where n is the deactivation coefficient for the loss of n-hexane conversion. The values of n for the different samples are presented in the last row of Table 3.1.

3.4.2. Effect of isomorphous substitution

The results of the n-hexane cracking studies carried out on H-Al-ZSM-48, H-Ga-ZSM-48 and H-Fe-ZSM-48 are presented in Table 3.2. At identical reaction conditions, the conversion of n-hexane decreases in the order Al-> Ga- > Fe-. All the three catalysts had similar SiO_2/M_2O_3 (M = Al, Ga and Fe) molar ratios and n-hexane sorption values (Table 2.4, Chapter 2). The specific catalytic activities (SCA) of the catalysts are 1.2×10^{-3}, 1.1×10^{-3} and 0.8×10^{-3}, for H-Al-ZSM-48, H-Ga-ZSM-48 and H-Fe-ZSM-48 respectively. The number of total acid sites in the three isomorphs (2,5 and 6; Table 2.4, chapter 2) are 0.11, 0.10 and 0.08 mmol/g, while the number of strong acid sites are 0.03, 0.03 and 0.02 mmol/g. It is found that the SCA values for the three samples are related to the number of strong acid sites in the samples. Similar variations in the strength of acid sites on isomorphous substitution by Fe and Ga has already been reported *[10]*. The activity of the three catalysts with duration of run is presented in (Fig. 3.2). It is found that both the Al-ZSM-48 and Ga-ZSM-48 deactivate faster than to Fe-ZSM-48 at similar reaction conditions. The deactivation coefficients for the three samples are, respectively, 0.17, 0.14 and 0.10 (Table 3.2). The lower deactivation rate of Fe-ZSM-48 is also probably related to its lower activity (Table 3.2).

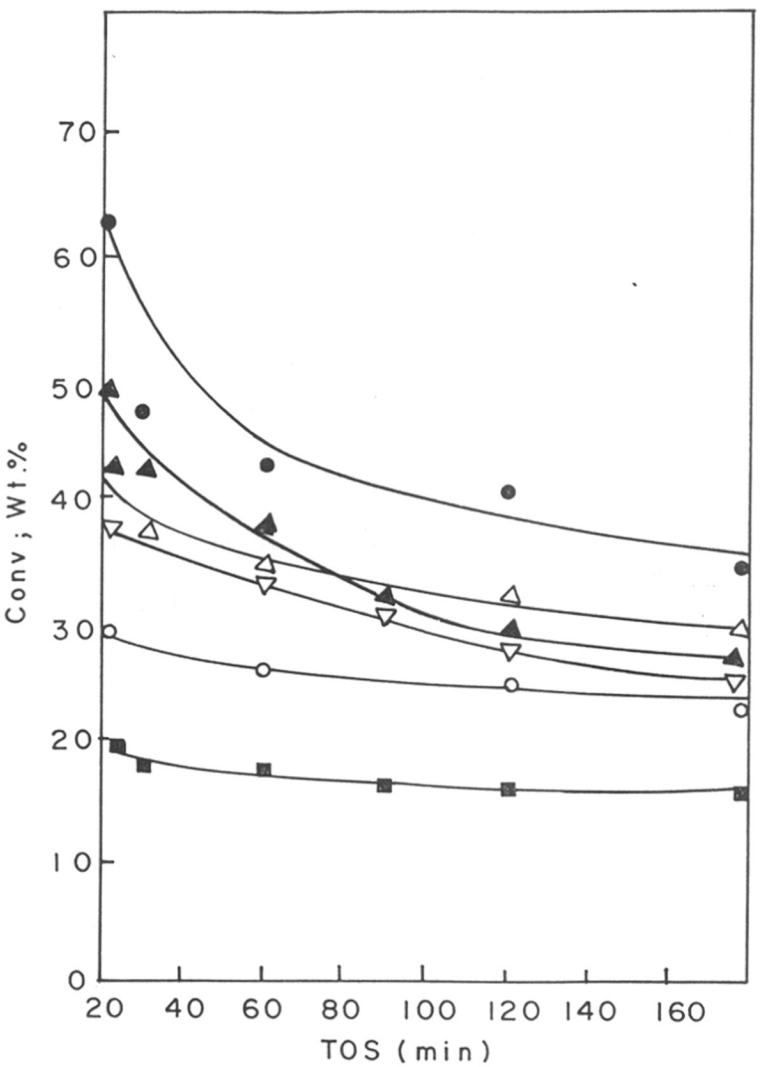

Fig. 3.2. Influence of duration of run on conversion of n-hexane over Al-, Ga-, and Fe-ZSM-48 and ZSM-48 with different SiO_2/Al_2O_3 ratios: (▲) Al-ZSM-48 (SiO_2/M_2O_3.= R = 307; (△) Ga-ZSM-48 (R = 309); (○) Fe-ZSM-48 (R = 314); (●) Al-ZSM-48 (R = 228); (▽) Al-ZSM-48 (R = 394); (■) Al-ZSM-48 (R = 605).

3.4.3. Effect of process parameters

The effect of temperature on n-hexane conversion and product distribution are presented in Fig. 3.3. As expected, both conversion and deactivation rate increase with increasing temperature. Besides, the olefin to paraffin ratios (C_2-C_4) also increase with increasing temperature. Interestingly, the iC_4 / nC_4 ratio (0.2 at 703K and 1.0 at 773K) also increases with temperature which is the opposite of what is expected from thermodynamics. Apparently, factors other than thermodynamics such as pore size effects play an important role in product formation. Fig. 3.4 shows the influence of WHSV on the conversion of n-hexane and product distribution. Conversion of n-hexane decreases rapidly from 62.7% to 48.9% on increasing the WHSV from 1.5 to 2.5, though no major decrease in conversion is noticed on further increase in WHSV. It is possible that the change in conversion is less at higher space velocities due to intraporous diffusion effects. Fig. 3.5 shows the effect of H_2 partial pressure on product distribution. Conversion of n-hexane decreases with increasing partial pressure of H_2 presumably due to a negative order with respect to H_2.

3.4.4. Effect of size of the substrate

The relative rate constants for the cracking of n-heptane, n-hexane, 3-methylpentane and 2,2-dimethylbutane over H-ZSM-48 (SiO_2/Al_2O_3 = 228) are presented in Table 3.3. Earlier workers *[11]* had reported that the cracking of n-hexane over H-ZSM-5 follows a first order rate law. The apparent first order rate constants (k) were derived from the equation, $k = (1/w) \ln [1/(1-x)]$, where w = the weight of the catalyst in g, and x = fractional conversion *[11]*. The lower cracking rates observed for 3-methyl pentane and 2,2-dimethyl butane are due to diffusion effects and spatial constraints inside the pores. Based on their studies on

Table 3.2

Influence of isomorphous substitution on n-hexane cracking

	H-Al-ZSM-48	H-Ga-ZSM-48	H-Fe-ZSM-48
Conversion (wt.%)	47.8	42.9	29.7
Product distribution (wt.%)			
C_1	2.7	3.0	1.1
$C_2^= + C_2$	17.2	17.0	13.2
$C_3^= + C_3$	50.2	50	51.1
$C_4 + C_4^=$	20.0	19.3	19.8
C_5	0.9	0.3	0.6
C_6 isomers	7.4	9.5	13.1
others	1.6	0.9	1.1
SCA[a] (10^{-3})	1.2	1.1	0.8
n[b](10^{-1})	1.7	1.4	1.0

Reaction conditions : Temperature (K) = 773; pressure = 1 atm; H_2 : nC_6 (mole) = 1.5; TOS = 20min; WHSV (h^{-1}) = 1.5: [a]SCA = No. of n-hexane molecules converted/Al^{3+}. Sec; [b]Deactivation coefficient (for conversion of n-hexane) determined (0 to 3 h) by fitting into Voorhies' equation ($C = a.t^{-n}$, where C = conversion, t = time on stream, n = deactivation coefficient and a = constant) *[9]*.

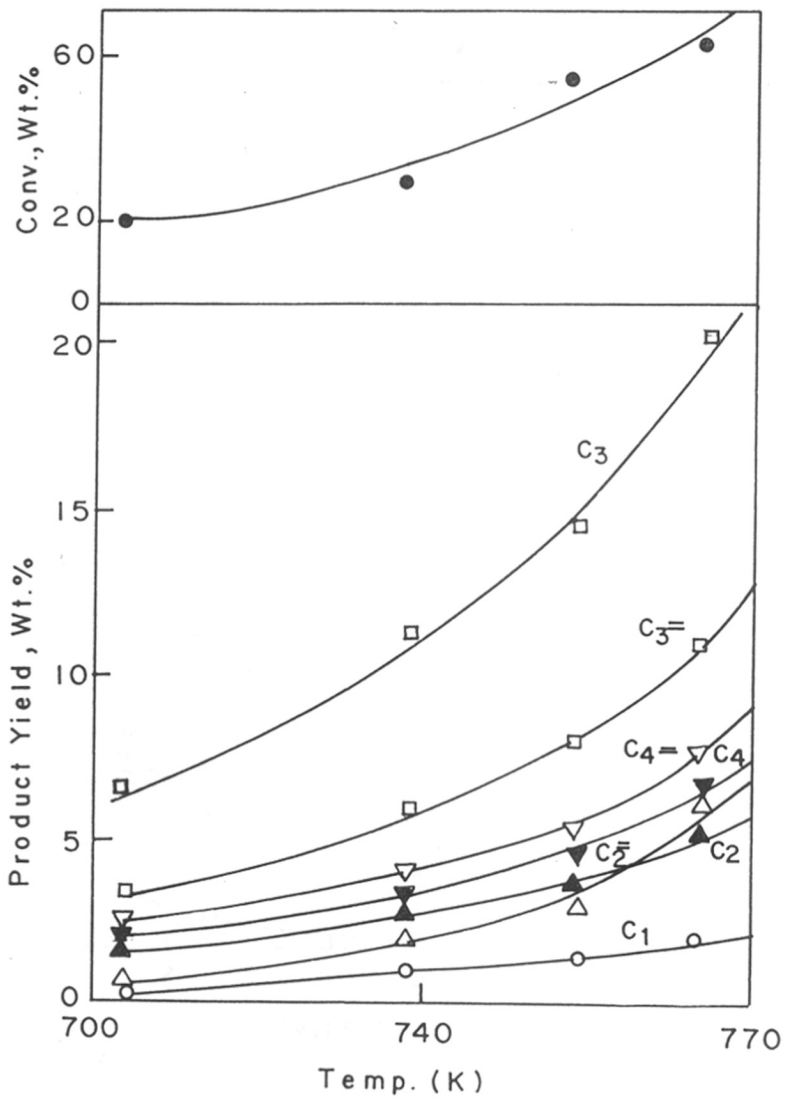

Fig. 3.3. Influence of temperature on n-hexane conversion and product yield over ZSM-48 (C_1, C_2, C_3, C_4 paraffins; $C_2^=$, $C_3^=$, $C_4^=$ olefins).

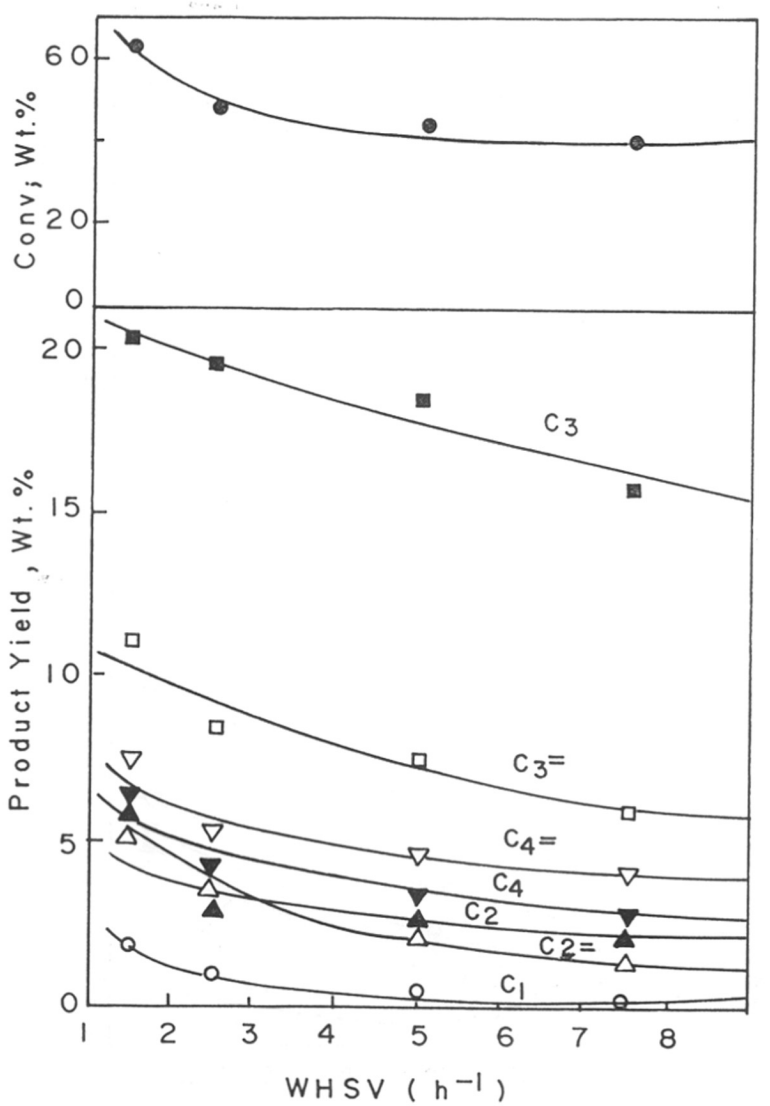

Fig. 3.4. Influence of WHSV on n-hexane conversion and product yield over ZSM-48 (C_1, C_2, C_3, C_4 paraffins; $C_2^=$, $C_3^=$, $C_4^=$ olefins).

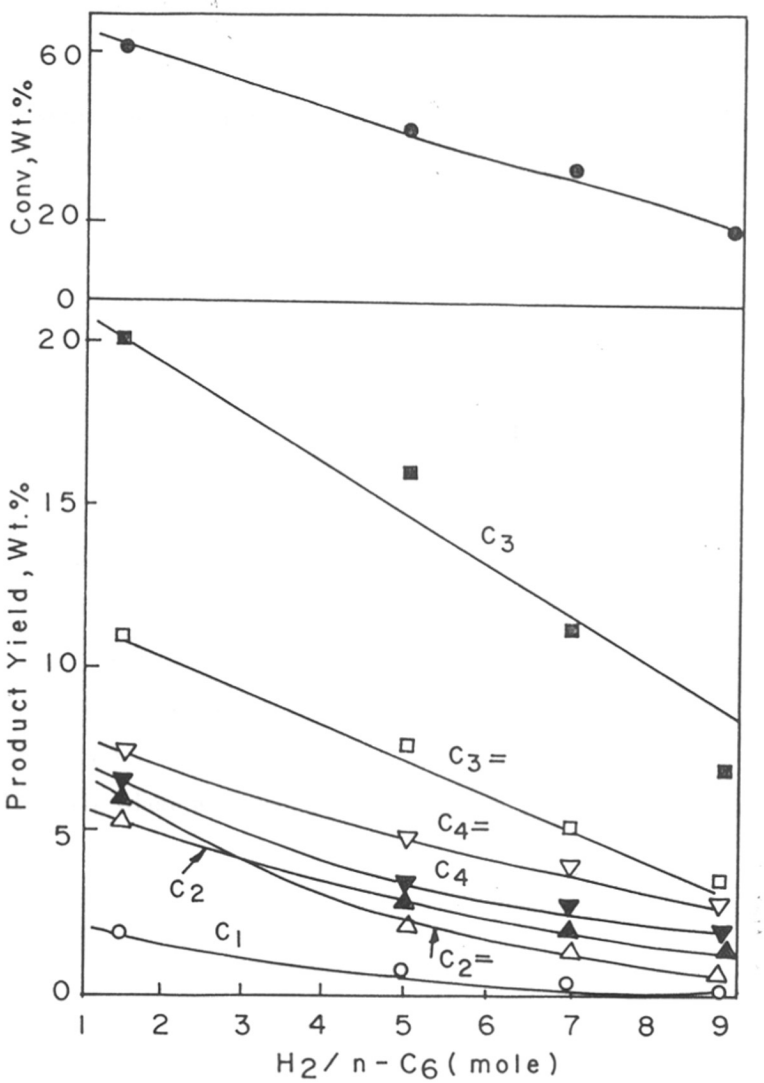

Fig. 3.5. Influence of (H_2/n-hexane) molar ratio on n-hexane conversion and product yield over ZSM-48 (C_1, C_2, C_3, C_4 paraffins; $C_2^=$, $C_3^=$, $C_4^=$ olefins).

Table 3.3

Relative rate constants and product distribution in the catalytic cracking of paraffins

	n-heptane	n-hexane	3-methylpentane	2,2-dimethylbutane
Conversion (wt%)	88.1	62.8	37.4	10.52
k_{rel}[a]	2.0	1.0	0.5	0.1
C_1	1.5	3.2	3.7	9.8
$C_2 + C_2^=$	11.4	17.7	10.9	22.1
$C_3 + C_3^=$	29.3	49.5	36.3	28.1
$C_4 + C_4^=$	22.5	20.8	18.0	16.1
C_5	2.4	1.2	2.8	3.0
C_6 isomers	24.4	4.8	20.3	13.4
Others	8.5	2.8	8.0	7.5

Reaction conditions: Temperature (K) = 773; pressure = 1 atm; H_2 : n-C_6 (mole) = 1.5; TOS = 20 min; WHSV (h^{-1}) = 1.5.

[a]K_{rel} = (1/w)ln [1/(1-x)], where w = weight of the catalyst in g, and x = fractional conversion [11].

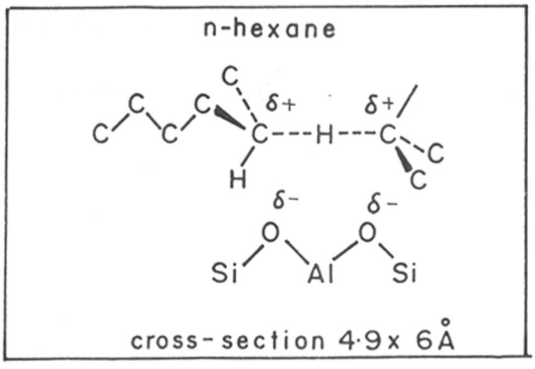

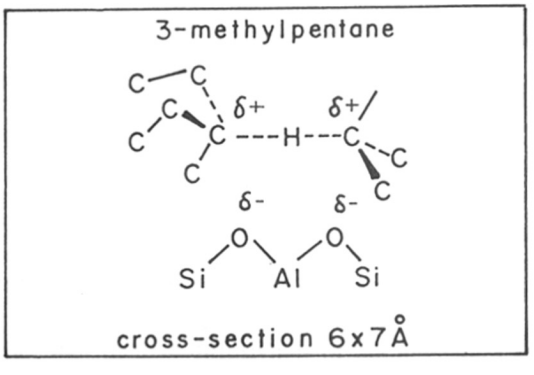

Fig. 3.6. Effective size of the transition state complexes for n-hexane and 3-methylpentane *[12]*.

cracking reactions over ZSM-5, Haag *et al. [12]* have proposed the formation of bimolecular transition state complexes during the cracking of paraffin molecules (Fig. 3.6). They have observed that the differences in the rate constants in the cracking of paraffins are not caused by the differences in diffusional mass transport between these molecules, but are mainly due to steric inhibition (in the pores of the zeolite) to the formation of the transition state complexes during the cracking of the molecules. The dimensions of the transition state complexes for n-hexane, 3-methylpentane, and 2,2-dimethylbutane are, respectively, (4.9 × 6.0 Å), (6.0 × 7.0 Å) *[12]* and (6.7 × 8.7 Å) *[13]*. These values are significantly larger than the pore dimension of ZSM-48 (5.3 × 5.6 Å). The relative cracking rates (k_{rel}) of n-hexane, 3-methylpentane, 2,2-dimethylbutane and n-heptane at 623K (WHSV = $4h^{-1}$, press. = 1atm) for ZSM-5 (SiO_2/Al_2O_3 = 79) are 1.0, 0.5, 0.1, 1.5 respectively *[14]*, which are similar to the values, 1.0, 0.5, 0.1 and 2.0, found by us for ZSM-48 at 773K (Table 3.3). The values reported by Haag *et al.[12]* are 1.0, 0.71, and 0.13, respectively, for n-hexane, 3-methylpentane and 2,2-dimethylbutane at 811K for ZSM-5 with an average crystal diameter of 2.7μm. The similarities in the values (k_{rel}) for the two different zeolites with different pore architectures (3-D for ZSM-5 and 1-D for ZSM-48) probably suggests that relative diffusivities of the molecules are more important in determining relative cracking rates.

3.5. Conclusions

The isomorphous substitution of Al by Ga or Fe and decreasing the Al^{3+} concentration decreases the conversion of n-hexane probably due to the decrease in strength and (or) number of acid sites. Conversion of n-hexane decreases with increasing space velocity and hydrogen partial pressure. Cracking activity depends on the concentration of strong acid sites.

Part 2

3.6. n-HEXANE CRACKING MECHANISM OVER H-ZSM-48

3.7. INTRODUCTION

Most of the kinetic studies reported on the cracking of C_6-paraffins have been conducted over HY and USHY (components of FCC catalysts) and detailed kinetic studies of paraffin cracking over the medium pore zeolites is scarce. Recent kinetic and mechanistic studies of the cracking of C_6-paraffins reveal that the cracking process follows both protolytic and chain reaction modes *[15-18]*. In this context, it is interesting to examine the mechanism of n-paraffin cracking over a medium pore zeolite such as H-ZSM-48.

3.8. EXPERIMENTAL

The feed n-hexane (>99%) was obtained from Merck (Bombay, India) and used without further purification. Preliminary thermal cracking experiments were carried out by pumping n-hexane through the reactor packed with inert quartz at different experimental conditions. The experiments were performed to determine the extent of the contribution of noncatalytic cracking to the total conversion of n-hexane. Thermal cracking was less than 1.2 wt.% at all the conditions. In any case, the data obtained over ZSM-48 were corrected for thermal cracking effects. Details of the experimental set-up and product analysis are described in Chapter 2.

3.9. RESULTS AND DISCUSSION

3.9.1. Theory

The kinetic model used in this study was proposed by Groten *et al.[19]*. The model accounts for monomolecular protolysis and bimolecular chain processes. Catalytic decay is accounted for by using a time on stream decay function. It assumes that the same sites

catalyze both the mechanisms and the surface reaction is the rate controlling step. An effective methodology for determining the initial selectivity of products from the experimental product yield and conversion data has been defined by Ko *et al. [20]*. For each reaction, the yield of the product is plotted against the conversion of the feed. Each of the plots is enveloped by a single curve, called the optimum performance envelope (OPE), which describes the selectivity behavior for a product as the catalyst decay approaches zero. Figures 3.7-3.9 show some of the OPE plots obtained in n-hexane cracking at 693, 723 and 773K. Initial weight selectivities of the products were estimated from the initial slope of the conversion vs. the yield of the product. The initial weight selectivities of the different products are presented in Table 3.4. Initial molar selectivities (Table 3.5) were calculated from the initial weight selectivities given in Table 3.4, using the relationship: molar selectivity = weight selectivity x (molecular weight of the feed / molecular weight of product).

Solution of the model equation yields the rate equation

$$dx/d\tau = \frac{[A_1\{(1-x\}/(1+\varepsilon x)\} + A_2\{(1-x)/(1+\varepsilon x\}^2](1+Gt)^{-N}}{1 + B\{(1-x)/(1+\varepsilon x)\}} \qquad [2]$$

where "x" is the instantaneous fractional conversion of the reactant, "τ" is the space time, "G" is the deactivation rate constant, "N" is the decay exponent, and "ε" is the volume expansion coefficient. A detailed development of the Eq. [2] is described in Appendix 1.

Considering the equilibrium between olefins and the corresponding carbenium ions, the constants A_1, A_2 and B are defined as *[19]*:

$$A_1 = \frac{(\sum k_{Mi})K_A + [\sum_i (\sum_j k_{cj})_i K_i f_i] C_{A0}}{1 + \sum K_i f_i C_{Ao}} [S]_o, \qquad [3]$$

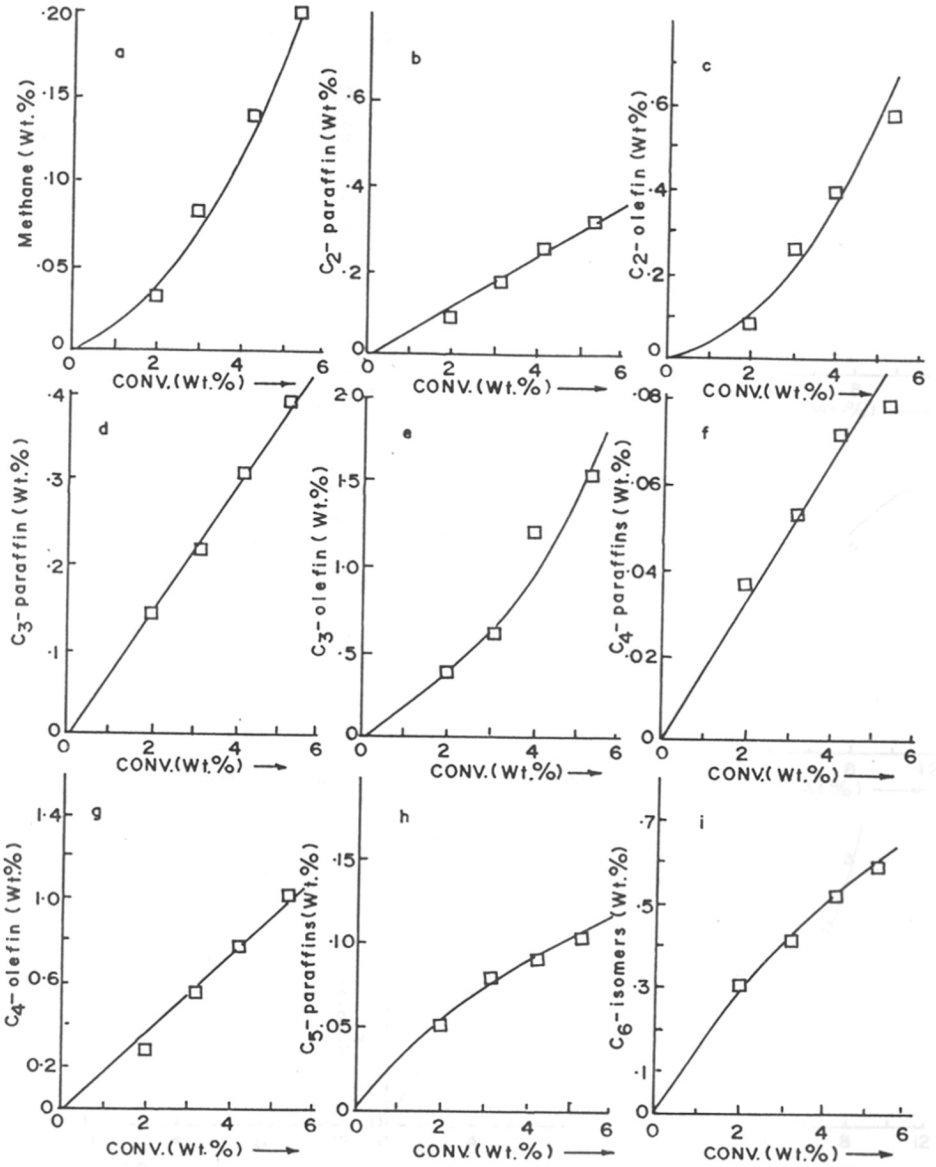

Fig. 3.7. Optimum performance envelopes for the products of the reaction of n-hexane over H-ZSM-48 at 693K: (a) methane; (b) C_2-paraffin; (c) C_2-olefin; (d) C_3 -paraffin; (e) C_3-olefin; (f) C_4-paraffins; (g) C_4-olefins; (h) C_5-paraffins; (i) C_6-isomers.

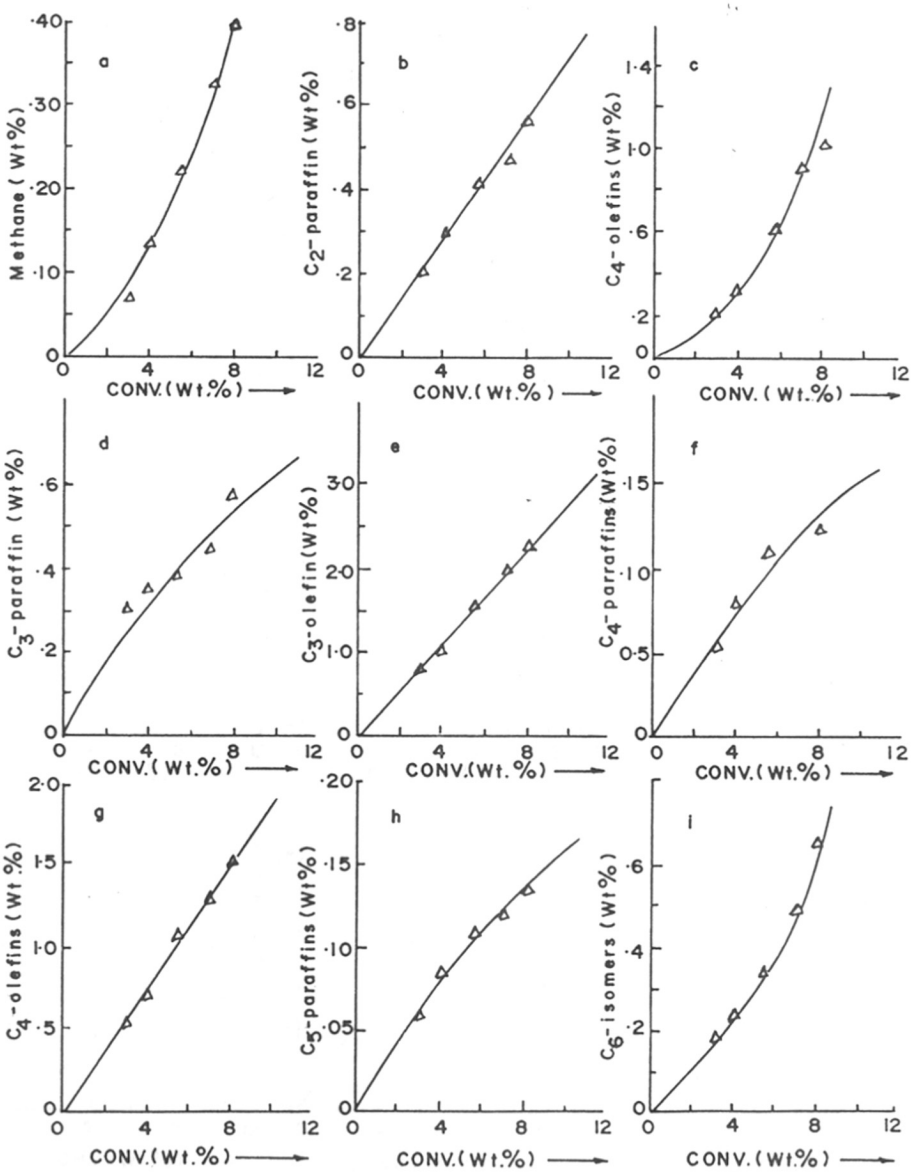

Fig. 3.8. Optimum performance envelopes for the products of the reaction of n-hexane over H-ZSM-48 at 723K: (a) methane; (b) C_2-paraffin; (c) C_2-olefin; (d) C_3 -paraffin; (e) C_3-olefin; (f) C_4-paraffins; (g) C_4-olefins; (h) C_5-paraffins; (i) C_6-isomers.

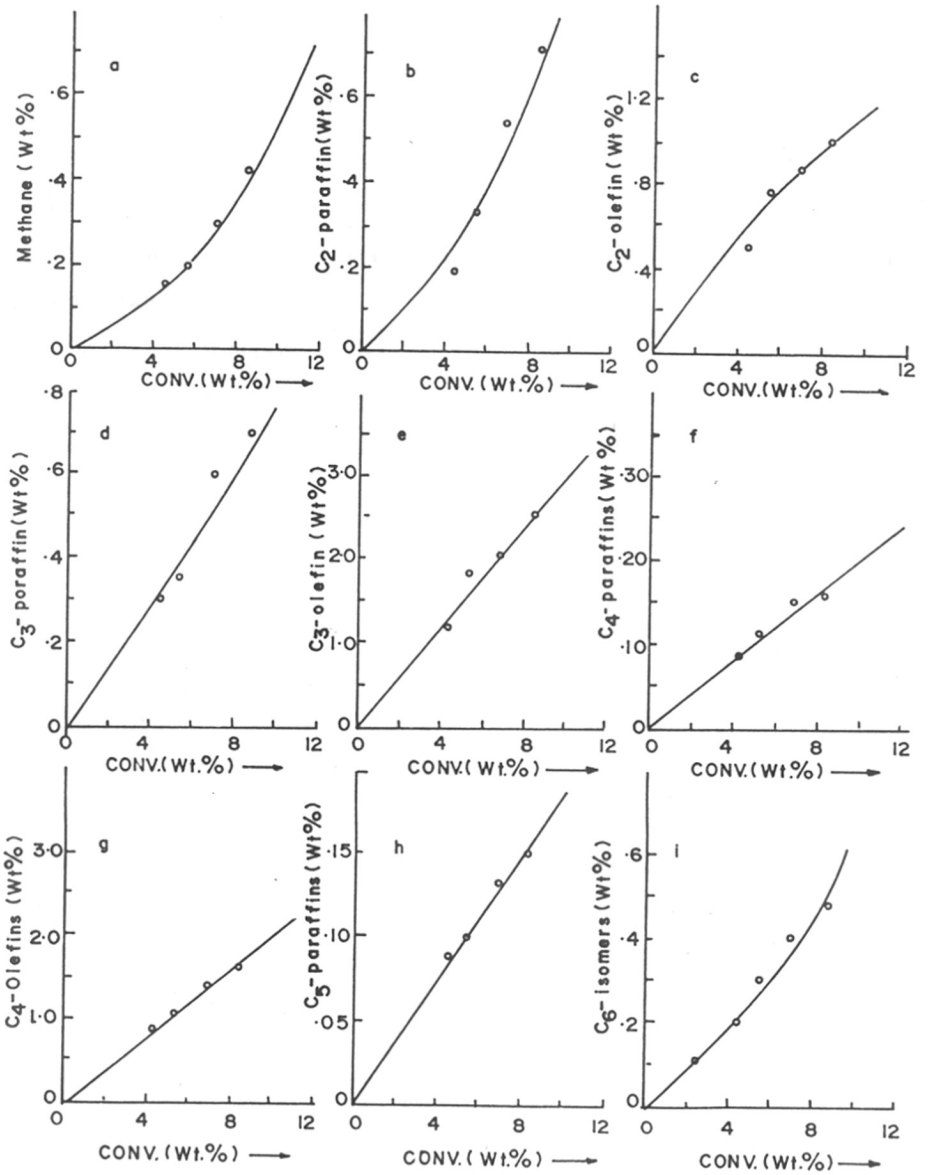

Fig. 3.9. Optimum performance envelopes for the products of the reaction of n-hexane over H-ZSM-48 at 773K: (a) methane; (b) C_2-paraffin; (c) C_2-olefin; (d) C_3 -paraffin; (e) C_3-olefin; (f) C_4-paraffins; (g) C_4-olefins; (h) C_5-paraffins; (i) C_6-isomers.

Table 3.4

Initial Weight Selectivities for Cracking Products from n-hexane over ZSM-48 in the temperature range 693-773K

	Temperature (K)		
Product	693	723	773
H_2	0.0064	0.0044	0.0035
C_1	0.0424	0.0543	0.0644
C_2-paraffin	0.0733	0.0799	0.0827
C_2-olefin	0.1009	0.1247	0.1459
C_3-paraffin	0.0640	0.0839	0.0926
C_3-olefin	0.2881	0.2637	0.2540
C_4-paraffins	0.0169	0.0209	0.0250
C_4-olefins	0.1791	0.1953	0.2058
C_5-paraffins	0.0142	0.0167	0.0193
C_5-olefins	0.0342	0.0407	0.0486
C_6-isomers	0.1200	0.0800	0.0300
C_6-olefins	0.0606	0.0391	0.0342
Coke	0.0203	0.0130	0.0091
Total	1.0204	1.0166	1.0153

Table 3.5

Initial Molar Selectivities for Cracking products from n-hexane over ZSM-48 in the temperature range 693-773K

	Temperature (K)		
Product	693	723	773
H_2	0.0300	0.0381	0.0431
C_1	0.0300	0.0372	0.0431
C_2-paraffin	0.1702	0.2296	0.2379
C_2-olefin	0.3102	0.3839	0.4480
C_3-paraffin	0.1248	0.1639	0.1829
C_3-olefin	0.5897	0.6404	0.6675
C_4-paraffins	0.0237	0.0311	0.0370
C_4-olefins	0.2867	0.3011	0.3160
C_5-paraffins	0.0167	0.0203	0.0236
C_5-olefins	0.0410	0.0498	0.0589
C_6-isomers	0.1130	0.0960	0.0320
C_6-olefins	0.0614	0.0399	0.0348
Coke	0.0159	0.0099	0.0069

$$A_2 = \frac{-[\sum_i (\sum_j k_{cj})_i K_i f_i] C_{A0}}{1 + \sum K_i f_i C_{Ao}} [S]_o , \qquad [4]$$

$$\text{and } B = \frac{[K_A - (\sum_i K_i f_i)] C_{A0}}{1 + \sum K_i f_i C_{Ao}}, \qquad [5]$$

where,

k_{Mi} is the rate constant of a feed molecule undergoing ith mode of monomolecular protolysis,
k_{Cj} is the rate constant of a carbenium ion $[C_jH_{2j+1}]^+$ and a feed molecule undergoing the jth mode of bimolecular chain reaction,
K_A is the adsorption constant of the feed molecule,
K_i is the adsorption constant of the ith product,
C_{Ao} is the initial concentration of the reactant,
$[S]_o$ is the initial concentration of the active sites and
f_i is the molar selectivity of the ith product.

The optimum values of the kinetic parameters A_1, A_2, B, G and N at different temperatures were determined using the nonlinear optimization technique based on Marquardt's method *[21]* and have been listed in Table 3.6. Using the optimum parameter values (Table 3.6), the differential Eq. [2] was integrated using the fourth order Runge-Kutta method. Fig. 3.10 shows the good fit of the experimental values of the fractional conversions of n-hexane as a function of space time for different reaction times with the theoretical curves.

3.9.2. Catalytic Cracking

Data in Tables 3.4 and 3.5 show that the major initial products are C_2, C_3 and C_4 olefins, including various skeletal isomers of the feed such as: 2,2-dimethylbutane, 2,3-dimethylbutane, 2-methylpentane and 3-methylpentane. Other important initial products

include C_2, C_3 paraffins and C_6^+ aliphatics. Small amounts of C_1, C_4 and C_5 paraffins were also detected in the product mixture.

Initial selectivities for the C_1-C_5 paraffins and C_2-, C_4-, and C_6-olefins increased with increasing temperature while those for C_6-skeletal isomers, C_3-olefin, C_6-olefins and coke decreased with temperature. The same trend was observed in the selectivities of the cracking products in the reaction of n-heptane over USHY *[22]*. This suggests that at high temperatures, the isomeric products are again cracked to produce C_1-C_5 species.

3.9.3. Reaction mechanism

The formation of C_1-C_6 paraffins and olefins can be explained as follows: the initial process involves the protonation of n-hexane on a Brönsted acid site to form a $[C_6H_{15}]^+$ carbonium ion. This carbonium ion decomposes to form either hydrogen and a n-hexane carbenium ion $[C_6H_{13}]^+$ or into a smaller paraffin $[C_{6-n}H_{2(6-n)+2}]$ and a small carbenium ion $[C_nH_{2n+1}]^+$ (where n changes from 2 to 5) which replaces the proton on the Brönsted base. All the protolytic cracking steps can be written explicity as:

$$C_6H_{14} + H^+B^- \rightarrow C_6H_{15}^+B^- \rightarrow H_2 + C_6H_{13}^+B^- \quad [6]$$
$$\rightarrow CH_4 + C_5H_{11}^+B^- \quad [7]$$
$$\rightarrow C_2H_6 + C_4H_9^+B^- \quad [8]$$
$$\rightarrow C_3H_8 + C_3H_7^+B^- \quad [9]$$
$$\rightarrow C_4H_{10} + C_2H_5^+B^- \quad [10]$$

Depending on the probabilities of the various steps, the carbenium ions in Eqs. [6]-[10] can either desorb as an olefin or participate in bimolecular chain reactions. The general form of a bimolecular reaction between a carbenium ion and a gas phase feed molecule can be written as:

$$C_6H_{14} + [C_nH_{2n+1}]^+B^- \rightarrow C_mH_{2m+2} + [C_kH_{2k+1}]^+B^- \ (n \neq m), \quad [11]$$

where $2 \leq n \leq 6$, $2 \leq m \leq 6$, and $2 \leq k \leq 6$.

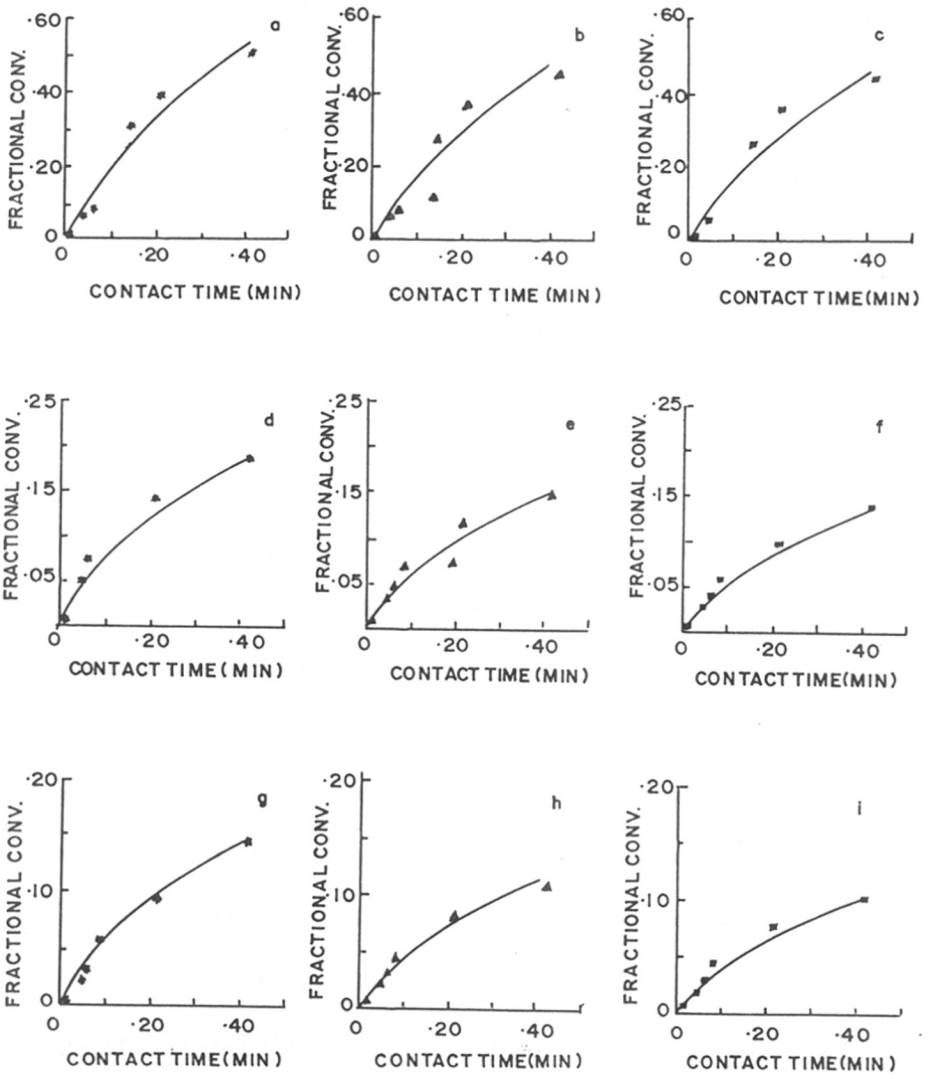

Fig. 3.10. Theoretical and experimental conversions at different temperatures and at different times on stream over H-ZSM-48: Theoretical values (line), experimental values (points): (a - c) at 693K; (d - f) at 723K; (g - i) at 773K; times on stream = 5 min (✱); 15 min (▲); 30 min (■).

The chain transfer process involves the rearrangement of the adsorbed carbenium ions before disproportionation or desorption occurs. When such a rearrangement is followed by a hydride transfer from n-hexane to the rearranged carbenium ion, isomeric paraffins are produced according to the general expression

$$C_6H_{14} + i\text{-}[C_nH_{2n+1}]^+B^- \rightarrow i\text{-}C_nH_{2n+2} + [C_6H_{13}]^+B^- \qquad [12]$$

After hydride transfer from n-hexane, the carbenium ion $[C_6H_{13}]^+B^-$ is formed, which undergoes a number of hydride shifts to form a variety of C_6 isomers. In the last step or in the chain termination step, desorption of the carbenium ion takes place as an olefin after β-scission or remains on the surface to form coke.

The results in Table 3.6, reveal that cracking of n-hexane over H-ZSM-48 proceeds predominantly via a monomolecular protolytic pathway and the probability of the protolytic cracking increases with temperature. Table 3.6, shows that both the parameters A_1 and A_2, increase with increasing temperature, and at all temperatures the value of A_1 is greater than the corresponding value of A_2. It is known that in a system where chain cracking is kinetically significant, the parameter A_2 will be negative and smaller in magnitude than A_1. The sum of A_1 and A_2 which is related to the contribution of the monomolecular process to the total conversion is found to increase with temperature. Thus it can be concluded that chain mechanism becomes much less significant than the protolytic process at higher temperatures.

The parameter B as described in Eq. [5] signifies the relative value of the adsorption constants of the reactant and products. The values for B are found to increase (more positive) with increasing temperature. The change in the magnitude of B from -0.918 at 693K to -0.901 at 773K suggests that the products are more strongly adsorbed on the active sites at lower temperatures and start desorbing at higher temperatures. The same trend in values of B has

been observed in n-nonane cracking over HY also *[23]*, whereas a reverse trend was observed during the cracking of n-hexadecane *[15]* and 2,2,4-trimethylpentane over HY in the temperature range, 573-673K. Therefore, it can be inferred that the competitive adsorption between the reactant and the products during paraffin cracking depends upon the feed and product properties and perhaps also on the catalyst characteristics.

The large consistently negative values of B imply that

(i) $\Sigma K_i f_i C_{Ao} > 1$, [13]

i.e., the system is in the region of high surface coverage by the reaction products

and

(ii) $\Sigma K_i f_i > K_A$, [14]

which indicates that the products are more readily adsorbed than the reactant. Eq.[5] upon substituting from Eq.[13] , results into

$$B = \frac{K_A}{\Sigma K_i f_i} - 1, \qquad [15]$$

which can be further simplified as

$$B + 1 = \frac{K_A}{\Sigma K_i f_i}, \qquad [16]$$

$$= \frac{K_A}{K_P . \Sigma f_i}, \qquad [17]$$

where $K_p = \Sigma K_i.f_i / \Sigma f_i$, is the weight averaged adsorption constants for the product species.

Eq. [17] can be rearranged to give

$$K_A / K_P = (B + 1) \Sigma f_i . \qquad [18]$$

Eq. [5] after substitution from Eq.[14] and simplification reduces to

$$K_P = \frac{-B}{(1 + B) \Sigma f_i C_{A0}} \qquad [19]$$

K_A / K_P (Eq. [18]) is representative of the ratio of adsorption constants for the reactant and products. The K_A / K_P (Eq. [18]) and K_P (Eq. [19]) values were calculated separately at different temperatures and are presented in Table 3.6. The data in Table 3.6, suggest that the reactant competes for adsorption sites more successfully at higher reaction temperatures, whereas, the K_P values indicate a rapid decrease in the surface coverage by products at higher temperatures. The slope of the plot of log (K_A / K_P) vs. 1/T (Fig.3.11) gives the difference in enthalpy of adsorption between the feed and the average product. The value of $\Delta\Delta H_{ads}$ ($\Delta H_P - \Delta H_A$) is 1.95 kcal/mole as calculated using Van't Hoff relationship *[24]* in the temperature range 693-773K. It is apparent that at high temperatures, under either of the two assumptions, the reactant will compete for adsorption sites more successfully.

Further information about the rate constant is obtained by adding Eqs. [3] and [4] to get

$$A_1 + A_2 = \frac{\Sigma k_{Mi.} K_A}{1 + \Sigma K_{pi} f_i C_{Ao}} [S]_o . \qquad [20]$$

By rearranging the Eqs. [20] and [5] the total specific rate of monomolecular cracking can be extracted as

$$\Sigma k_{Mi} [S]_o = \frac{A_1 + A_2}{B + 1} (1/K_A + C_{Ao}). \qquad [21]$$

Substituting Eq. [13], into Eq. [21] we get

$$\Sigma k_{Mi}[S]_o = \frac{A_1 + A_2}{B + 1}(C_{Ao}). \qquad [22]$$

Further, the substitution of Eq. [14] into Eq. [21] results in

$$\Sigma k_{Mi} K_A[S]_o = \frac{A_1 + A_2}{B + 1}. \qquad [23]$$

The values of $\Sigma k_{Mi}[S]_o$ and $\Sigma k_{Mi} K_A[S]_o$ under high and low surface coverage conditions respectively, were calculated (see Table 3.6). The slope of the plot of $\ln\{\Sigma k_{Mi}[S]_o\}$ vs 1/T and $\Sigma k_{Mi} K_A[S]_o$ vs 1/T yields the apparent activation energies for these two cases (Figs. 3.12a & 3.12b). Figs. 3.12a & 3.12b show the nonlinear increase in the monomolecular protolytic cracking rate constant values with increasing temperature. This finding is consistant with the product selectivity data (Tables 3.4 and 3.5) which show that the relative importance of the various cracking modes changes with temperature *[25]*. The E_a values for high and low surface coverage conditions are 21.0 kcal/mole and 19.3 kcal/mole respectively, which are much lower than the C-C bond dissociation energy (81 kcal/mole) *[26]*. A low activation energy has also been observed for cumene cracking over HY zeolite *[26]*.

The higher initial selectivities of C_4 and C_3 olefins, compared to the C_2 olefin (Table 3.4) can be explained by considering the formation of a bimolecular transition state complex during hydride transfer from n-hexane to lower olefins. According to Haag *et al. [12]* the cross-section of the transition state complex during the hydride transfer reaction between a secondary carbenium ion and n-hexane is 4.8×6.0 Å. The sizes of the transition state complexes between n-hexane and a primary carbenium ion or a tert-butyl carbenium ion are 4.8×6.1 Å or 5.2×6.7 Å, respectively *[13]*. This implies that the reaction between n-hexane

Table 3.6

Optimum and Calculated values of Kinetic Parameters in the Cracking of n-hexane over H-ZSM-48 in the temperature range 693-773K

Kinetic parameters	Temperatures (K)		
	693	723	773
A_1 (min^{-1})	0.168	0.304	0.978
A_2 (min^{-1})	-0.009	-0.095	-0.100
B	-0.918	-0.913	-0.901
G (min^{-1})	90.03	98.00	99.99
N	0.301	0.260	0.221
K_A/K_P[a]	0.143	0.168	0.201
K_P[b] (lit/mol)	377.38	337.73	298.73
C_{A0} (mol/lit)	0.017	0.016	0.015
log (K_A/K_P)	-0.844	-0.774	-0.696
$\Sigma k_{Mi}[S]_o$[c] ($mol.lit^{-1}.min^{-1}$)	0.033	0.038	0.133
$\Sigma k_{Mi} K_A[S]_o$[d] (min^{-1})	1.970	2.403	8.868
ln $\{\Sigma k_{Mi}[S]_o\}$	-3.411	-3.270	-2.017
ln$\{\Sigma k_{Mi} K_A[S]_o\}$	0.678	0.876	2.182

[a]Determined according to Eq. [18].

[b]Determined according to Eq. [19].

[c]Determined according to Eq. [22].

[d]Determined according to Eq. [23].

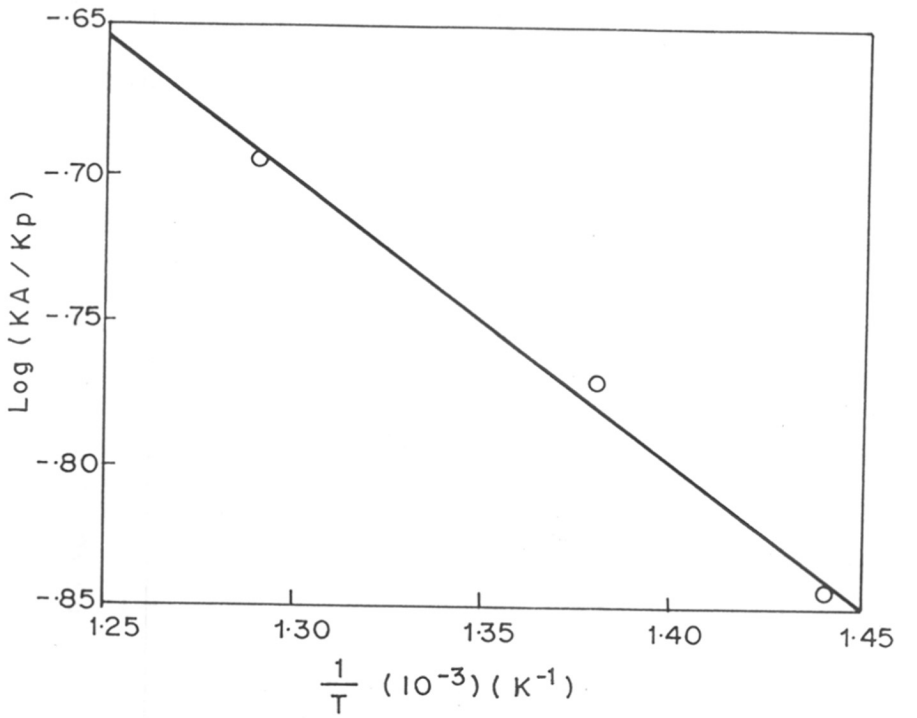

Fig. 3.11. Variation of log (K_A/K_P) with reaction temperature for n-hexane conversion over H-ZSM-48.

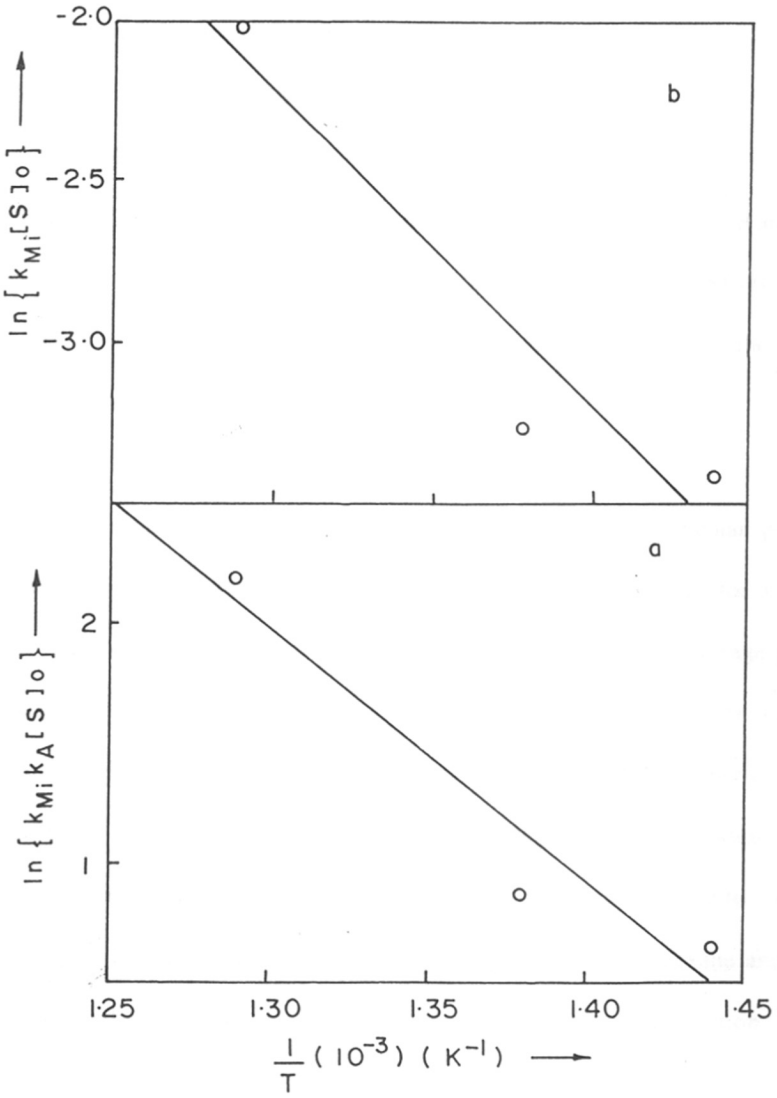

Fig. 3.12. Arrhenius plot for n-hexane protolytic cracking on H-ZSM-48 in the temperature range 693-773K: (a) high surface coverage condition; (b) low surface coverage condition.

and the tert-butyl carbenium ion should be strongly constrained inside the pores of ZSM-48, since the cross-section of ZSM-48 is 5.3×5.6 Å. Lukyanov *et al. [27]* have showed that the hydrogenation activity of C_3 and C_4 olefins depends on the void space inside the zeolite. Among HY, H-mordenite and H-ZSM-5, H-mordenite had the highest hydride transfer activity, whereas H-ZSM-5 had the least activity. By comparing our results, with those obtained over H-ZSM-5 *[28]* at the same temperature, it is found that the initial selectivity for C_4 paraffins are more in H-ZSM-5 as compared to H-ZSM-48. This may be due to the greater formation of the bimolecular hydride transfer transition state complex at the channel intersections in H-ZSM-5.

3.10. Conclusions

In this part a general kinetic model that includes both monomolecular protolytic cracking and bimolecular chain cracking mechanisms is shown to be applicable for a medium pore zeolite like H-ZSM-48. The ratio of the adsorption of the feed and the average product, as well as the change in enthalpy show that the probability of the adsorption of the reactant is greater (compared to the product) at higher temperatures. This explains the higher probability of the monomolecular processes at higher temperatures during n-hexane cracking over H-ZSM-48. The lower yield of C_4 paraffins compared to C_3 and C_2 paraffins is due to the strong steric inhibition to the formation of a transition state complex between n-hexane and a tert-butyl carbenium ion in the channels of H-ZSM-48 during the hydride transfer reaction.

Appendix 1

The assumptions involved in the development of the general model *[19]* are:

(a) all cracking reactions are irreversible and

(b) surface reactions are rate limiting

The initiating monomolecular reaction involves the adsorption of the reactant as a carbonium ion followed by the protolysis, resulting in the formation of a gas phase paraffin and a residual surface carbonium ion. The residual surface ion can desorb to form an olefin product or undergo a bimolecular reaction with a second gas phase reactant molecule. A simplified scheme of kinetically important reactions can be represented by

$$A + S \underset{K_{Pi}}{\overset{K_A}{\longrightarrow}} AS \xrightarrow[A]{\sum k_{Mi}} n_i P_i + S \qquad [1]$$

$$P_i + S \longrightarrow P_i S \xrightarrow[(\sum k_{Cj})_i]{} n_i P_i + S \qquad [2]$$

where A is the reactant, P_i the ith product, S an active site on the catalyst, K_A and K_{Pi} are the equilibrium adsorptoion constants for the reactant, A, and the ith product, respectively, $\sum k_{Mi}$ is the sum of the rate constants for the various modes of the monomolecular cracking, while $(\sum k_{Cj})_i$ is the sum of the rate constants for the bimolecular reaction between the ith surface species and the reactant, and n is the stoichiometric factor for the formation of the ith product.

A differential rate expression is obtained by assuming that the surface reactions are rate-limiting and that all adsorption reactions are at equilibrium. The surface concentrations of the adsorbed reactant and products can be expressed as

$$[AS] = K_A[S]\,[A]; \qquad [3]$$

$$[P_iS] = K_{Pi}[P_i]\,[S]. \qquad [4]$$

The expression governing the time rate of change in A will be

$$-r_A = (\sum k_{Mi})\,[AS] + (\sum_i (\sum_j k_{Cj})_i\,[P_iS])\,[A] \qquad [5]$$

Using Eqs., [3] and [4] to substitute for the surface concentrations in [5] gives

$$-r_A = (\sum k_{Mi})\,K_A[S]\,[A] + (\sum_i (\sum_j k_{Cj})_i\,K_{Pi}[P_i])\,[S][A] \qquad [6]$$

Next, a site balance is carried out on the active sites. There are three possible states in which a site may exist: in a pristine state, free of adsorbed species; with an adsorbed reactant or a product of reaction on it; or it may be deactivated. It is assumed that the sites decay according to the time-on-stream function. If subscripts 0 and d represents initial sites and deactivated sites, respectively, then a balance on the sites gives

$$[S] = [S]_o - [AS] - \sum_i[P_iS] - [S]_d \qquad [7]$$

$$[S] = [S]_o - \left[K_A\,[A] + \Sigma_i K_{pi}\,[P_i]\right][S] - [1 - (1 + Gt)^{-N}]\,[S]_o \qquad [8]$$

where $(1 + Gt)^{-N}$ is the fraction of sites still active at time t. Solving for [S] and substituting into [6] results in

$$-r_A = \frac{[(\sum k_{Mi})K_A\,[A] + (\sum_i (\sum_j k_{Cj})_i\,K_{Pi}[P_i])[A]]\,[S]_o\,(1 + Gt)^{-N}}{1 + K_A\,[A] + \sum K_{Pi}[P_i]} \qquad [9]$$

It is assumed that the concentration of product species, $[P_i]$, involved in the bimolecular cracking and competitive adsorption reactions are proportional to the conversion of the reactant thus:

$[P_i] = f_i\,([A]_o - [A])$, where f_i represents the moles of ith product formed per mole of feed reacted, i.e, the molar selectivity. The molar selectivity of the ith product is the sum over all

reactions of the probability S_j, for each reaction, times the stoichiometric factor for the production of i in this jth reaction, n_j. Thus,

$$f_i = \sum_j (S_j n_j). \qquad [10]$$

Summing over all i products gives

$$\sum_i \sum_j (S_j n_j)_i = \sum_i f_i = 1 + \varepsilon. \qquad [11]$$

where ε is the volume expansion coefficient for the reaction and is assumed to be constant with respect to conversion. This parameter is experimentally determined using initial selectivity data.

It is convenient to express the concentration of the reactant in terms of the dimensionless variable x, the fractional conversion of the reactant:

$$[A] = [A]_o \frac{(1 - x)}{(1 + \varepsilon x)} \qquad [12]$$

$$= C_{Ao} \frac{(1 - x)}{(1 + \varepsilon x)} \qquad [13]$$

The reactions under consideration here are normally carried out in plug-flow reactors. Recalling that the design equation for a plug flow reactor is

$$- r_A = C_{Ao} \frac{dx}{d\tau} \qquad [14]$$

where τ is the space time.

Using these relationships and Eq. [9] gives

$$dx/d\tau = \frac{[A_1\{(1-x\}/(1+\varepsilon x)\} + A_2\{(1-x)/(1+ \varepsilon x\}^2] (1 + Gt)^{-N}}{1 + B\{(1-x)/(1 +\varepsilon x)\}}, \qquad [15]$$

$$A_1 = \frac{(\sum k_{Mi})K_A + [\sum_i (\sum_j k_{cj})_i K_i f_i] C_{A0}}{1 + \sum K_i f_i C_{Ao}} [S]_o, \qquad [16]$$

$$A_2 = \frac{-\left[\sum_i \left(\sum_j k_{cj}\right)_i K_i f_i\right] C_{A0}}{1 + \sum K_i f_i C_{Ao}} \quad [S]_o \text{ and} \qquad [17]$$

$$B = \frac{\left[K_A - \left(\sum_i K_i f_i\right)\right] C_{A0}}{1 + \sum K_i f_i C_{Ao}}. \qquad [18]$$

References

1. Plank, C. J., Rosinski, E. J., and Hawthorne, W. P., *Ind. Eng. Chem. Prod. Res. Dev.*, **3,** 165 (1964).
2. Plank, C. J., Rosinski, E. J., and Givens, E. N., US. Pat 4,141,859 (1979).
3. Chester, A. W., Cormier, W. E., and Stoner., A., US. Pat 4368,114 (1983).
4. Cumming, K. A., and Wojciechowski, B. W., *Catal. Rev. Sci. Eng.*, **38,** 101 (1996).
5. Dercroocq, D., "Catalytic Cracking of Heavy Petroleum Fractions", Technip 1984, p 32.
6. Valyocsik, E. W., Eur. Patent, 0142317 (1984).
7. Pines, L. A., Maher, P. J., and Watcher, W. A., *J. Catal.*, **85,** 466 (1984).
8. Corma, A., Fornes, V., Monton, J. B., and Orchilles, A. V., *J. Catal,* **107,** 288 (1987).
9. Voorhies', A., *Ind. Eng. Chem.*, **37,** 318 (1945).
10. Chu, C. T .W., and Chang, C. D., *J. Phys. Chem.*, **89,** 1569 (1985).
11. Wang, I., Chen, T. J., Chao, K. J., and Tsai, T. C., *J. Catal.*, **60,** 140 (1979).
12. Haag, W. O., Lago, R. M., and Weisz, P. B., *Faraday Discussion.*, **72,** 317 (1982).
13. Size of the intermediate for 2,2-dimethylbutane is calcuted using INSIGHT II module supplied by Biosym. Inc, using a Silicon Graphics Work Station (Indigo 2).
14. Borade, R. B., Hegde, S. G., Kulkarni, S. B., and Ratnasamy, P., *Appl. Catal.*, **13,** 27 (1984).
15. Abbot, J., and Wojciechowski, B. W., *J. Catal.*, **113,** 353 (1988).
16. Abbot, J., *J. Catal.*, **126,** 628 (1990).
17. Wielers, A. F. H., Vaarkamp, M., and Post, M. F. M., *J. Catal.*, **127,** 51 (1991).
18. Zhao, Y., Bamwenda, G. R., and Wojciechowski, B. W., *J. Catal.*, **142,** 465 (1993).
19. Groten, W. A., and Wojciechowski, B. W., *J. Catal.*, **140,** 262 (1993).
20. Ko, A. N., and Wojciechowski, B.W., *Prog. React. Kinet.*, **12,** 201 (1983).
21. Marquardt, D. W., "An Algorithm for Least Squares Estimation of Non Linear Parameters", J. Soc. Ind. Appl. Math, Vol 11, 1963, p 431.
22. Corma, A., Monton, J. B., and Orchilles, A.V., *Appl. Catal.*, **16,** 59 (1985).
23. Abbot, J., and Wojciechowski, B. W., *J. Catal.*, **109,** 274 (1988).

24. Clark, A., "The theory of Adsorption and Catalysis", Academic Press, New York, 1970.
25. Zhao, Y., Bamwenda, G. R., Groten, W. A., and Wojciechowski, B. W., *J. Catal.*, **140,** 243 (1993).
26. Best, D. A., and Wojciechowski, B. W., *J. Catal.*, **47,** 343 (1977).
27. Lukanov, D. B., *J. Catal.*, **147,** 494 (1994).
28. Abbot, J., *Appl. Catal.*, **57,** 105 (1990).

CHAPTER IV

AROMATIZATION OF (C_4-C_6) HYDROCARBONS

4.0. INTRODUCTION

The transformation of lower hydrocarbons (C_2-C_6) into aromatics over zeolites is an industrially important reaction. A number of processes such as Cyclar (BP-UOP) *[1]*, M-2 forming (Mobil) *[2]* and Aroforming (IFP-SALUTEC) *[3]* for the transformation of C_2-C_6 hydrocarbons are available. These processes are believed to be based on promoted H-ZSM-5. The aromatization of C_3-C_5 hydrocarbons over H-ZSM-5 has been studied by many authors *[1-7]*. The excellent activity of ZSM-5 in aromatizing alkanes has been attributed mainly due to the high acidity and correct pore geometry. In this context, it is interesting to compare the performance of other medium-pore high silica zeolites with different pore geometries. It has been observed that the addition of promoters such as Ga_2O_3 or ZnO to the zeolite (HZSM-5) improves its aromatization activity *[8-9]*. The Ga-oxide provides sites necessary for dehydrogenation activity *[10]*. A favourable combination of Lewis and Brönsted acidity has been suggested to be a necessary condition for an active and selective catalyst for the aromatization of lower alkanes *[11]*. The yield of aromatics become significant only at temperatures beyond 753K and the reaction is often conducted around 800K. At these elevated temperatures, catalyst deactivation tends to be rapid necessitating frequent regenerations. In fact, the Cyclar process operates in a continuous catalyst regeneration mode *[1]*

At low temperatures, the ΔG_F (free energy of formation) values of the paraffins are lower than those of the corresponding olefins, and thus the hydrogenation of the olefins readily occures, whereas, at high temperatures the dehydrogenation of the paraffins is thermodynamically favoured (Fig.4.1). For example, at temperatures lower than 1093K, the hydrogenation of ethene has a negative change in free energy, and the reaction is thermodynamically favoured. At 1093K, the lines of ethane and ethene intersect, (Fig. 4.1) no change of free energy in the reaction is observed, and the equilibrium is at an intermediate

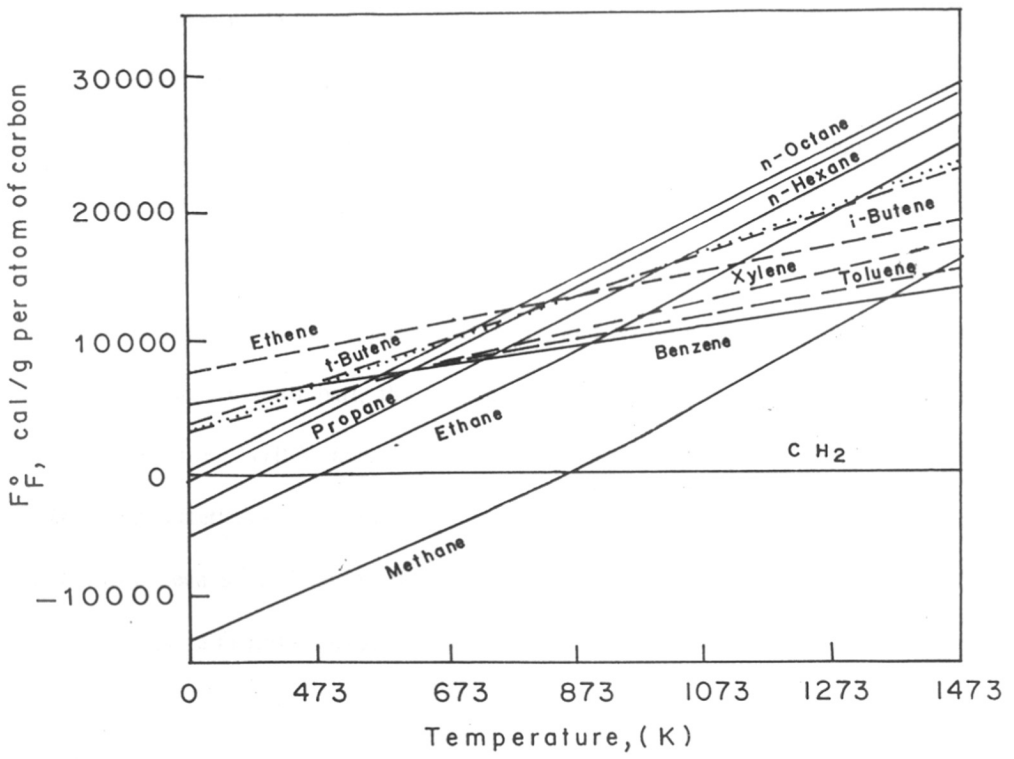

Fig. 4.1. Free energy of formation of hydrocrarbons, per carbon atom, as a function of temperature.

position. At higher temperatures, ethane has a higher free energy of formation than ethene, and dehydrogenation is more favoured. The temperature of inversion of the hydrogenation-dehydrogenation equilibrium is lower when the number of carbon atoms in the molecule is larger. Fig.4.1 shows that, at high temperatures, aromatic hydrocarbons are more stable than the corresponding paraffins. For this reason, paraffin dehydrocyclization is thermodynamically favoured under these conditions *[12]*.

This chapter is made up of three parts; in the first part, a comparative study of the aromatization of n-butane, 1-butene and n-hexane over the three medium pore zeolites, ZSM-5, ZSM-22 and EU-1, is discussed; in the second part, the influence of different promoters such as Ga_2O_3, ZnO, Cr_2O_3 and Fe_2O_3 on product yields and deactivation characteristics of promoted H-ZSM-5 in the aromatization of n-hexane is discussed. The effect of reaction pressure and the presence of added gases such as H_2 and N_2 on catalyst deactivation is also discussed; finally in the third part, the influence of different process parameters such as temperature, pressure, WHSV and H_2:oil (mole ratio) on the product yield and the deactivation characteristics of platinum promoted Ga_2O_3/H-ZSM-5 at different reaction conditions have been studied during the aromatization of a commercial mixture of C_5-C_7 hydrocarbons (light raffinate) is reported.

Part-1

4.1. A COMPARISON OF THE 1-BUTENE, n-BUTANE AND n-HEXANE AROMATIZATION ACTIVITIES OF THE THREE MEDIUM PORE ZEOLITES, ZSM-5, ZSM-22 AND EU-1.

4.2. EXPERIMENTAL

Samples of ZSM-22 and EU-1 used in these studies were synthesized as per published procedure. The detailed synthesis procedures of these catalysts have been described in chapter 2. The Na-form of these zeolites were converted into the NH_4^+-form by repeated exchanges (thrice) with ammonium nitrate solution. The NH_4^+-form of these zeolites were then dried and calcined in air to yield H-forms. The H-zeolites were compacted into discs (20mm x 2mm) using a hydraullic press and then broken into pieces (16-20 mesh). Generally 2-3 g samples diluted with 5ml quartz chips of the same size were used in the catalytic studies. The experimental setups used in the studies and methodology for product and coke analysis have been reported in chapter 2.

4.3. AROMATIZATION OF 1-BUTENE

4.4. RESULTS AND DISCUSSION

4.4.1. Influence of reaction temperature

The results of the transformation of 1-butene over the three catalysts at different temperatures in the range 723-813K are presented in Fig.4.2. The conversion of 1-butene (100 - %1-butene in the product) is more over ZSM-5 and ZSM-22 than over EU-1. The values of conversion for ZSM-5, ZSM-22 and EU-1 are, respectively, 96.78%, 91.02% and 79.97% at 723K and 99.08%, 96.73% and 92.02% at 813K. If one were to consider the other C_4 compounds in the products as unconverted material, then the conversion values for ZSM-5,

ZSM-22 and EU-1 will be, respectively 82.03%, 55.76% and 19.62% at 723K and 90.85%, 81.30% and 58.34% at 813K. It appears, therefore that EU-1 is much less active than the other two zeolites even though they all possess similar SiO_2/Al_2O_3 ratio (Table 2.5 ; chapter 2). If we examine the product distribution over the three zeolites, we find that the yield of aromatics decreases in the order ZSM-5 > ZSM-22 > EU-1.

A comparative distribution of the products over the three zeolites at the same operating conditions are presented in Table 4.1. In general, toluene is the major aromatic compound produced, while xylenes are the least produced. This is surprising, as one would expect 1-butene to dimerize to yield mostly xylenes. Their reduced yield is apparently due to their undergoing rapid disproportionation, transalkylation and dealkylation reactions producing toluene as one of the products.

Under the reaction conditions, only traces of the primary product, viz., C_8 aliphatics were detected in the mixture of products. As seen from the sequence of the reactions shown above, low molecular weight (C_1-C_3) hydrocarbons are also produced in large amounts from a number of side reactions.

The yields of benzene and toluene increase with temperature for all the three zeolites, while the yield of the C_8 aromatics remains nearly constant over ZSM-5 and EU-1 (Fig. 4.2). The near constant yields of the C_8 aromatics (the primary aromatic compounds) in the product on increasing the temperature is a result of their undergoing further transformation to yield the other aromatics and light gases. The yield of the C_1-C_2 fraction decreases (Fig. 4.2) in the case of ZSM-22 (along with an increase in C_8 aromatics) suggesting that at least a part of the C_1 and C_2 fractions is produced from the dealkylation of the C_8 aromatic fraction. The reason for the above build up of the C_8 aromatics at higher temperatures, which is the reverse of the trend observed over ZSM-5 and EU-1 is not clear. However, the yield of total aromatics increases

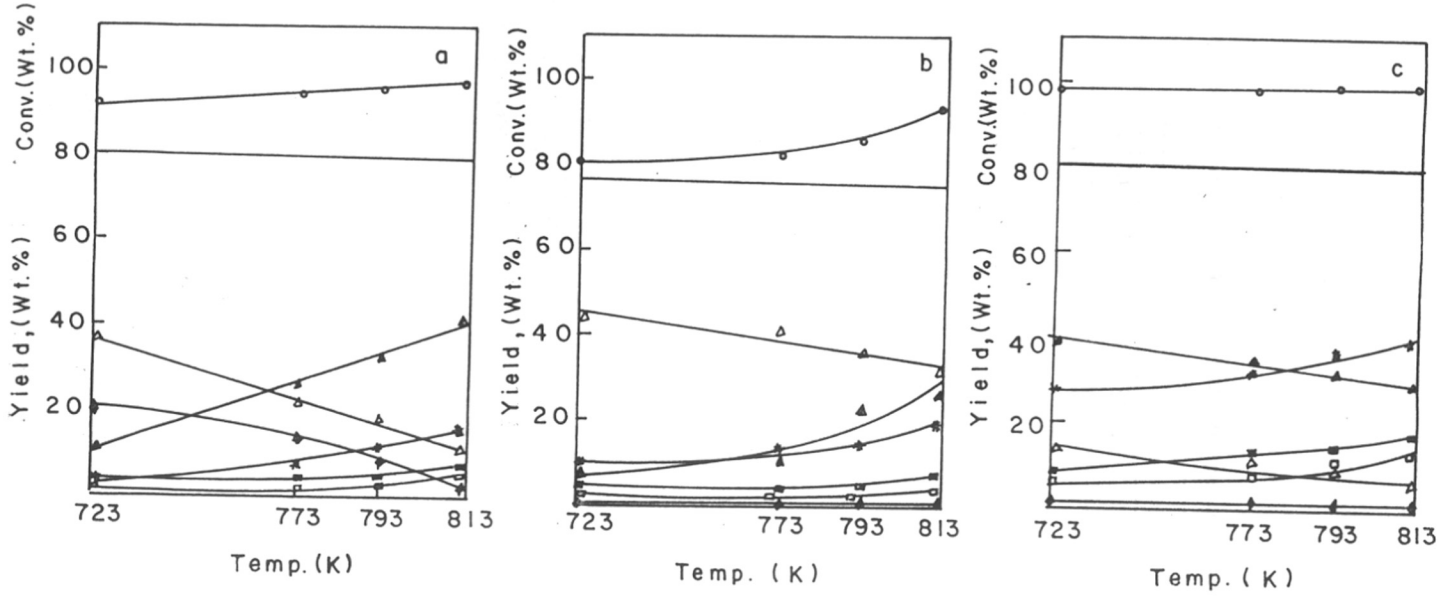

Fig. 4.2. Influence of temperature on conversion and product yield for the aromatization of 1-butene (a) ZSM-22; (b) EU-1; (c) ZSM-5: (▲) $C_3 + C_3^=$; (△) $C_4 + C_4^=$; (♦) C_5 - C_8 alip.; (✱) Arom.; (■) Tol; (□) Bez.
Reaction conditions: WHSV (h^{-1}) = 2; pressure = 0.1MPa; N_2/ 1-butene (mole) = 1.5; TOS = 1h.

Table 4.1

Product distribution over the three zeolites for 1-butene aromatization

	Product distribution (wt.%)		
	H-ZSM-5	H-ZSM-22	H-EU-1
% Conversion	98.6	95.0	85.2
∑Aromatics	32.3	13.1	10.0
C_1	2.0	1.9	1.3
$C_2 + C_2^=$	21.9	15.0	3.9
$C_3 + C_3^=$	34.3	30.4	31.4
$C_4 + C_4^=$	7.8	28.2	50.2
C_5^+	1.3	10.8	1.4
Benzene	9.5	2.2	1.9
Toluene	17.1	5.9	4.9
C_8 Aromatics	5.8	4.8	3.9
C_8^+	0.3	0.8	1.0

Reaction conditions: Temperature = 793K; WHSV (h^{-1}) = 2; H_2/1-butene (mole) = 1.5; pressure = 0.1 MPa; TOS = 1h.

(as expected) with temperature. An interesting observation is the yield of large quantities (12% at 823K) of the C_5^+ fraction over ZSM-22 when compared to the trace quantities (<1%) obtained over the other two zeolites. Besides, the yield of C_5^+ increases with temperature in the case of ZSM-22 (Fig. 4.2) while it decreases in the case of ZSM-5 and EU-1. It is probable that the restricted pore system in the ZSM-22 and its weak acidity (see Table 4.1) are mainly responsible for the build up of the intermediate C_8 aromatics and C_5^+ aliphatic compounds.

Under these conditions, a significant amount of C_3 's are also formed. Abbot *et al. [13]* studied the cracking of C_6-C_{16} alkanes over HY and concluded that the cracking reaction is initiated by the direct C-C cleavage of linear alkanes and proceeds through the formation of a carbonium ion intermediate. The carbonium ion thus formed releases a proton and produces the corresponding olefins. Based on the experimental data for n-butane cracking of over H-ZSM-5, Ono *et al. [6]* have shown that the ratio of different carbonium ions formed during cracking is: $C_3H_7^+ : C_2H_5^+ : C_4H_9^+ = 42 : 38 : 20$. This observation explains the higher yield of C_3's during aromatization of paraffins and olefins.

4.4.2. influence of added gases on catalyst deactivation

The deactivation rate of the three zeolites in the presence of the diluent gases, N_2 and H_2 are presented in fig. 4.3. It is found that catalyst deactivation is faster in nitrogen than in hydrogen (Fig. 4.3) for all the zeolites. This is probably due to hydrogenation of the polyunsaturated hydrocarbons (coke precursors) in the hydrogen atmosphere. ZSM-5 deactivates at a slower rate than the others, especially in N_2, although it produces larger amounts of aromatics. The reasons for the greater stability of ZSM-5, may be the greater propensity of ZSM-5 to crack down coke precursors due to its greater acidity (Table 2.5; chapter 2) and the faster desorption of the coke precursors through the more open (3D) and

relatively large pore system in ZSM-5. In general, the yield of aromatics is more in the presence of N_2 than H_2.

4.5. AROMATIZATION OF n-BUTANE

4.6. RESULTS AND DISCUSSION

The results of the transformation of n-butane at identical conditions over ZSM-5, ZSM-22 and EU-1, are presented in Table 4.2. It is observed that n-butane is much less reactive than 1-butene. Even H-ZSM-5 converts only 58.7% of n-butane while it converts 98.6% of 1-butene. Comparing tables 4.1 and 4.2, we note that the aromatic yields are more in the case of ZSM-5 during 1-butene aromatization than when n-butane is used as the feed. In the case of EU-1 and ZSM-22 the aromatic yields are similar with both reactants.

4.7. AROMATIZATION OF n-HEXANE

4.8. RESULTS AND DISCUSSION

4.8.1. Influence of reaction temperature

The influence of temperature of the reaction on conversion and product yields over the three zeolites is presented in Fig. 4.4. The conversion of n-hexane over ZSM-5 is nearly 100% at all the temperatures in the range, 723-813K. In the same range of temperatures, the conversion is between 60 to 90% in the case of ZSM-22 and between 43 to 51% in the case of EU-1. The critical diameter of n-hexane is 0.47 nm and its length is 1.03 nm *[14]*. The cracking of n-hexane over ZSM-5 has been reported by previous workers *[15,16]* to be free of diffusion effects even in crystallites of sizes exceeding 5 μm. It is therefore very likely that n-hexane conversion is not diffusion limited in our case also. As all the zeolites have similar SiO_2/Al_2O_3 ratios, the lower conversions recorded over ZSM-22 and EU-1 may be due to differences in acid strength.

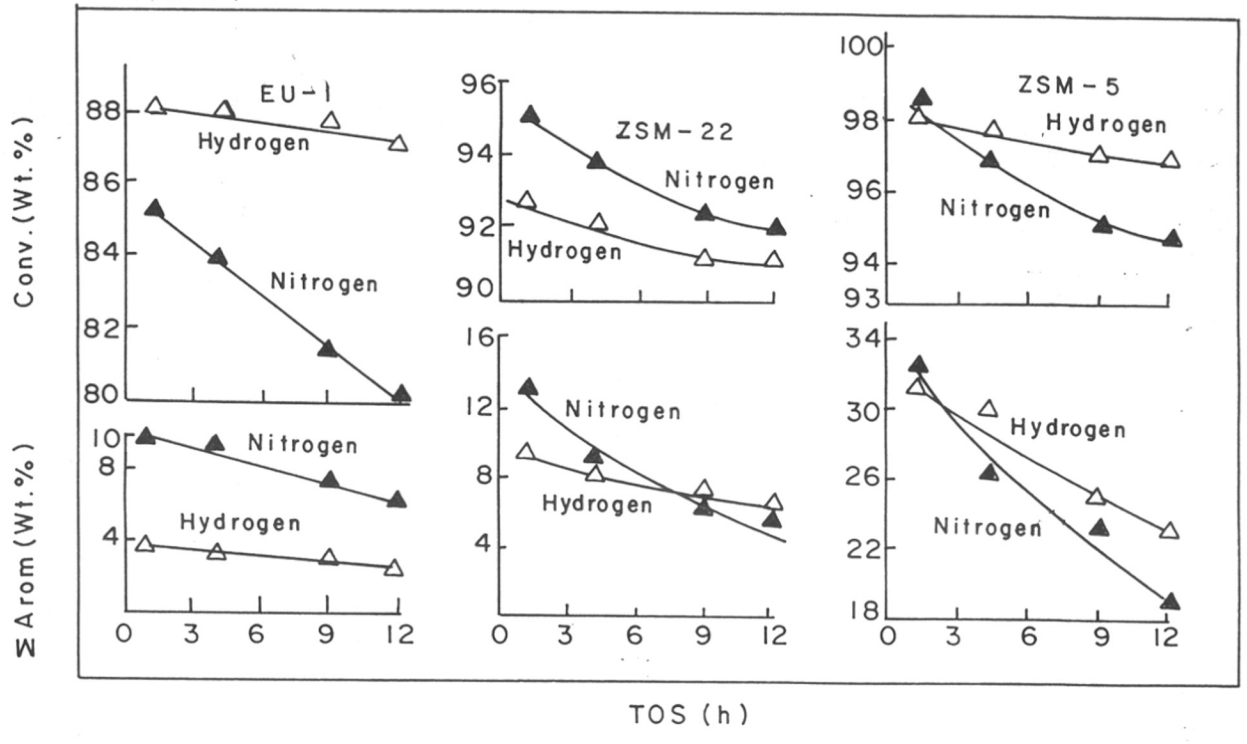

Fig. 4.3. Deactivation of catalysts with duration of run for the aromatization of 1-butene.
Reaction conditions: Temperature = 793K; WHSV (h^{-1}) = 2; pressure = 1 atm; Gas/ 1-butene (mole) = 1.5.

Table 4.2

Product distribution over the three zeolites for n-butane aromatization

	Product distribution (wt.%)		
	H-ZSM-5	H-ZSM-22	H-EU-1
% Conversion	58.7	42.2	39.5
∑Aromatics	16.1	10.9	10.1
C_1	4.2	4.7	4.3
$C_2 + C_2^=$	17.5	19.7	20.2
$C_3 + C_3^=$	36.4	36.3	36.2
$C_4 + C_4^=$	11.3	10.2	10.6
C_5^+	3.2	3.2	3.0
Benzene	5.8	5.0	4.0
Toluene	14.5	14.5	14.7
Ethyl benzene	0.8	0.7	0.8
Xylenes	5.5	4.8	5.3
C_8^+	0.8	0.9	0.8

Reaction conditions: Temperature = 793K; WHSV (h^{-1}) = 2; H_2/n-butane (mole) = 1.5; pressure = 0.1 MPa; TOS = 1h.

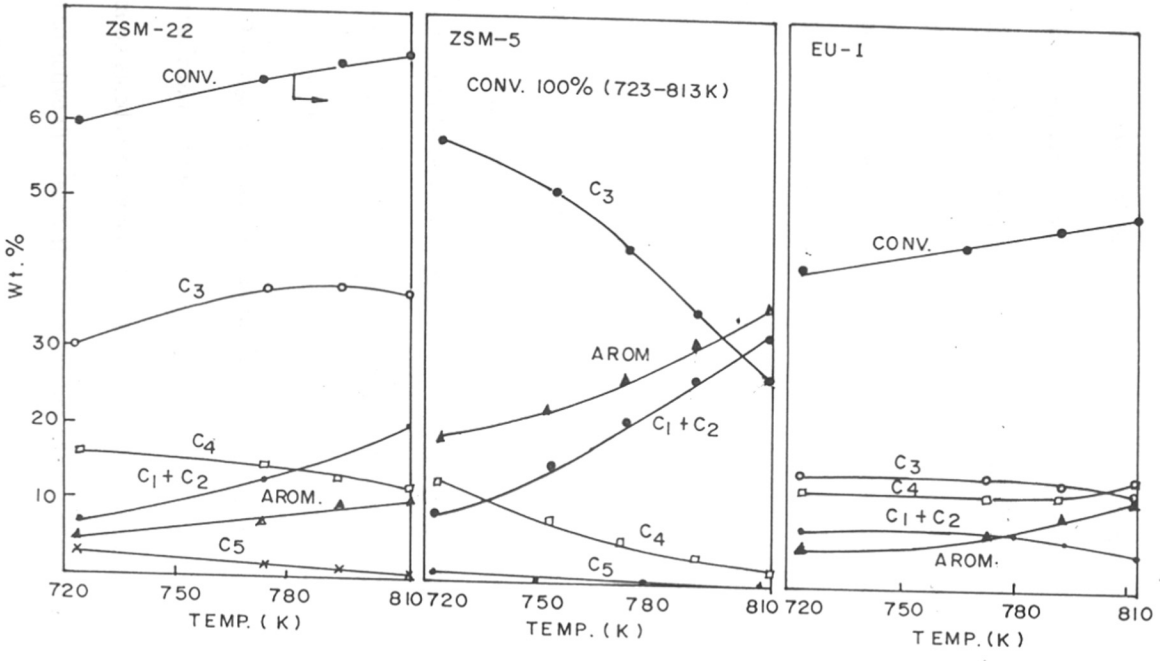

Fig. 4.4. Influence of temperature on conversion and product yield for the aromatization of n-hexane. Reaction conditions: WHSV (h^{-1}) = 2; pressure = 1 atm; H_2 / n-C_6 (mole) = 1.5; TOS = 1h.

The apparent activation energies (E_a) for the cracking of n-hexane are 19 ± 2 and 22 ± 3 KJ/mole for EU-1 and ZSM-22 in the temperature range 573 to 673K, while the activation energy is 60 ± 4 KJ/mole for ZSM-5 in the temperature range 533 to 593K. The rates of n-hexane cracking at 573K (WHSV, $2h^{-1}$; H_2/n-C_6 (mole), 1.5; pressure (total), 1 atm) for ZSM-5, ZSM-22 and EU-1 are respectively, 3.6×10^{-6}, 7.4×10^{-7} and 5.8×10^{-7} moles/g/sec. The small E_a values for EU-1 and ZSM-22 also suggest the possibility of diffusion effects in these catalysts. In addition, other factors arising from the difference in the location of the T_d-Al^{3+} sites and the inherent differences in activity per Al site could also explain the lower activities of ZSM-22 and EU-1 when compared to ZSM-5.

The yield of aromatics is significantly greater over ZSM-5 than over ZSM-22 or EU-1. Apparently, again the pore size restrictions are responsible for the poorer aromatic yields over ZSM-22 and EU-1. The critical diameter of the benzene ring is 0.68 nm *[14]* which is larger than the maximum pore diameters of these zeolites. In the case of ZSM-5, the aromatic compounds can easily be formed at the channel intersections. EU-1 produces (Fig 4.4) slightly more aromatics than ZSM-22 (12.3 % vs 10.8%) at 813K even though the conversion is lower (49.2% vs 89%). Again the C_8^+ aromatics yield is also larger (2.52% vs 0.88%) at this temperature (Fig. 4.4). It appears that the large side pockets (in EU-1; see chapter 1, section) are responsible for the greater yields of aromatics.

4.8.2. Influence of contact time

The data obtained at different contact times for the three catalysts are presented in Fig 4.5. ZSM-5 is so active that nearly the same amount of aromatics (about 10.5%) is produced at a contact time nearly 10 and 8 times smaller than over ZSM-22 and EU-1, respectively ((W/F) = 0.05 h for ZSM-5, 0.48 h for ZSM-22 and 0.40 h for EU-1). The n-hexane conversions at these contact times are 78% for ZSM-5, 87% for ZSM-22 and 50% for EU-1.

At the same contact time of 0.48 h, the yield of aromatics is nearly three and two times greater over ZSM-5 than over ZSM-22 and EU-1, respectively.

4.8.3. Influence of added gas on catalyst deactivation

The deactivation characteristics of the three zeolites (at 793K) are presented in Fig. 4.6. ZSM-5 deactivates the least even though it produces the greatest amount of aromatics. No significant decrease in conversion is noticed over ZSM-5 for about 50 h on stream (conversion ~ 100%) in both H_2 and N_2 atmospheres. On the other hand, ZSM-22 and EU-1 deactivate quickly, with both conversion and aromatic yields decreasing rapidly with time (Fig. 4.6). The deactivation is faster in the presence of N_2. Apparently, the presence of H_2 helps in the removal of coke precursors from the catalyst surface leading to a longer life. The reason normally given for the low coking tendency of ZSM-5 is that bimolecular reactions involving larger molecules leading to coke cannot take place inside the narrow pores of ZSM-5 (restricted transition state selectivity) *[17]*. The faster deactivation of ZSM-22 and EU-1 (also with similar narrow pores) compared to ZSM-5 is probably due to the unidimensional nature of the pore systems in EU-1 and ZSM-22 as opposed to the 3D pore system in ZSM-5 and the faster desorption of the coke precursors through the more open and relatively larger pore system in ZSM-5.

4.9. A comparison of aromatization of different hydrocarbons

A comparison of the aromatization of n-butane, 1-butene and n-hexane over H-ZSM-5 is presented in Table 4.3. Both the 1-butene and n-hexane crack rapidly, the conversion being 91.4 and 100%, at 793K, while the conversion of n-butane is only 58.7% at the same reaction condition. The yield of aromatics is about 32% from 1-butene and n-hexane, while it is only 16.1% from n-butane. Thermodynamic data suggest that hydrocarbon-to-aromatic conversion becomes more favourable as the carbon number increases. Also, the formation of aromatics is

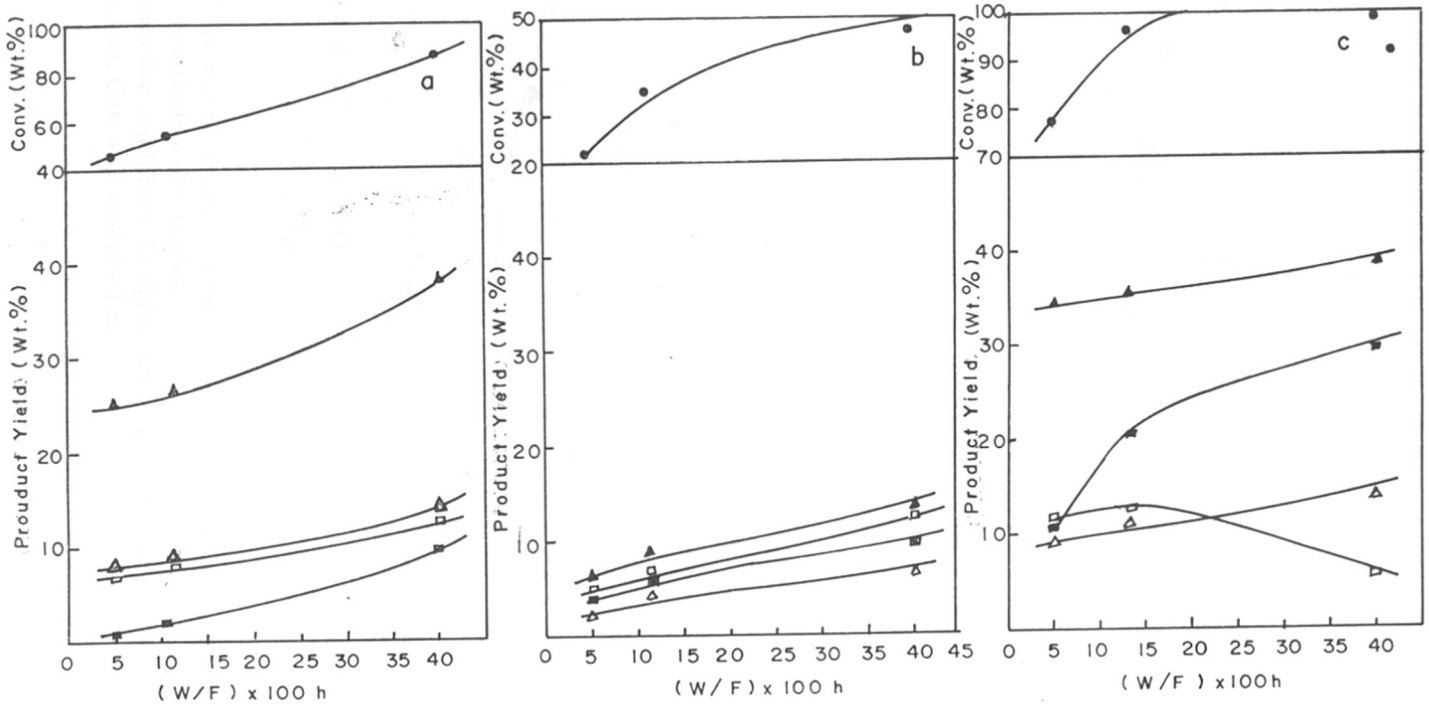

Fig. 4.5. Influence of n-hexane contact time on conversion and product yield (a) ZSM-22; (b) EU-1; (c) ZSM-5: (▲) $C_3 + C_3^=$; (△) $C_2 + C_2^=$; (□) $C_4 + C_3^=$; (■) aromatics .
Reaction conditions: Temperature = 793K; pressure = 1atm; H_2 / n-C_6 (mole) = 1.5; TOS = 1h.

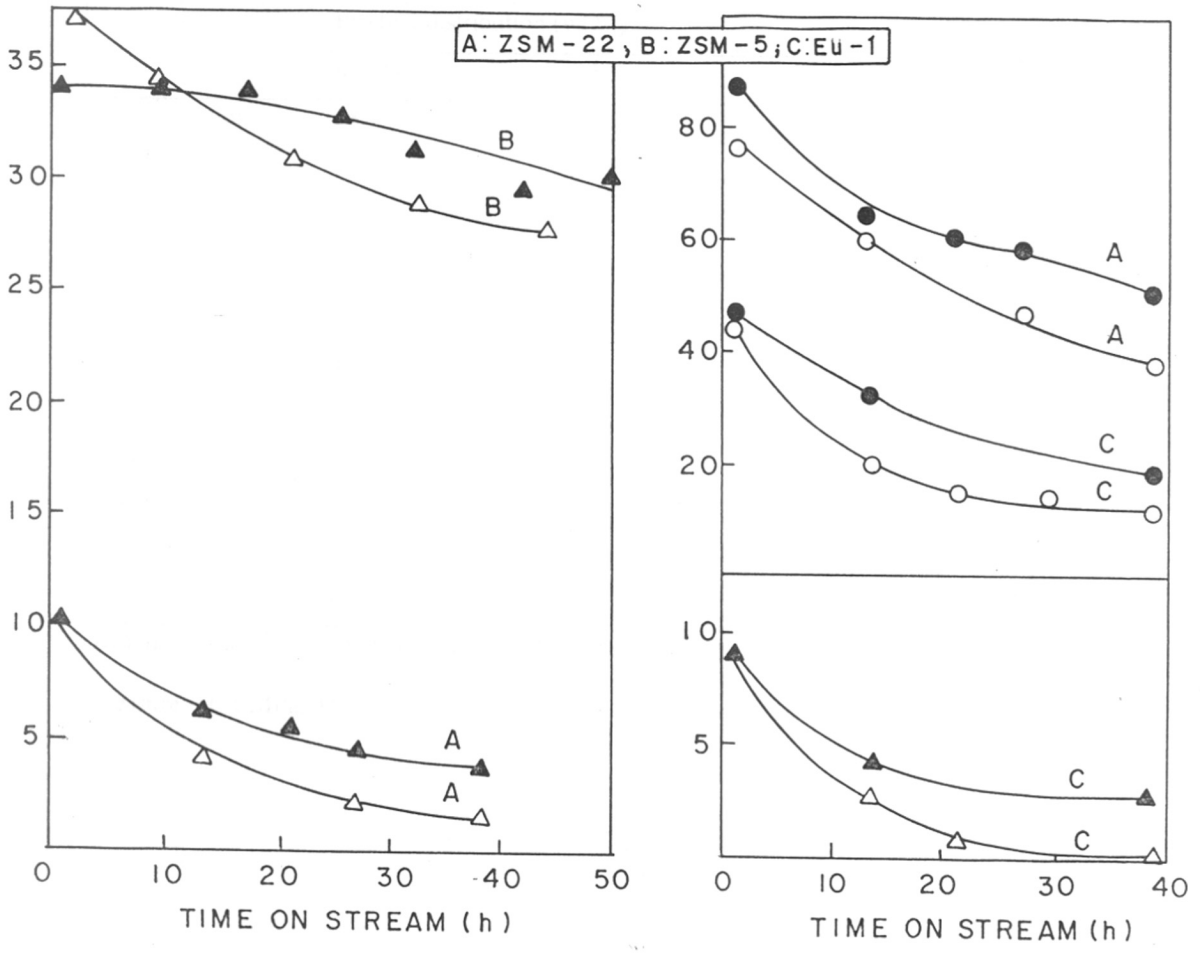

Fig. 4.6. Influence of duration of run on conversion and aromatic yield for the aromatization of n-hexane.
Reaction conditions: Temperature = 793K; WHSV (h^{-1}) = 2; pressure = 1 atm; Gas/ n-C_6 (mole) = 1.5.

Table 4.3

Aromatization of n-butane, 1-butene and n-hexane over H-ZSM-5

	Product distribution (wt.%)		
	n-butane	1-butene	n-hexane
% Conversion	58.7	98.6	100
∑Aromatics	16.1	32.3	32.1
C_1	4.2	2.0	11.3
$C_2 + C_2^=$	17.5	21.9	15.8
$C_3 + C_3^=$	36.4	34.3	36.3
$C_4 + C_4^=$	11.3	7.8	4.1
C_5^+	3.2	1.3	0.3
Benzene	5.8	9.5	8.1
Toluene	14.5	17.1	13.1
C_8 aromatics	6.3	5.8	6.7
C_8^+	0.8	0.3	4.2

Reaction conditions: Temperature = 793K; WHSV (h^{-1}) = 2; H_2/hydrocarbon (mole) = 1.5; pressure = 0.1 MPa; TOS = 1h.

more favoured from olefins than from paraffins of the same carbon number. Thus, from the thermodynamic considerations, one would expect greater conversion of n-hexane and 1-butene into aromatics (at 773K) when compared to n-butane.

4.10. Conclusions

The experimental data suggest that lower alkanes dimerize over protonic sites of the strongly acidic zeolites. The dimers may isomerize and decompose to produce a variety of compounds depending on the path of the reaction.

Though, at the temperature of the reaction, dehydrogenation of alkanes to alkenes is thermodynamically not a very favoured reaction, the aromatization reaction is highly favoured (Table 4.5). From the kinetic angle, the quick removal of the alkenes formed from alkanes is required to attain a high conversion rate of alkanes. The removal of alkenes by oligomerization depends on the strength of the acid sites.

Among the catalysts studied, ZSM-5 shows greater activity than ZSM-22 and EU-1 during the transformation of n-butane, 1-butene and n-hexane to aromatics. Though all the catalysts have similar SiO_2/Al_2O_3 ratio, their acid strengths are different (Table 2.5; chapter 2). ZSM-5 which has a greater acidity is found to aromatize hydrocarbons better. Apart from zeolite acidity, other factors like reactant and product diffusivities and the maximum space available inside the pore are also responsible in deciding conversion and product selectivities.

Part-2

4.11. AROMATIZATION OF n-HEXANE OVER Zn, Ga, Fe AND Cr-PROMOTED H-ZSM-5

4.12. EXPERIMENTAL

The physicochemical properties of the catalysts used in these reactions were discussed in chapter 2 (Table 2.5). Pure n-hexane was used in these studies. The catalytic experiments were carried out in a commercial high pressure reactor (Autoclave Engineers, Erie, USA). The catalysts were activated before runs by drying at 793K with N_2 (6h). After the catalytic runs, the coke contents of the catalysts were estimated by careful burning of the hydrocarbon deposits with O_2 at 773K. The gases were passed through a bed of Pt (0.3%) -Al_2O_3 at 773K prior to their absorption in alkali and estimation (of CO_2) by titrimetric methods. Mass balances of the runs and details of the product analysis were described in chapter 2.

4.13. RESULTS AND DISCUSSION

4.13.1. Influence of promoters on product yields

A comparison of product yields obtained over H-ZSM-5 and promoted H-ZSM-5 catalysts is presented in Table 4.4. The comparative study was carried out at atmospheric pressure in N_2 (n-hexane: N_2 (mole) = 1.5). The conversion of n-hexane (n-C_6) was 100% over all the catalysts at the temperature of the study (793K). From the point of aromatic production, the catalysts can be arranged in increasing order of activity as follows: Cr_2O_3/H-ZSM-5 < Fe_2O_3/H-ZSM-5 < H-ZSM-5 < Ga_2O_3/H-ZSM-5 < ZnO/H-ZSM-5. Zn and Ga-oxides promote the aromatization reaction while Cr and Fe-oxides decrease the aromatization. The lower yield of aromatics is accompanied by an increase in the yield of C_2-C_4 saturates (Table 4.4). The increased production of saturates is probably due to the greater

Table 4.4

Product distribution over metal promoted H-ZSM-5 catalysts

Product distribution (wt%)	H-ZSM-5	Ga_2O_3 / H-ZSM-5	ZnO / H-ZSM-5	Fe_2O_3 / H-ZSM-5	Cr_2O_3 / H-ZSM-5
C_1	0.6	3.5	3.9	2.8	4.3
C_2 (=)	3.0	6.0	7.3	1.4	3.5
C_2	15.8	13.9	13.3	10.0	15.6
C_3 (=)	3.3	3.4	4.5	6.4	3.7
C_3	31.9	18.4	17.7	37.0	36.0
i-C_4	1.7	2.0	1.1	7.3	3.3
n-C_4	1.8	2.2	1.2	7.9	4.5
C_4 (=)	1.7	2.6	1.8	3.8	1.8
C_5-C_8 (alip)	1.0	0.9	0.3	2.4	7.0
Benzene	8.5 (0.23)[a]	12.5 (0.26)	14.9 (0.31)	3.8 (0.18)	3.9 (0.19)
Toluene	16.9 (0.44)	20.1 (0.43)	19.2 (0.40)	8.0 (0.39)	8.1 (0.41)
Xylenes	8.3 (0.21)	9.2 (0.20)	9.5 (0.19)	5.7 (0.28)	6.1 (0.31)
Ethyl benzene	0.8	0.6	0.3	0.5	0.4
C_8^+	4.7 (0.12)	4.7 (0.10)	5.0 (0.10)	3.0 (0.15)	1.8 (0.09)
∑Aromatics	39.2	47.1	48.9	21.0	20.3

Reaction conditions: Temperature = 793K; WHSV (h^{-1}) = 2; N_2 : n-C_6 (mole) = 1.5; pressure = 1atm; TOS = 1h; n-C_6 conversion was 100% in all experiments.

[a]Values in the brackets are the ratios of the components in total aromatics. The break-up of aromatics at equilibrium (800K) in the case of toluene disproportionation is: C_6 = 0.32; C_7 = 0.41; C_8 = 0.23 and C_8^+ = 0.04, and the case of xylene disproportionation it is C_6 = 0.06; C_7 = 0.24; C_8 = 0.41 and C_8^+ = 0.29 *[32]*.

hydrogenation activity possessed by these promoters (Cr- and Fe-oxides) which, in all likelihood, are present as lower valent reduced species under the reaction conditions. The promoters Zn and Ga produce less saturates and more olefins than H-ZSM-5. Increased yields of aromatics and lower yields of saturates over Ga and Zn promoted H-ZSM-5 have been reported by earlier workers during the aromatization of lower alkanes and alkenes *[3,6]*. The promoting action of both Ga- and Zn-oxides has been attributed to their ability to dehydrogenate alkanes and the production of allylic species. The yield of CH_4 is higher in the case of all the promoted catalysts than over H-ZSM-5. Presumably, the reduced forms of the promoters possess some hydrogenolysis activity. Kanai and Kawata *[8,9]* have also observed higher yields of aromatics during the aromatization of n-hexane over H-ZSM-5 doped with ZnO and Ga_2O_3.

In the case of Ga_2O_3 promoted H-ZSM-5 Kanai and Kawata *[8]* have reported an aromatic yield enhancement of about 50% at a loading of 3 wt% Ga_2O_3 (from Fig.1 in Ref. *[8]*) during the aromatization of n-hexane. On the other hand Ono *et al. [18]* have reported 2 and 3 fold yield (aromatic) enhancements by Ga_2O_3 during the aromatization of n-pentane and propane respectively. Kanai and Kawata *[8]* have reported that selectivity to aromatics decreases in the order : Galloaluminosilicate > Ga-exchanged H-ZSM-5 > Ga_2O_3/H-ZSM-5 > H-ZSM-5. Besides Kanai *[19]* has also reported that the pretreatment temperature influences the aromatics selectivity of Ga_2O_3/H-ZSM-5. In the case of ZnO promoted catalysts also, the enhancement of aromatization selectivity depends on the substrate. For example, during the aromatization of butane, the aromatics selectivity increased 6-fold on incorporation of ZnO into H-ZSM-5 *[20]*, though the increase was only 2-fold during the aromatization of butene-1 *[15]*. The 20-25 % enhancement in aromatics yield on the addition of Ga and Zn oxides reported here is quite small in comparison to the literature reports presented above.

Apparently many factors such as the concentration and method of loading the promoters, the properties (SiO_2/Al_2O_3; crystallite size) of the base H-ZSM-5, the process parameters, the duration of the run and the nature of the substrate determine the level of enhancement of aromatics selectivity by Ga_2O_3 and ZnO.

Based on an estimate of the H_2-produced at zero-aromatics selectivity, Kanai and Kawata *[8,19]* have concluded that over H-ZSM-5, the aromatization proceeds through the cracking of n-hexane, while it proceeds mainly through the dehydrogenation of n-hexane to n-hexene and subsequent cracking of the hexene to lower olefins over Ga_2O_3/H-ZSM-5. Both types of cracking reactions take place over ZnO/H-ZSM-5. Both the ZnO and Ga_2O_3 promoted catalysts operate by a bifunctional mechanism, the ZnO and Ga_2O_3 promoters taking part in both the initial dehydrogenation of n-hexane and also in the dehydrogenation of the cyclic oligomeric species into aromatics. It is interesting to note that, even though n-hexane is used as the feed, the major product is toluene (Table 4.4). An examination of the Eqs. (10 to 13; Table 4.5) reveals that the change in free energy (ΔG_r) accompanying the formation of an aromatic molecule increases in the order, m-xylene < toluene < benzene. However, at the conditions of the experiment, the aromatic molecules produced will undergo rapid isomerization / disproportionation reactions (14 and 15; Table 4.5) and the product pattern obtained is mainly due to these reactions. An examination of the break-up of the different components in the aromatics fraction (Table 4.4) reveals that the distribution of aromatics is reasonably similar to what one would expect from the disproportionation of toluene (see footnote of Table 4.4). Even though toluene is the major aromatic product over the different catalysts, the small variations in the distribution of aromatics observed over the different catalysts (Table 4.4) suggest that the interconversion of aromatics is influenced by the promoters presumably via changes in the acidity and pore size characteristics.

Table 4.5

Reactions in the aromatization of n-hexane

No	Reaction	ΔG_r (K cal)	Equilibrium conversion (x)		
			1 bar	1 bar (H_2)	15 bar (H_2)
1	n-C_6 → n-$C_6^=$ + H_2	4.83	0.214	0.073	0.005
2	n-$C_6^=$ → $C_3^=$ + $C_3^=$	-8.27			
3	n-C_6 → C_3^- + $C_3^=$	-7.81	0.996	0.998	0.970
4	n-C_6 → C_2^- + $C_4^=$	-7.83			
5	$C_3^=$ + H_2 → C_3^-	-4.37	0.755	0.906	0.995
6	$C_4^=$ + H_2 → C_4^-	-5.13	0.804	0.938	~1
7	2$C_3^=$ → n-$C_6^=$	8.27	0.003	0.002	0.027
8	$C_3^=$ + $C_4^=$ → n-$C_7^=$	8.19			
9	2$C_4^=$ → n-$C_8^=$	8.11			
10	n-C_6 → Bz + 4H_2	-20.24			
11	2n-C_6 → Bz + 2C_3^- + 3H_2	-32.42			
12	2n-C_6 → Tol + C_2^- + C_3^-	-37.82			
13	2n-C_6 → Xyl + 2C_2^- + 3H_2	-40.32			
14	2Tol → Bz + m-Xyl	2.90			
15	m-Xyl → TMB + Tol	0.05			

Saturates denoted by "-" and olefins by "=" ; $C_4^=$ to $C_8^=$ refers to 1-olefins; Bz = benzene; Tol = toluene; Xyl = m-xylene; TMB = 1,2,4-trimethyl benzene.

Previous studies on Ga and Zn impregnated H-ZSM-5 samples have suggested that most of the Ga and Zn are present away from the cation exchange sites and reside as Ga_2O_3 or ZnO in the calcined samples. However, a small amount of Ga^{3+}or Zn^{2+} ions may replace acidic protons in bridging hydroxyls, there by decreasing Brönsted acidity, though the extracrystalline Ga_2O_3 or ZnO species would not affect the Brönsted acidity *[21]*.

The probability of introduction of cations into high silica zeolites depends on the physico-chemical properties of the metal oxides, such as, melting point, sublimation temperature, the diffusivity of the metal oxides through the pores and the strength of the acidic sites, which are considered as powerful traps for the migrating cations. These aspects can be examined further by TPR measurements which could help in determining the location, dispersion and the interaction between the oxide species with zeolite matrix.

Zn species have a significant effect on the distribution of aromatics, the formation of less bulky products like benzene is more favourable on ZnO/H-ZSM-5 than on H-ZSM-5 (Table 4.4) *[22]*. The TPR spectrum of ZnO/H-ZSM-5 (Fig. 2.8; chapter 2) suggests that ZnO is well dispersed in the channels of the zeolites. Therefore the observed higher benzene yield is probably due to the diffusion limitations posed by the Zn species within the channel of the zeolite.

Recent reports suggest that the reduction of Ga^{3+} in Ga_2O_3/H-ZSM-5 is influenced by the intimacy of the mixing between the two components *[23]*. The initial reduction of Ga^{3+} species produces GaH_x (+ δ oxidation state) species, which migrates from the outer surface into the intracrystalline voids in the zeolite due into its higher volatility and loss of coordination during reduction. This $Ga^{+\delta}$ ion has been suggested to possess an oxidation state between 0 to 1 and coordinated to the equivalent of a single basic oxygen ion *[23]*. These species are believed to possess dehydrogenation / hydrogenation properties. The TPR spectrum of Ga_2O_3

/H-ZSM-5 (Fig. 2.8; chapter 2) and the amount of H_2 consumption (Table 2.6; chapter 2) suggests that an appreciable amount of Ga^{+3} ions were converted to Ga^{+} (~ 60%).

4.13.2. Influence of promoters on catalyst deactivation

In the aromatization of alkane over H-ZSM-5, the yield of aromatics is significant only beyond 753K. Typically, temperatures in the range 773-813K are preferred. At these high temperature, coke deposition and catalyst deactivation are rapid. By virtue of its special pore dimensions and poor hydrogen transfer ability, H-ZSM-5 generally deactivates slower than other zeolites through coke lay down. Even so, deactivation rates are rapid, limiting the economic attractiveness of this process.

The influence of promoters on the deactivation rate (aromatics-loss) are presented in Fig. 4.7. The experiments were carried out in N_2 (n-C_6 : N_2 (mole) = 1.5) at atmospheric pressure. The catalysts generally deactivate rapidly in the beginning and then the deactivation becomes less rapid. Visual inspection of Fig. 4. shows that the rate of deactivation is different over the different catalysts. To get a better appreciation of the deactivation rate, the aromatic yields at different times on stream were fitted into the Voorhies' equation *[24]*, $k = at^{-n}$; n is the deactivation coefficient for the loss of aromatics. The values of n for the different catalysts are presented in Table 4.6 along with the coke content of the catalysts at the end of the run. It is noticed that the coke contents are related to the amount of aromatics produced by the catalysts and not to the deactivation coefficients. The order of aromatics production and coke deposition is nearly the same: Zn > Ga > H > Cr ~ Fe. This is probably due to the fact that coke (polyunsaturated compounds) and aromatics have common precursors. The deactivation coefficient is large for the poor promoters, Fe_2O_3 and Cr_2O_3 (Table 4.6). ZnO/H-ZSM-5 deactivates faster than H-ZSM-5 while Ga_2O_3/H-ZSM-5 deactivates slower. The more rapid deactivation of ZnO has already been reported *[25]*. It has been suggested to be due the

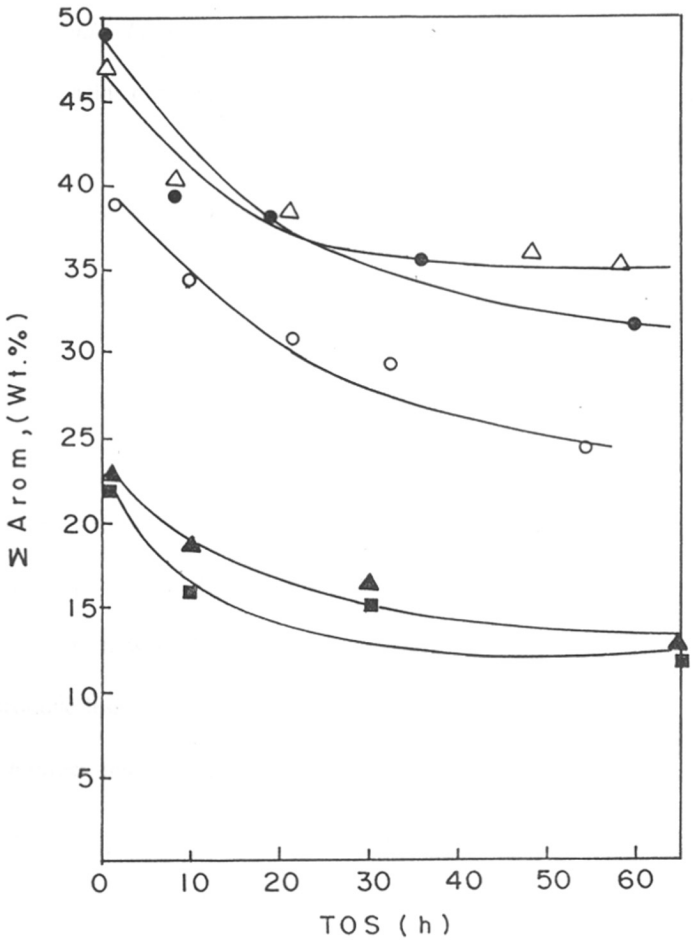

Fig. 4.7. Influence of duration of run of aromatics over promoted H-ZSM-5 catalysts.
Reaction conditions: Temperature = 793K; WHSV (h^{-1}) = 2; pressure = 1 atm; N_2 / n-C_6 (mole) = 1.5: (○) H-ZSM-5; (●) ZnO/H-ZSM-5; (△) Ga_2O_3/H-ZSM-5; (▲) Cr_2O_3/H-ZSM-5; (■) Fe_2O_3/H-ZSM-5.

reduction of ZnO to Zn metal during the reaction and its loss as vapor *[25]*. It appears more likely that the deactivation in the case of ZnO/H-ZSM-5 in our experiments is due to more rapid coke deposition (Table 4.6) brought about by the reduced Zn species.

4.13.3. Influence of added gas and total pressure on product yields

The product yields obtained over H-ZSM-5 at atmospheric pressure and 15 bars (total pressure) in the absence and presence of added gases (n-C_6 : gas (mole) = 1.5) are reported in Table 4.7. Besides, the results obtained over ZnO and Ga_2O_3 promoted catalysts in the presence of H_2 (1 bar) are also reported in the table. As the reaction involves olefinic intermediates, one would expect a large decrease in the yield of aromatics when H_2 is added and on increasing the total pressure. In the case of H-ZSM-5, the addition of N_2 increases the yield of aromatics, while H_2-addition decreases the yield. Increasing the pressure decreases the yield of C_6-C_8 aromatics, but has little influence on total aromatics yield when no added gas is present. When N_2 is present (at 15 bar), the yield of total aromatics is only marginally more, but significantly less than when H_2 is present (Table 4.7). The Ga_2O_3 and ZnO promoted catalysts also produce less aromatics in the presence of H_2 than in the presence of N_2 (Table 4.4 and 4.7), the effect being more pronounced in the case of Zn. The increase in aromatics production on addition of N_2 is probably a consequences of the inert gas dilution effect which increases the equilibrium conversion values for many of the olefin and aromatics production reactions such as 1 to 4 and 10 to 13 (Table 4.5).

Table 4.5 indicates that the dehydrogenation of n-hexane (reaction 1) is much less thermodynamically favored than the cracking of n-hexane and n-hexene (reactions 3-4) at 800K. Besides, the former reaction is very much suppressed by added H_2 and high pressures than the cracking reactions (Table 4.7). The hydrogenation of the intermediate C_3-C_4 olefins (reactions 5 and 6; Table 4.5) is also very much enhanced by H_2 and high pressures. However,

Table 4.6

Influence of promoters on the deactivation rate and coke lay down

Catalyst	Deactivation coefficient (n)[a]	Coke (wt%)[b]
H-ZSM-5	0.085	10.5
Ga_2O_3 / H-ZSM-5	0.068	11.3
ZnO / H-ZSM-5	0.092	15.5
Cr_2O_3 / H-ZSM-5	0.170	10.0
Fe_2O_3 / H-ZSM-5	0.139	9.0

Reaction conditions: 793K; WHSV (h^{-1}) = 2; N_2 : n-C_6 (mole) = 1.5; pressure = 1 atm.

[a]Deactivation coefficient (for total aromatics) determined by fitting into the Voorhies' equation *[24]*

[b]after a time on stream of 60h.

Table 4.7

Influence of added gas and pressure on the aromatization of n-hexane

	H-ZSM-5						ZnO/ H-ZSM-5	Ga_2O_3/ H-ZSM-5
	Atmospheric			15 bar			Atmospheric	
	n-C_6	n-C_6 + N_2	n-C_6 + H_2	n-C_6	n-C_6 + N_2	n-C_6 + H_2	n-C_6 + H_2	n-C_6 + N_2
C_1	1.0	0.6	1.9	8.1	8.1	6.1	8.4	9.7
C_2(=)	4.0	3.0	3.4	4.7	5.0	4.1	1.3	0.8
C_2	16.8	15.8	13.8	27.4	23.4	33.6	22.0	12.6
C_3 (=)	3.1	3.3	4.0	4.4	4.7	4.4	0.8	0.7
C_3	33.8	31.9	36.2	15.2	16.6	12.5	21.8	23.8
i-C_4	1.6	1.7	2.7	0.7	1.3	3.7	0.6	2.1
n-C_4	2.1	1.8	4.8	0.9	1.6	5.0	2.0	3.7
C_4 (=)	1.2	1.7	1.2	0.1	0.2	1.0	0.6	0.3
C_5-C_8 (alip)	1.0	1.0	0.8	2.3	2.1	1.3	0.5	1.1
Benz	8.9	8.5	7.1	6.9	6.1	6.1	12.3	10.2
Tol	16.0	16.9	12.8	11.4	11.4	9.9	15.4	19.0
Xyls	7.3	8.3	6.7	5.7	6.7	4.8	9.3	12.2
EB	0.7	0.8	0.6	0.7	0.9	0.3	0.3	0.6
C_8^+	2.5	4.7	4.0	11.5	11.9	7.2	4.7	3.2
∑Arom	32.4	39.2	31.2	36.2	37.0	28.3	42.0	45.2

Reaction conditions: Temperature = 793K; WHSV (h^{-1}) = 2; N_2 (or H_2) : n-C_6 (mole) = 1.5; TOS = 1h

as the aromatics production reactions are the most favoured (reactions 10-13) at the operating conditions, their production is understandable. Aromatics are believed to be formed (over zeolites) from alkene-oligomers by successive deprotonation and hydride transfer reactions *[26]*. These reactions occur rapidly on the surface of H-ZSM-5 and the intermediate alkenes are rapidly converted as fast as they are formed. Besides, these reactions are probably not sensitive to the added molecular H_2. Additionally, steric factors inside the pores of ZSM-5 might also favour the stabilization of the oligomers (reactions 7 and 9; Table 4.5) as Ψ-cyclic intermediates and their rapid dehydrogenation to aromatics. The formation of Ψ-cyclic intermediates has been suggested by Derouane *et al.[27]* in the reforming of n-paraffins over Pt-KL).

Overall, as aromatics production is a dehydrogenation reaction, a decrease in aromatics yield on addition of H_2 or increasing the pressure is expected purely from thermodynamic reasons. However, due to the large number of reactions and the complexity of the reaction network it is not possible to predict the extent to which the added H_2 will reduce the aromatics yield. Though reports on the influence of H_2 on the aromatization reaction over ZSM-5 catalysts are limited, they do confirm our observations *[28,29]*. The decrease in aromatics production over ZnO and Ga_2O_3 promoted catalysts is not more than that the observed over H-ZSM-5 suggesting that the initial dehydrogenation of n-hexane (reaction 1; affected by H_2) may not be the important (rate determining) reaction in the aromatization of n-hexane over ZSM-5 based catalysts.

4.13.4. Influence of added gas and total pressure on catalyst deactivation

Fig. 4.8 and Table 4.8 present the results of the influence of added gas and total pressure on the deactivation of the catalysts. The results indicate that deactivation rate and coke deposition are lowered by the presence of H_2. N_2, however increases the deactivation

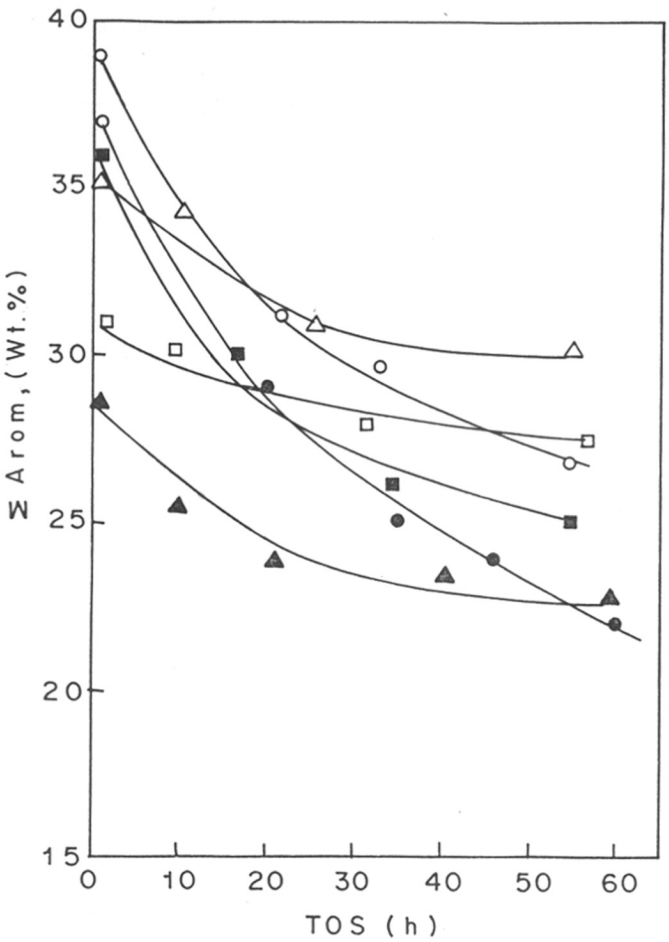

Fig. 4.8. Influence of duration of run on yield of aromatics over H-ZSM-5 in the presence of added gases.
Reaction conditions: Temperature = 793K; WHSV (h^{-1}) = 2; Gas/ n-C_6 (mole) = 1.5: (△) n-C_6 (atm); (□) n-C_6 + H_2 (atm); (○) n-C_6 + N_2 (atm); (■) n-C_6 (15 atm); (▲) n-C_6 + H_2 (15 atm); (●) n-C_6 + N_2 (15 atm).

Table 4.8

Influence of pressure and added gases (H_2 or N_2) on the deactivation rate and coke lay down

Pressure	Deactivation coefficient (n)[a]			Coke (wt%)[b]		
	n-C_6	n-C_6 + N_2	n-C_6 + H_2	n-C_6	n-C_6 + N_2	n-C_6 + H_2
Atmospheric	0.045	0.085	0.032	9.4	10.5	5.7
15 bar	0.087	0.112	0.053	12.3	11.9	10.0

Reaction conditions: Temperature = 793K; WHSV (h^{-1}) = 2; N_2 (or H_2) : n-C_6 (mole) = 1.5,

[a]Deactivation coefficient (for total Aromatics) determined by fitting into the Voorhies' equation *[24]*

[b]after a time on stream of 60h.

rate. The deposition of coke over zeolite catalysts during hydrocarbon transformations has been extensively investigated *[30,31]*. The type of coke and its toxicity has been reported to be different on different zeolites. H-rich (soft) coke has been found to be less toxic than the harder graphitic coke. The coke formed on ZSM-5 has been shown to be richer in hydrogen than the coke formed over mordenite and USY *[31]*. Apparently, the hydrogen externally added during the aromatization reaction over ZSM-5 catalysts helps in increasing the hydrogen content (softness) of the coke, thereby reducing its toxicity to the reaction. It is also likely that the added H_2 decreases the coking rate by decreasing the concentration of the polyunsaturated coke-precursors.

Increasing the pressure of the reaction increases both deactivation rate and coke deposition. Apparently, at higher pressure, large molecular products are produced, through condensation/polymerization reactions deactivating the active centers more rapidly by increasing coke deposition.

4.14. Conclusions

The aromatization of n-hexane over H-ZSM-5 is enhanced by the promoters ZnO and Ga_2O_3 while Fe_2O_3 and Cr_2O_3 decrease the aromatization. Both ZnO and Ga_2O_3 comtaining catalysts deactivate less. Significant production of aromatics occurs over the catalysts even in the presence of H_2 at 15 bars (total pressure). Addition of H_2 deacrases deactivation and coke deposition. It appears that the aromtization of n-hexane over ZSM-5 based catalysts takes place via cracking of n-hexane into C_3 and C_4 olefins, the oligomerization of the olefins into Ψ-cyclic intermediates inside the pore system and the subsequent dehydrogenation via disproportionation and H-transfer reactions.

Part 3

4.15. AROMATIZATION OF LIGHT RAFFFINATE OVER H-ZSM-5 BASED CATALYSTS

All the studies reported so far in this thesis were carried out using pure model hydrocarbons, especially n-hexane. It was next decided to examine the possibility of aromatizing a low value light hydrocarbon mixture (mostly in the C_6 range) available in a refinery into high value aromatics. The purpose of this study was partly to establish the influence of isomeric hexanes on the aromatization reaction. Besides, these studies will also demonstrate the influence of minor amounts of olefinic impurities on the performance of the catalyst. A commercial light raffinate obtained from a refinery was used in these studies. A simplified scheme for the production of the raffinate (in the refinery) is shown below:

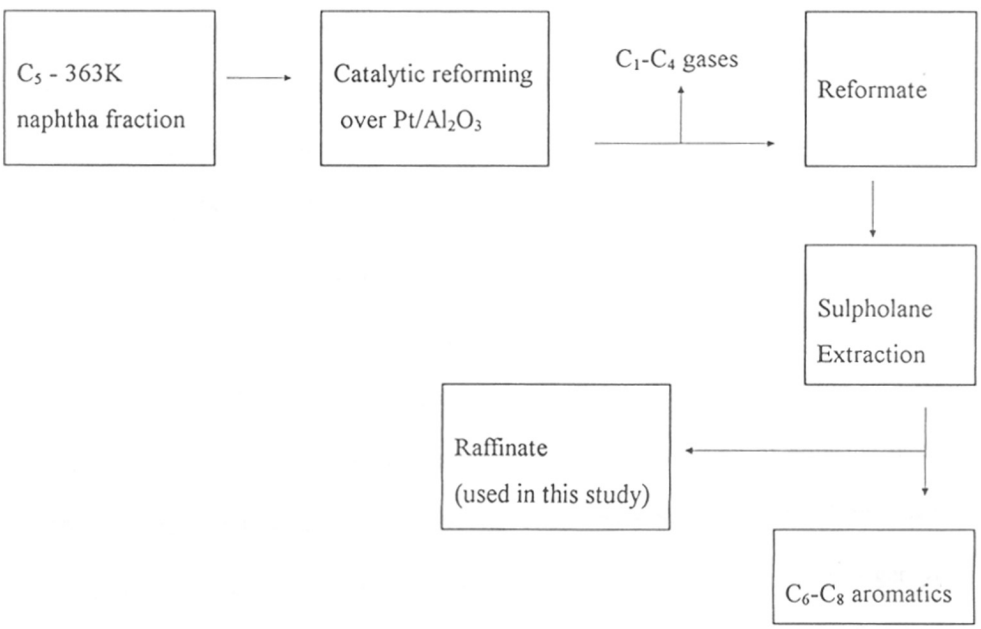

The composition of the raffinate used is given in table 4.9. Besides, a small amount of (<1 wt.%) of olefins were also present in the raffinate. These have not been included in the

table. The C_6-fraction (non-aromatic) of the mixture was nearly 75% while the C_5 and C_7 fractions were 13.4 and 7.9 wt.%, respectively. The aromatics content was 4.3 wt.%.

4.16. EXPERIMENTAL

The catalytic studies were carried out in a commercial high pressure reactor (Twin Reactor, Hungary; reactor volume = 200ml). Generally 20-30 g catalyst (with binder) was used in the studies. The catalysts were extrudates (1/16") broken into small pieces (2 mm dia). Extrudate samples were loaded with Ga_2O_3 (3 wt.%) by impregnation using $Ga(NO_3)_3$ (Aldrich) and calcined at 773K in dry air. For the platinum promoted Ga_2O_3/H-ZSM-5 sample, both the metals were introduced by co-impregnation using chloroplatinic acid and gallium nitrate. The platinum and Ga_2O_3 contents of the samples were 0.05 % and 3% respectively. Catalysts were loaded in the mid section of the reactor. Ceramic beads were used to preheat the feed and to support the catalyst bed. Both the gaseous and liquid products were collected, analyzed and the mass balance carried out. Details of the reactor setup, mass balance and product analysis have been discussed in chapter 2.

4.17. RESULTS AND DISCUSSION

4.17.1. Aromatization of raffinate over H-ZSM-5

The product yields from the aromatization of n-hexane and the raffinate over H-ZSM-5 are compared in Table 4.10. n-hexane produces slightly less aromatics (26.6%) than the raffinate (29.3%) at identical conditions. Although, the conversion of both the feeds were 100% at the temperature of the study (793K). The lower yield of aromatics from n-hexane is accompanied by higher yields of C_3 and C_4 fractions (Table 4.10). The larger yield of aromatics from raffinate is likely to be due to the presence of small quantites of olefins in the feed. Olefins form carbocations rapidly on the catalyst surface, the carbocations acting as reaction initiators. During aromatization, the raffinate produces more C_1 and C_2 hydrocarbons

Table 4.9

Typical composition of the raffiante feed

Hydrocarbon	Concentration (wt.%)
C_5- hydrocarbons	
i-C_5	6.9
n-C_5	6.5
C_6-hydrocarbons	
2,2-dimethylbutane	4.0
2,3-dimethylutane	5.8
2-methylpentane	21.8
3-methylpantane	16.8
n-hexane	21.1
methylcyclopentane	4.9
C_7-hydrocarbons	
2,4-dimethylpentane	2.1
3-methylcyclohexane	2.2
n-heptane	1.8
others[*]	1.8
Aromatics	
Benzene	1.0
Toluene	2.9
C_8-aromatics	0.3
C_8^+-aromatics	0.1

[*]Others include C_7^+ - aliphatics and C_6-C_8 olefins

(Table 4.10), probably due the cracking of the branched C_5-C_7 isomeric hydrocarbons present in the feed (Table 4.9). The influence of temperature on product yield is presented in figure 4.9. The general trends of product yield changes with temperature are very similar to those observed for n-C_6 (Fig. 4.4).

4.17.2. Aromatization studies over Ga_2O_3 /H-ZSM-5

It was already reported in part 2 that promoters like Ga_2O_3 and ZnO increase the aromatic yield. ZnO/H-ZSM-5 deactivates faster than H-ZSM-5 while Ga_2O_3/H-ZSM-5 deactivates slower. Because of slower deactivation, and the higher stability of Ga_2O_3, Ga_2O_3/H-ZSM-5 was used in these studies. A comparative study of the aromatization of the raffinate over H-ZSM and Ga_2O_3/H-ZSM-5 is presented in Table 4.11. The conversion of the raffinate was 100% over both the catalysts at the range of temperatures studied. From the point of aromatics production, Ga_2O_3/H-ZSM-5 is more active than H-ZSM-5. The lower yield of aromatics over H-ZSM-5 is accompanied by an increase in the yield of C_2-C_4 saturates (Table 4.11).

The influence of duration of run on aromatics production over Ga_2O_3/H-ZSM-5 is presented in Fig. 4.10. It is noticed that the deactivation of the catalyst was rapid in the case of the raffinate feed than when n-hexane was used as feed (compare with Fig. 4.8; section 4.13.4). This is probably due to the presence of small amounts of olefinic components (~1%) in the feed. Hence it was decided to incorporate a small amount of a hydrogenation component, namely Pt (0.05 wt.%) to Ga_2O_3/H-ZSM-5 and study its influence on catalyst performance including its rate of deactivation. In the following sections the effect of process parameters such as temperature, space velocity, H_2/raffinate (mole) ratio and aging characteristics are described for the aromatization of the raffinate over Pt-promoted Ga_2O_3/H-ZSM-5.

Table 4.10

Influence of feed on aromatization activity of H-ZSM-5

Product distribution (wt%)	Catalyst: H-ZSM-5	
	Feed	
	Raffinate	n-hexane
C_1	4.6	3.9
C_2 (=)	10.0	5.5
C_2	21.0	12.4
C_3 (=)	9.8	8.8
C_3	18.2	30.6
i-C_4	2.1	4.5
n-C_4	2.5	4.7
C_4 (=)	1.7	1.2
C_5-C_8 (alip)	0.8	0.9
Benzene	5.9	4.0
Toluene	11.0	8.9
Xylenes	6.2	8.2
Ethyl benzene	0.8	0.7
C_8^+	5.4	4.8
$\sum$Aromatics	29.3	26.6

Reaction conditions: Temperature = 793K; WHSV (h^{-1}) = 2; H_2 : oil (mole) = 2.0; pressure = 5 bar; TOS = 1h.

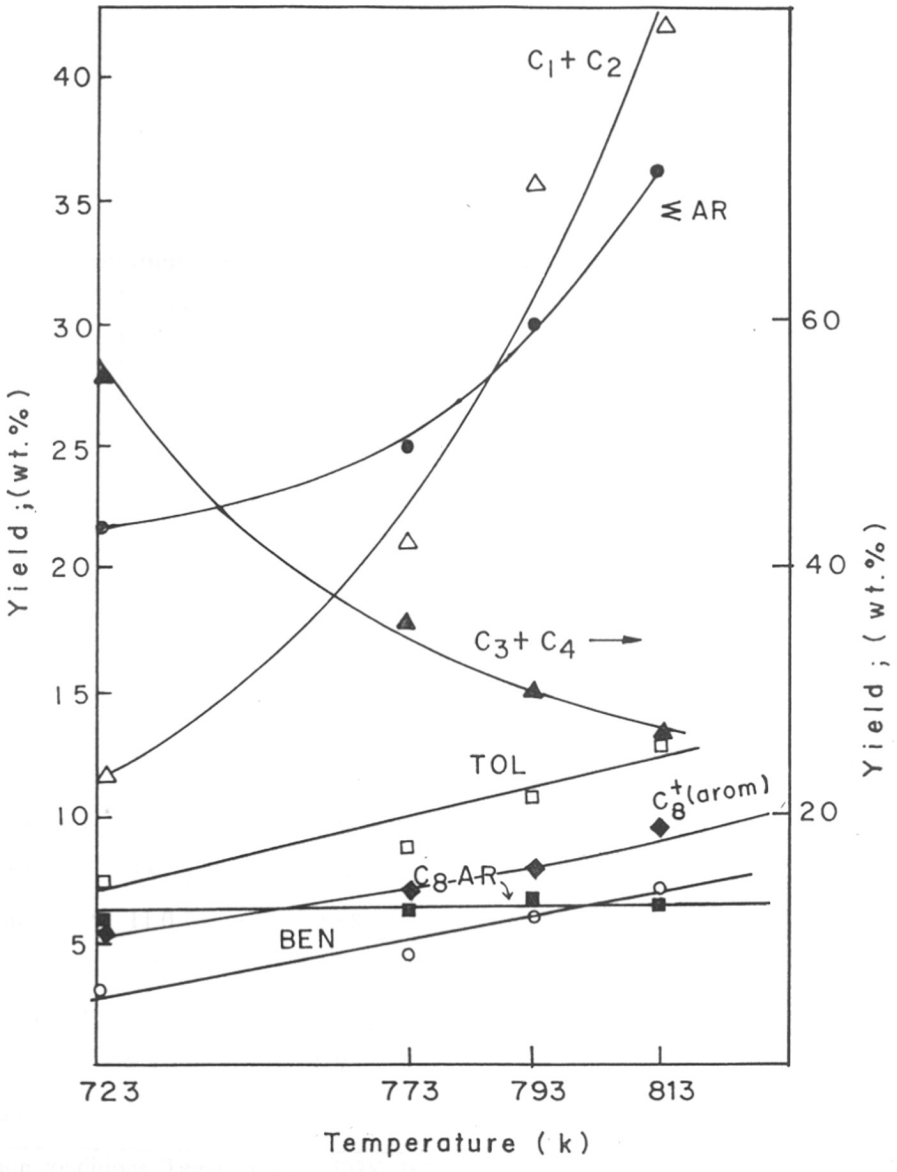

Fig. 4.9 Influence of temperature on product yield during the aromatization of raffinate over H-ZSM-5.
Reaction conditions: WHSV (h^{-1}) = 2; H_2/raffinate (mole) = 1.5; pressure = 5 atms; TOS = 1h .

Table 4.11

Product distribution over metal promoted H-ZSM-5 catalysts

Product distribution (wt.%)	H-ZSM-5	Ga_2O_3 / H-ZSM-5	Pt/ Ga_2O_3 / H-ZSM-5
C_1	4.6	6.5	11.8
C_2 (=)	10.0	7.0	9.8
C_2	21.0	18.9	14.6
C_3 (=)	9.8	9.0	7.2
C_3	18.2	18.4	10.8
i-C_4	2.1	0.4	0.1
n-C_4	2.5	0.5	0.2
C_4 (=)	1.7	1.6	1.4
C_5-C_8 (alip)	0.8	0.9	1.5
Benzene	5.9	9.6	9.8
Toluene	11.0	12.8	13.6
Xylenes	6.2	5.0	6.7
Ethyl benzene	0.8	0.5	0.7
C_8^+	5.4	8.9	11.8
∑Aromatics	29.3	36.8	42.6

Reaction conditions: Temperature = 793K; WHSV (h^{-1}) = 2; H_2 : oil (mole) = 2.0; pressure = 5 bar; TOS = 1h.

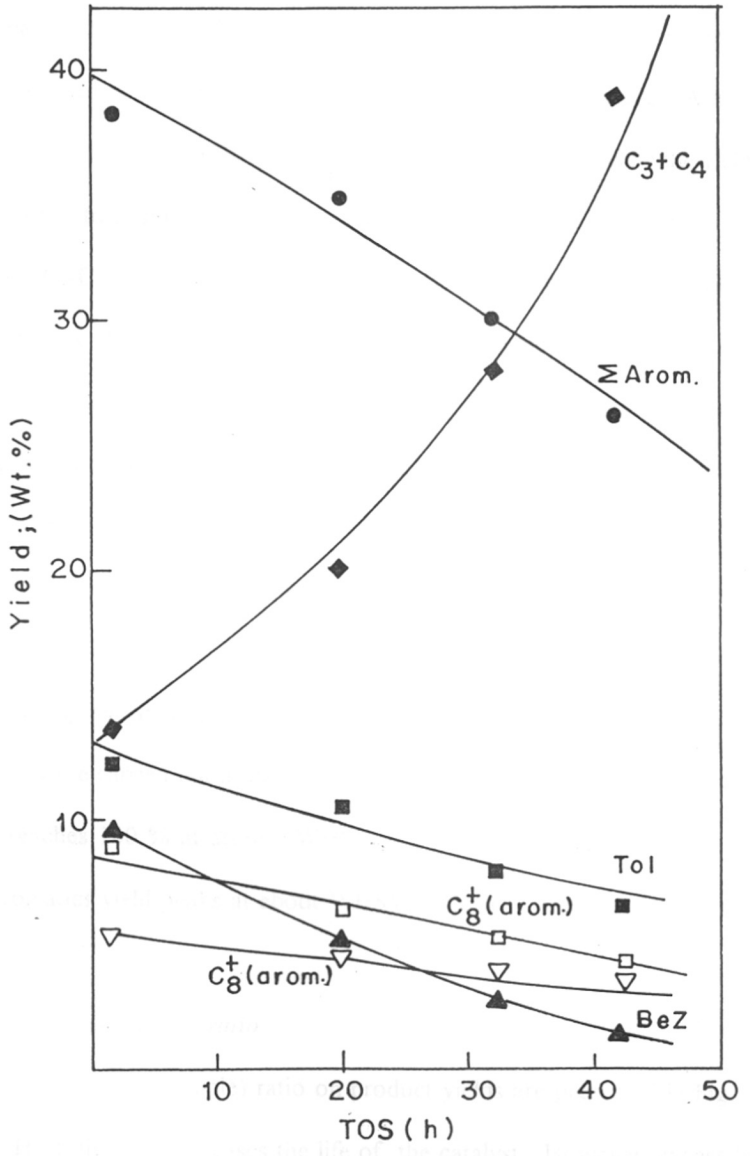

Fig. 4.10 Influence of time on stream on product yields during the aromatization of raffinate over Ga_2O_3/H-ZSM-5.
Reaction conditions: Temperature = 793K; WHSV (h^{-1}) = 2; H_2/raffinate (mole) = 1.5; pressure = 5 atms.

4.17.3. Influence of temperature

The aromatization of the raffinate was carried out in the temperature range 723-813K. It is found that the yield of aromatics increases with increasing temperature. A maximum of 51% aromatic yield is noticed at 813K. The yields of $C_1 + C_2$ increases while the yields of $C_3 + C_4$, which transform into aromatics decrease rapidly with increasing temperature (Fig 4.11). The unsaturates (C_2-C_4) are slightly more at higher temperatures as expected from thermodynamic reasons. In general, the yields of aromatics are more over Pt/Ga_2O_3/H-ZSM-5 than over H-ZSM-5 and Ga_2O_3/H-ZSM-5 (Table 4.11). Though Pt itself is a catalyst for aromatizing hydrocarbons, it appears that the increase in aromatics is not due to the direct activity of Pt as the Pt content is very small (0.05%). It is more likely that it acts as a promoter. It is possible that it helps in the reduction of the Ga_2O_3 species into more active lower valent material *[29]*.

4.17.4. Influence of space velocity

The studies were carried out in the WHSV (h^{-1}) range between 0.5 to 9.2. Conversion of the raffinate reaches 100 % at around WHSV ~ 2 h^{-1}. The data reported in Fig. 4.12, reveal that the aromatics yield peaks at about WHSV ~ 1.6 h^{-1}. The gas yields are higher at lower conversions.

4.17.5. Influence of H_2/oil (mole) ratio

The influence of H_2/oil (mole) ratio on product yields are presented in Fig. 4.13. A small amount of H_2 in the feed increases the life of the catalyst. However, excess hydrogen decreases aromatics yield. The data reveal that the yield of aromatics decreases significantly beyond H_2/oil (mole) = 1.5 (Fig. 4.13). The yield of $C_3 + C_4$ increases, but the increase of C_3 is more than that of C_4.

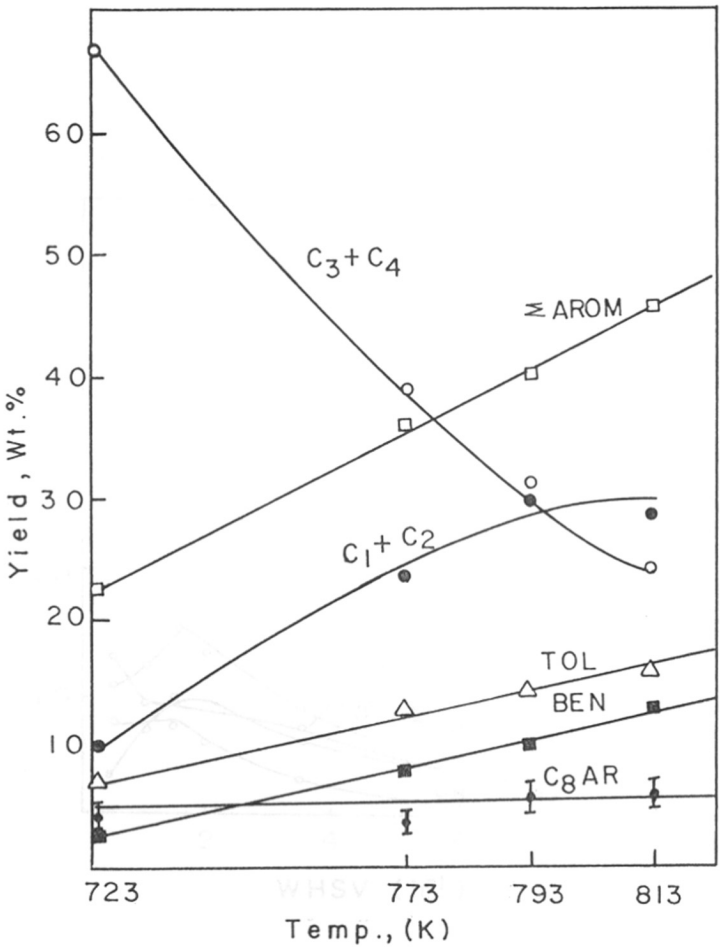

Fig. 4.11. Influence of temperature on product yield during the aromatization of raffinate over $Pt/Ga_2O_3/H$-ZSM-5.
Reaction conditions: WHSV (h^{-1}) = 2; H_2/raffinate (mole) = 1.5; pressure = 5 atms; TOS = 1h .

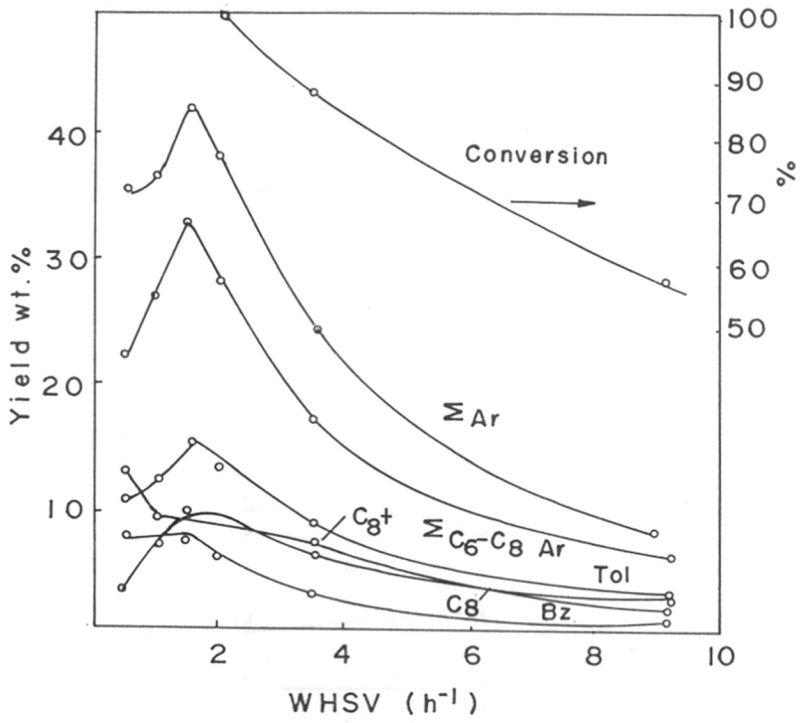

Fig. 4.12. Influence of space velocity on product yield during the aromatization of raffinate over $Pt/Ga_2O_3/H$-ZSM-5.
Reaction conditions: Temperature = 793K; H_2/raffinate (mole) = 1.5; Pressure = 5 atms; TOS = 1h.

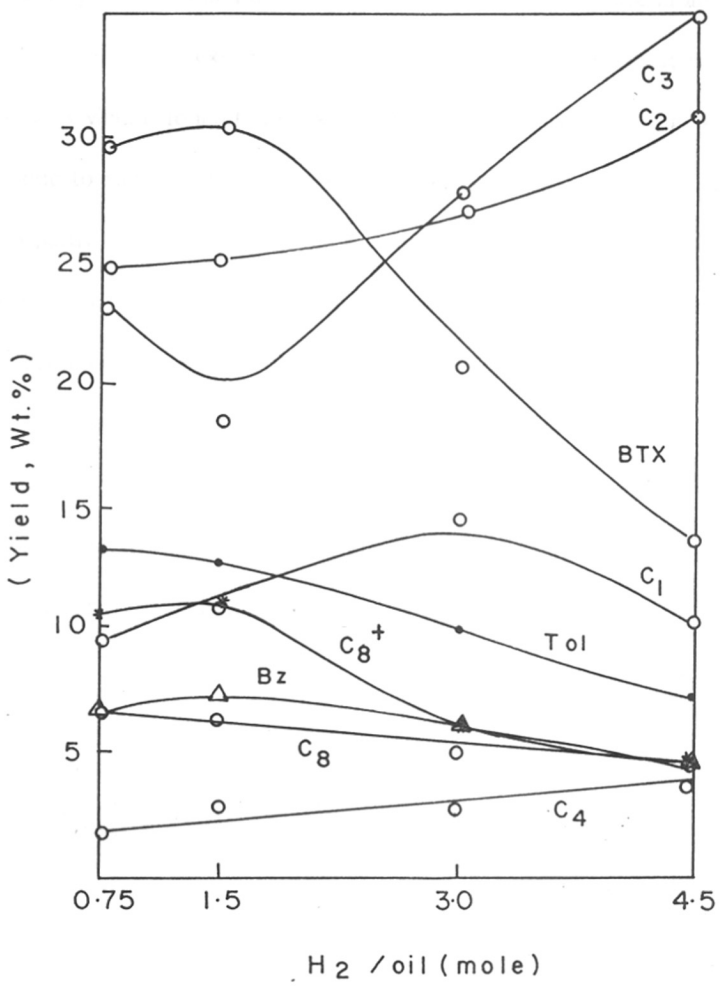

Fig. 4.13. Influence of H_2/oil (mole) on product yield during the aromatization of raffinate over Pt/Ga_2O_3/H-ZSM-5.
Reaction conditions: Temperature = 793K; WHSV (h^{-1}) = 2; pressure = 5 atms; TOS = 1h.

4.17.6. Influence of pressure

As aromatics production is a dehydrogenation reaction, a decrease in aromatics yield on increasing the pressure is expected purely from thermodynamic reasons. However, surprisingly, the BTX yield is found to increase slightly at higher pressures (Fig. 4.14). This is probably partly due to suppression of the initial rapid deactivation (less than 2 h time on stream) and also partly to the increase in the rate of dimerization of C_3 and C_4 olefins into precursors of aromatics. Low pressures lead to more propylene and C_4 hydrocarbons.

4.17.7. Aging Characteristics

The aging characteristics of Pt/Ga_2O_3/H-ZSM-5 is compared with that of Ga_2O_3/H-ZSM-5 in Fig. 4.15. It is apparent that the addition of a small quantity of Pt reduces the deactivation of the catalyst. This is probably due to the hydrogenation of polyolefinic coke precursors formed on the surface into more benign material by the Pt.

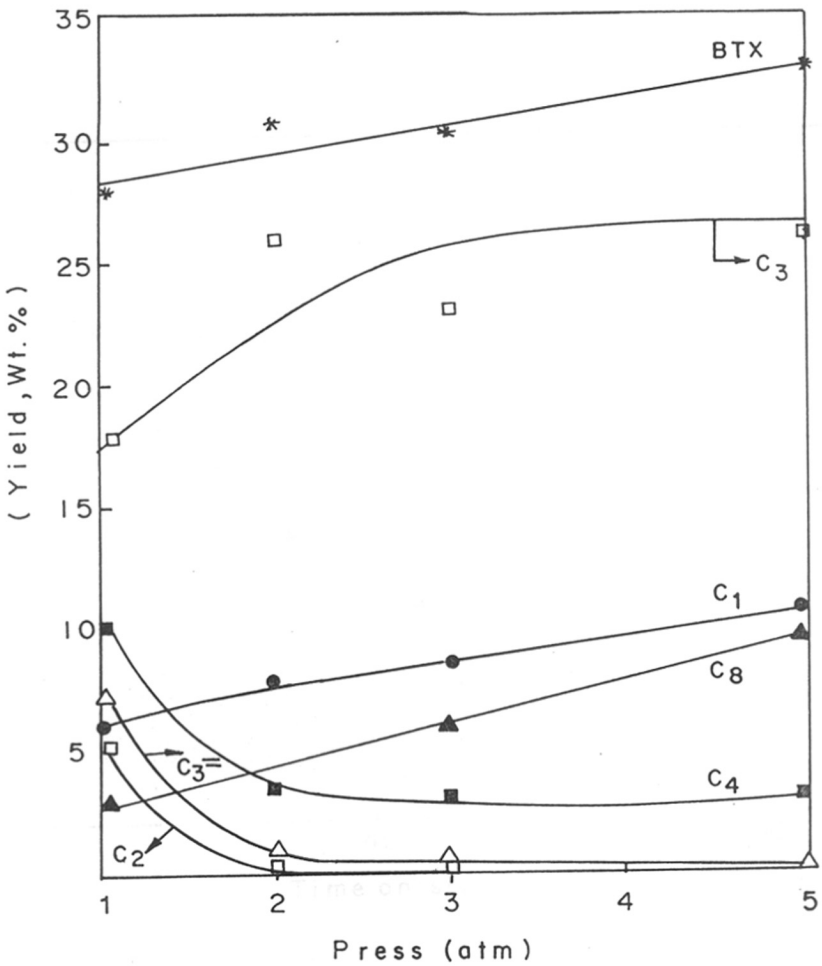

Fig. 4.14. Influence of reaction pressure on product yield during the aromatization of raffinate over $Pt/Ga_2O_3/H$-ZSM-5.
Reaction conditions: Temperature = 793K; WHSV (h^{-1}) = 2; H_2/raffinate (mole) = 1.5; TOS = 1h.

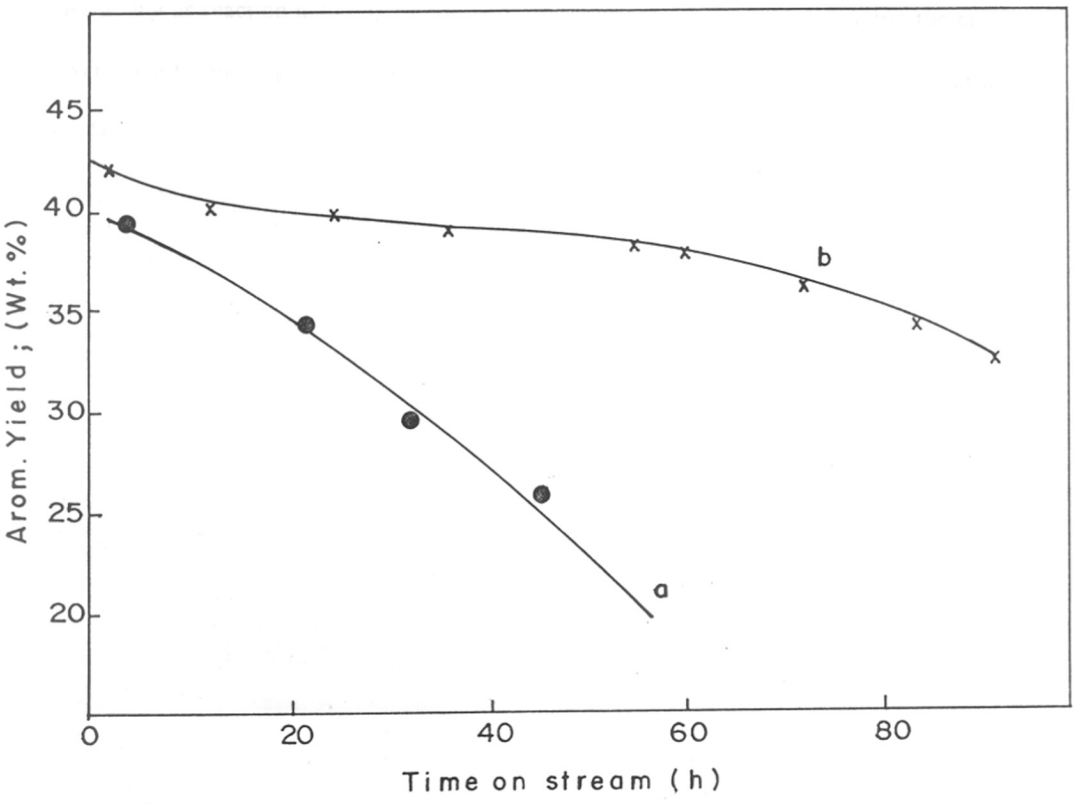

Fig. 4.15. Influence of the duration of run on aromatics yield during the aromatization of raffinate over Ga_2O_3/H-ZSM-5 and Pt/Ga_2O_3/H-ZSM-5.
(a) Ga_2O_3/H-ZSM-5; (b)Pt/Ga_2O_3/H-ZSM-5.
Reaction conditions: Temperature = 793K; WHSV (h^{-1}) = 1.6; pressure = 5 atm; TOS = 1h.

4.18. Conclusions

Studies on a mixed hydrocarbon feed have indicated that the aromatization is not affected due to the presence of branched hydrocarbons. The enhancement of aromatization observed in the case of the raffinate feed may be due to the presence of small amounts of olefins acting as reaction initiators by forming carbocations rapidly. As noticed in the case of n-hexane, Ga_2O_3 increases the aromatization activity of H-ZSM-5 in the case of the raffinate feed also. The presence of olefinic material in the feed increases the deactivation rate of Ga_2O_3/H-ZSM-5 (Fig. 4.15). However, the addition of small amounts of Pt (0.05%) reduces the deactivation rate. The addition of Pt also enhances the aromatization activity of Ga_2O_3/H-ZSM-5.

References

1. Chen, N.Y., and Yan, T. Y., *Ind. Eng. Process. Des. Dev.*, **25,** 151 (1986).
2. Johnson, J. A., Weiszmann, J. A., Hilder, G. K., and Hall, A. H. P., paper presented at the 1984 Annual Meeting, March 25-27, 1984, San Antonio, TX.
3. Guisnet, M., and Gnep, N. S., *Appl. Catal.*, A. General, **89,** 1 (1992).
4. Mole, T., Anderson, J. R., and Creer, G., *Appl. Catal.*, **17,** 141 (1985).
5. Wang, I., Chen, T. J., Chao, K. J., and Tsai, T. C., *J. Catal.*, **60,** 140 (1979).
6. Ono, Y., *Catal. Rev. Sci. Eng.*, **34,** 179 (1992).
7. Sirokman, G., Sendoda, Y., and Ono, Y., *Zeolites,* **6,** 299 (1986).
8. Kanai, J., and Kawata, N., *J. Catal.*, **114,** 284 (1988).
9. Kanai, J., and Kawata, N., *Appl. Catal.*, **55,** 115 (1989).
10. Khodakov, A.Yu., Kustov, M. L., Bondarenko, N. T., Dergachev, A. A., Kanzansky, B. V., Minachev, M. Kh., Borbely, G., and Beyer, K. H., *Zeolites*, **10,** 603 (1990).
11. Minachev, M. Kh., and Dergachev, A. A., *Catal. Today*, **13,** 645 (1992).
12. Parera, J. M., and Figoli, N. S., in "Catalytic Naphtha Reforming, Science and Technology", Dekker, 1995, p. 47.
13. Abbot, J., and Wojciechowski, B. W., *J. Catal.*, **115,** 1 (1989).
14. Vedrine, J. C., "Solid State Chemistry in Catalysis", (R.K. Grasselli and J.F. Brazdil, Eds.), ACS Symposium Series, Vol., 279, p. 257. Am. Chem. Soc., Washington, DC, 1985.
15. Voogd, P., and Van. Bekkum, H., *Appl. Catal.*, **59,** 311 (1990).
16. Haag, W. O., Lago, R. M., and Weisz, P. B., *Faraday. Discuss. Chem. Soc.*, **72,** 317 (1982).
17. Csicsery, S. M., *Zeolites*, **4,** 202 (1984).
18. Ono, Y., Nakatani, H., Kitagawa, H., and Suzuki, E., *Stud. Surf. Sci. Catal.*, **44,** 279 (1988).
19. Kanai, J., *Stud. Surf. Sci. Catal.*, **44,** 211 (1988).
20. Ono, Y., and Kanae, K., *J. Chem. Soc. Faraday. Trans. I.*, **87,** 663 (1991).
21. Meitzner, G. D., Iglesia, E., Baumgartner, J. E., and Huang, E. S., *J. Catal.*, **140,** 209 (1993).
22. Guisnet, M., Gnep, N. S., Vasques, H., and Ribeiro, F. R., *Stud. Surf. Sci. Catal.*, **69,** 321 (1991).

CHAPTER V

SUMMARY

This thesis is a study of cracking and aromatization reactions of lower hydrocarbons (C_4-C_6) over pentasil group zeolites such as ZSM-5, ZSM-22, ZSM-48 and EU-1. The influences of various process parameters and catalyst promoters such as ZnO, Ga_2O_3 and Pt on aromatization activity and catalyst life have been examined. Considering the commercial importance of the aromatization processes, the transformation of a low value hydrocarbon mixture (light raffinate) into aromatics was also investigated.

The fundamental aspects of the hydrocarbon cracking mechanism is well understood for large pore zeolites. In this thesis, the hydrocarbon cracking mechanism over medium pore pentasil zeolites is examined using n-hexane as a model hydrocarbon and ZSM-48 as a model catalyst. The cracking model includes a monomolecular cracking path based on Langmuir adsorption isotherm as well as a bimolecular path following Rideal kinetics. The results of the different studies are summarized below:

Cracking of n-hexane over ZSM-48 and its Fe and Ga-isomorphs

- The isomorphous substitution of Al- by Ga and Fe and decreasing the Al^{3+} concentration significantly decreases the conversion of n-hexane over ZSM-48.
- All the catalysts deactivate rapidly in the biginning (within 1h) and then the deactivation becomes less rapid. The rate of deactivation increases with increasing reaction temperature and increasing Al^{3+} concentration. The Fe-isomorph of ZSM-48 deactivates less when compared to the Ga- and Al-isomorphs.
- The lower cracking rates of isomeric C_6-hydrocarbons like 3-methylpentane and 2,2-dimethylbutane are probably mainly due to differences in diffusion than to the steric inhibition (inside the pores of the zeolite) to the formation of the transition state complexes during cracking.
- A linear relationship between the concentration of stronger acid sites and specific catalytic

activities (molecules of n-C_6 converted/Al^{3+}.sec) has been found.

Hydrocarbon cracking mechanism in ZSM-48

- A general kinetic model that includes both monomolecular protolytic cracking and bimolecular chain cracking mechanism is shown to be applicable in the case of ZSM-48.
- The ratio of the adsorption of the feed and the average product, as well as the change in enthalpy of adsorption between the feed and the average product suggest that the adsorption of the reactant is more than the product at higher temperatures. This explains the higher probability of the monomolecular process compared to the bimolecular chain cracking process at higher temperatures.
- The lower yield of C_4 paraffins compared to C_3 and C_2 paraffins during cracking has been explained to be due to strong steric inhibition to the formation of a transition state complex between n-hexane and the corresponding carbonium ion in the channels during the hydride transfer reaction.

Aromatization of lower hydrocarbons (C_4-C_6) over three pentasil group zeolites (ZSM-5, ZSM-22 and EU-1)

- The yield of aromatics is significantly more over ZSM-5 than over the other two zeolites, ZSM-22 and EU-1 during the aromatization of C_4-C_6 hydrocarbons . Reaction temperature and space velocity have significant influence on the aromatics yield. At identical reaction conditions, ZSM-22 and EU-1 produce 10 and 8 times less aromatics than ZSM-5 during n-hexane aromatization probably due to the higher acid strength and optimal channel dimensions of ZSM-5. EU-1 produces more C_8^+ aromatics than ZSM-22 at 793K. The larger side pockets in EU-1 are probably responsible for the higher yields of C_8^+ aromatics.
- ZSM-5 deactivates less rapidly during n-hexane aromatization even though it produces

more aromatics. No significant decrease in conversion is noticed over ZSM-5 for about 50 h on stream in both H_2 and N_2 atmospheres. On the otherhand, ZSM-22 and EU-1 deactivate rapidly, with both conversion and aromatic yields decreasing rapidly with time.

Aromatization of n-hexane over Ga, Zn, Cr and Fe promoted H-ZSM-5

- Promoters such as ZnO and Ga_2O_3 impregnated into H-ZSM-5 increase the aromatic yield while Fe_2O_3 and Cr_2O_3 decrease the aromatic yield during the aromatization of n-hexane. Ga_2O_3 and ZnO promoted H-ZSM-5 deactivate less when compared to Fe_2O_3 and Cr_2O_3 promoted H-ZSM-5 at similar reaction conditions. The aromatization proceeds through cracking of n-hexane over H-ZSM-5, while it proceeds mainly through dehydrogenation of n-hexane to n-hexene, hexadiene or haxatriene and subsequent cracking of these species to lower olefins over Ga_2O_3/H-ZSM-5. The higher aromatic yield in Ga_2O_3/H-ZSM-5 is due to rapid cyclization of these allylic species over protonic sites. ZnO/H-ZSM-5 deactivates faster than H-ZSM-5 while Ga_2O_3/H-ZSM-5 deactivates slower. The deactivation coefficient is maximum for Fe_2O_3 and Cr_2O_3 containing samples.
- In the case of H-ZSM-5, the yield of C_8^+ aromatics increases with increasing pressure. When H_2 is present (at higher pressures), the yield of total aromatics is significantly less when compared to the presence of N_2 at similar conditions. As aromatics production is a dehydrogenation reaction, a decrease in aromatics yield on addition of H_2 or increasing the pressure is expected purely from thermodynamic reasons. Increasing the pressure of the reaction increases both deactivation rate and coke deposition because of an increase in the rate of condensation/polymerization reactions of the cracked olefins.

Aromatization of light raffinate

- Incorporation of a small amount of platinum (500 ppm) to Ga_2O_3/H-ZSM-5 improves both the aromatics yield and the life of the catalyst. The slower deactivation of platinum

promoted catalyst is probably due to the hydrogenation of the poly unsaturated hydrocarbons (coke precursors) over the metallic surface.

The process parameters like space velocity and H_2 partial pressure have significant influence on the total aromatics yield. However, the influence of H_2 partial pressure is less marked, though it has a considerable influence on the aging characteristics of the catalyst.

LIST OF PUBLICATIONS

1. A Comparison of Aromatization Activities of the Medium pore zeolites, ZSM-5, ZSM-22 and EU-1.
   D. Bhattacharya and S. Sivasanker, *J. Catalysis* 153 (1995) 353.

2. Characterization and Catalytic properties of Zeolite MCM-22.
   R. Ravisanker, **D. Bhattacharya**, N.E. Jacob and S. Sivasanker, *Microporous Material* 4 (1995) 83.
3. Synthesis, Characterization and Catalytic properties of the two novel Vanado-aluminosilicates with EU-1 and ZSM-22 structures.
   M. Chatterjee, **D. Bhattacharya,** N. Venkatathri and S. Sivasanker, *Catalysis Letter* 35 (1995) 313
4. Benzoylation of Benzene to Benzophenone over Zeolite Catalysts.
   A.P. Singh and **D. Bhattacharya,** *Catalysis Letter* 32 (1995) 327.
5. Benzoylation of Toluene with Benzoyl chloride over Zeolite Catalysts.
   A.P. Singh, **D. Bhattacharya** and S. Sharma, *J. Mol. Catal* 102 (1995) 139.
6. A Comparison of the Activity of ZSM-5, ZSM-22 and EU-1 Zeolites in the Aromatization of Butene-1.
   D. Bhattacharya and S. Sivasanker, *Catalysis Modern Trends,* N.M. Gupta and D.K. Chakrabarty (Editors) Narosa Publising House, p191.
7. Selective para Chlorination of Toluene to para Chlorotoluene (PCT) using Zeolite Catalysts.
   A.P. Singh, S.B. Kumar and **D. Bhattacharya,** *Catalysis Modern Trends,* N.M. Gupta and D.K. Chakrabarty (Editors) Narosa Publising House, p196.
8. Isomerization of o-dichlorobenzene over ZSM-5 and EU-1 Zeolite Catalysts.
   A.P. Singh, A. Paul, S. Sharma and **D. Bhattacharya**, *Catalysis Modern Trends,* N.M. Gupta and D.K. Chakrabarty (Editors) Narosa Publising House, p200.
9. Aromatization of n-Hexane over H-ZSM-5: Influence of promoters and added Gases.
   D. Bhattacharya and S. Sivasanker, *Appl. Catal* 141 (1996) 117.
10 Remarkable Change in the Regioselectivity of Benzoylation of Naphthalene using Zeolite H-beta Catalysts.
   D. Bhattacharya and A.P. Singh
   Poster Presentation at International Congress on Catalysis, Baltimore, USA, July 1996.
11. Studies on the cracking of n-Hexane over H-ZSM-48.
   D. Bhattacharya, M. Chatterjee and S. Sivasanker, *Reaction. Kinet. Catal. Lett* (in press).
12. Selective Benzoylation of Naphthalene to 2-benzoylnaphthalene using Zeolite H-beta Catalysts.
   D. Bhatttacharya, S. Sharma and A.P. Singh, *Appl. Catal* (in press)
13. The influence of Reaction Temperture on the Cracking Mechanism of n-Hexane over H-ZSM-48.
   D. Bhattacharya, S. S. Tambe and S. Sivasnker, *Appl. Catal* (communicated)
14. Benzylation of Naphthalene with Benzylchloride over Zeolite Catalysts.
   D. Bhattacharya, A. Pande and A.P. Singh. (manuscript in preparation)

PATENTS FILED

1. An Improved Process for the Preparation of Benzophenone.
   D. Bhattacharya, S.B. Kumar, A.P. Singh and P. Ratnasamy, Indian patent, Appl. No. 289/DEL/95.
2. An Improved Process for the Preparation of meta dichlorobenzene.
   D. Bhattacharya and A. P. Singh
   Indian Patent filed.
3. An Improved Process for the Preparation of a Crystalline Vanado-aluminosilicate with EUO Structure.
   D. Bhattacharya, M. Chatterjee and S. Sivasanker.
   Indian Patent filed.
4. An Improved Process for the Preparation of a Crystalline Vanado-aluminosilicate with TON Structure.
   D. Bhattacharya, M. Chatterjee and S. Sivasanker.
   Indian Patent filed.

TH-1057